



## Evaluation of uncertainties in the simplified fatigue method

A study on appendages in the splash zone of a semi-submersible platform

*Master's Thesis in the International Master's Programme Naval Architecture and Ocean Engineering*

MATTIAS FRÖSING AND  
RASMUS WESTERDAHL JANSSON

Department of Shipping and Marine Technology  
*Division of Marine Design, Research Group Marine Structures*  
CHALMERS UNIVERSITY OF TECHNOLOGY  
Göteborg, Sweden 2013  
Master's Thesis X-13/287



MASTER'S THESIS IN THE INTERNATIONAL MASTER'S PROGRAMME IN  
NAVAL ARCHITECTURE AND OCEAN ENGINEERING

# Evaluation of uncertainties in the simplified fatigue method

A study on appendages in the splash zone of a semi-submersible platform

MATTIAS FRÖSING AND RASMUS WESTERDAHL JANSSON

Department of Shipping and Marine Technology  
*Division of Marine Design*  
Research Group Marine Structures  
CHALMERS UNIVERSITY OF TECHNOLOGY  
Göteborg, Sweden 2013

Evaluation of uncertainties in the simplified fatigue method – a study on appendages  
in the splash zone of a semi-submersible platform

MATTIAS FRÖSING AND RASMUS WESTERDAHL JANSSON

© MATTIAS FRÖSING AND RASMUS WESTERDAHL JANSSON, 2013

Master's Thesis X-13/287

ISSN 1652-8557

Department of Shipping and Marine Technology

Division of Marine Design

Research Group Marine Structures

Chalmers University of Technology

SE-412 96 Göteborg

Sweden

Telephone: + 46 (0)31-772 1000

Cover:

Modern production platforms have a lot of external piping and other appendages attached to the columns. On the right-hand side, riser pipes and a riser guard that protects the pipes in case of collision can be seen. On the left-hand side, caissons and supports for sea water and ballast are installed.

Printed by Chalmers Reproservice  
Göteborg, Sweden 2013

Evaluation of uncertainties in the simplified fatigue method – a study on appendages in the splash zone of a semi-submersible platform

*Master's Thesis in the International Master's Programme in Naval Architecture and Ocean Engineering*

MATTIAS FRÖSING AND RASMUS WESTERDAHL JANSSON

Department of Shipping and Marine Technology

Division of Marine Design, Research Group Marine Structures

Chalmers University of Technology

## ABSTRACT

The use of external piping is becoming more common for semi-submersible platforms. Previous analyses have shown that uncertainties exist in how the methods used for assessing the fatigue limit state should be applied. One method of interest, which is offered by classification society rules for offshore structures, is the simplified fatigue method. The expression used for estimating fatigue damage only requires S-N parameters, distribution parameters of the stress range history and a design life.

The objective of this thesis has been to identify and evaluate factors that have a great influence on the calculated fatigue damage in the simplified fatigue method when applied on appendages in the splash zone. The evaluation was conducted on a case study regarding external piping on a semi-submersible production platform. By using a Weibull model to represent the stress-range distribution the following critical factors could be identified: the shape parameter, the reference stress range, and the chosen S-N parameters. Methods for assessing them individually were developed. An assumption of a linear relation between stress range and wave height was used. The distribution parameters could then be obtained using the results from a linear finite element analysis to scale the distribution of wave heights.

The conclusions obtained through the devised methods showed that the estimated damage is heavily dependent on how stress ranges are represented in the Weibull fit. This is dependent on both the shape parameter and the reference stress range. Contributions from stress ranges with a high magnitude dominate even though the occurrences of such stress ranges are very low. A subdivision of stress-range distributions corresponding to, for example, different wave headings gives improved estimates. More Weibull-like distributions can be obtained and scaled with the corresponding stress ranges. It was also noted that small changes in load input data increases the estimated fatigue damage significantly. Thus, it is very important to have an understanding of the uncertainties in the hydrodynamic analysis used for deriving the loads. Moreover, the choice of S-N data also shows a large impact, although it is hard to determine which weld classification should be used when only one reference stress range is considered.

It is important that future work is conducted in order to verify the simplified fatigue method. Different alternatives in deriving the wave-height distribution, or one of the other fatigue assessment methods offered by class could be used.

Key words: external piping, semi-submersible, simplified fatigue method, slamming, splash zone, wave statistics.



# Contents

ABSTRACT	I
CONTENTS	III
PREFACE	V
NOTATIONS	VII
ABBREVIATIONS	IX
1 INTRODUCTION AND MOTIVATION FOR STUDY	1
1.1 Background	1
1.2 Objectives of Investigation	3
1.2.1 Sub-targets	3
1.3 Methodology	4
1.4 Limitations and Assumptions	5
1.5 Outline of Thesis	6
2 FATIGUE ASSESSMENT ALTERNATIVES	7
2.1 Spectral-based Method	8
2.2 The Deterministic Method	9
2.3 The Simplified Fatigue Method	10
3 CASE STUDY	13
3.1 General	13
3.2 Input Data	15
3.2.1 Structure	15
3.2.2 Environment	16
3.2.3 Loads	16
4 IMPORTANT FACTORS IN THE SIMPLIFIED FATIGUE METHOD	19
4.1 Main Factors	19
4.1.1 Shape Parameter	19
4.1.2 Reference Stress Range	20
4.1.3 Fatigue Resistance	21
4.2 Alternatives in Methodology	22
5 LOAD ANALYSIS	27
5.1 Loads on Caissons	27
5.2 Loads on Support	29
5.2.1 Morison Forces	29
5.2.2 Slamming	30

6	STRUCTURAL RESPONSE ANALYSIS	33
6.1	Beam FE-model	33
6.1.1	Boundary Conditions	33
6.1.2	Load Application	34
6.2	3D FE-model	35
6.2.1	Mesh	35
6.2.2	Boundary Conditions	37
6.2.3	Load Application	37
6.3	Local Stress Analysis	39
6.3.1	The Hot-spot Method	39
6.3.2	Stress Derivation	40
7	ESTIMATION OF THE SHAPE PARAMETER	41
7.1	Determining the Distributions of Waves	41
7.2	Derivation of the Shape Parameter	43
8	FATIGUE DAMAGE	47
8.1	Calculation of Scale Parameter	47
8.2	Calculation of Fatigue Damage	49
8.2.1	The Nominal Method	50
8.2.2	Morison and Impact-separated Method	50
8.2.3	The Directional Morison Method	51
8.2.4	The Weather Conditional Method	52
9	FATIGUE DAMAGE RESULTS	53
10	DISCUSSION	61
11	CONCLUSIONS	63
12	FUTURE WORK	67
13	REFERENCES	69
	APPENDIX A: THE THEORY OF THE SIMPLIFIED FATIGUE METHOD	A1
	APPENDIX B: LOADS	B1
	APPENDIX C: STRUCTURAL MODELS	C1
	APPENDIX D: STRESS RESULTS	D1
	APPENDIX E: SHAPE PARAMETERS	E1
	E.1 List of Shape Parameters	E6
	APPENDIX F: SCALE PARAMETERS	F1
	APPENDIX G: S-N CURVES	G1

# Preface

This thesis is a part of the requirements for the master's degree in Naval Architecture and Ocean Engineering at Chalmers University of Technology, Göteborg, and has been carried out at the Division of Marine Design, Department of Shipping and Marine Technology, Chalmers University of Technology in cooperation with GVA Consultants, in Göteborg, between January and June of 2013.

We would like to acknowledge and thank our examiner and supervisor, Professor Jonas Ringsberg at the Department of Shipping and Marine Technology, for excellent guidance and support throughout the work with this thesis. We also thank Assistant Professor Wengang Mao at the Department of Shipping and Marine Technology for giving us feedback.

We would also like to thank our industry partner supervisor Philip Olin at GVA Consultants for the time and supervision he has given us. Moreover, we would like to thank Lic. Eng. Kjell Vågfelt, Structural Analysis Manager at GVA Consultants, for giving us the opportunity of producing this thesis.

Furthermore, we would like to thank Professor Igor Rychlik at the Division of Mathematical Statistics for taking the time to answer our questions.

Finally, we would like to express our gratitude to everyone at the GVA Consultants, Göteborg office, who have contributed with information and guidance during our work.

Note that some references used in this thesis are confidential. Referenced reports written by GVA Consultants are not publicly available. Anybody interested in taking part of these reports is referred to GVA headquarters in Göteborg.

Göteborg, June, 2013

Mattias Frösing and Rasmus Westerdahl Jansson



# Notations

## Roman upper case letters

$A$	Cross sectional area, m <sup>2</sup>
$A_p$	Projected area, m <sup>2</sup>
$C_A$	Added mass coefficient
$C_D$	Drag coefficient
$C_L$	Lift coefficient
$C_{Pa}$	Space average slamming pressure coefficient
$D_c$	Caisson diameter, m
$D$	Fatigue damage
$D_d$	Fatigue damage during the design life
$D_{life}$	Fatigue damage during an arbitrary life-time
$D_{ref}$	Reference fatigue damage
$E$	Young's modulus, GPa
$E(X)$	Expected value of random variable $X$
$F(X)$	Cumulative distribution function of random variable $X$
$F_x$	Distributed load in the x direction, N/m
$F_y$	Distributed load in the y direction, N/m
$H$	Wave height, m
$H_{lim}$	Cut-off for which waves with wave height over $H_{lim}$ cause slamming, m
$H_s$	Significant wave height, m
$L$	Caisson length, m
$N$	Number of cycles to failure at a specific stress range or stress range block
$N_d$	Number of cycles during the design life
$N_{life}$	Number of cycles for an arbitrary life-time
$N_{ref}$	Number of cycles where $S_{ref}$ is the maximum stress range during $N_{ref}$
$P(X)$	Probability density function of random variable $X$
$Q(X)$	Exceedance probability function of random variable $X$
$S$	Stress range, MPa
$S_{ref}$	Reference stress range, MPa
$T$	Wave period, seconds
$V$	Displaced volume, m <sup>3</sup>

### Roman lower case letters

$\bar{a}$	Interception of N-axis and S-N curve, cycles
$\bar{c}$	Interception of N-axis and second S-N curve in a two-slope S-N diagram, cycles
$f_{Sea-state}$	Relative frequency of the occurrence of a short term sea-state
$f_{Heading}$	Relative fraction of a wave heading
$f_{Weather}$	Relative fraction of a weather condition
$f_L$	Lift force per unit length, N/m
$f_N$	Normal force per unit length, N/m
$f_T$	Tangential force per unit length, N/m
$h$	Wave height, m
$m$	Inverse slope of S-N curve
$n$	Inverse of second slope of a two slope S-N curve
$n_i$	Number of cycles at a specific stress range or stress range block
$p$	Weighting exponent
$p_s$	Space average slamming pressure, Pa
$q$	Scale parameter
$s$	Stress range, MPa
$s_{s.i.}$	Stress at intersection of a two slope S-N curve, MPa
$s_{0.5t}$	Stress at 0.5 $t$ from hot spot location, MPa
$s_{1.5t}$	Stress at 1.5 $t$ from hot spot location, MPa
$s_{HS}$	Stress at hot spot location, MPa
$t$	Plate thickness, mm
$v$	Relative fluid particle velocity, m/s
$\dot{v}$	Relative fluid particle acceleration, m/s <sup>2</sup>
$z$	Gamma function cut-off parameter

### Greek upper case letters

$\Gamma$	Gamma function
$\Gamma_0$	Cut-off gamma function from 0 to $z$
$\Gamma_1$	Cut-off gamma function from $z$ to $\infty$

### Greek lower case letters

$\gamma$	Shape parameter
$\lambda$	Wave length, m
$\nu$	Poisson's ratio
$\rho$	Mass density of sea water, kg/m <sup>3</sup>
$\sigma$	Rayleigh parameter

## Abbreviations

ABS	American Bureau of Shipping
CFD	Computational Fluid Dynamics
DNV	Det Norske Veritas
FE	Finite Element
FLS	Fatigue Limit State
RP	Recommended Practice
S-N Curve	Stress-Life Curve (Wöhler curve)
ULS	Ultimate Limit State



# 1 Introduction and Motivation for Study

## 1.1 Background

The global economy is heavily dependent on petroleum products as a source of energy particularly with regard to transports and electricity, World Resource Institute (2000). In order to ensure sustainable development: “To meet the need of the present without compromising the ability of future generations to meet their own needs”, The World Commission on Environment and Development (1987), this dependency of fossil fuels needs to be reduced by switching to renewable and CO<sub>2</sub>-neutral sources of energy. Such a shift, however, will not happen over night.

In 2010, the Deepwater Horizon platform had an accident resulting in approximately 4.9 million barrels of oil being released into the Gulf of Mexico. The spill had a significant impact on the marine environment and is considered as one of the worst environmental disasters in the United States, Fruedenburg and Gramling (2011). As long as we as a society are dependent on this industry, it is important to ensure safe operations of offshore platforms in order to avoid accidents resulting in oil spill. Through increased knowledge of the methods used for evaluating the structural strength of offshore structures, future disasters may be avoided.

Modern semi-submersible production platforms are heavily equipped with machinery, pump equipment, treatment and distribution systems. All these systems require piping that has to exit or enter the platform in order perform its function. The piping can either be routed through the hull to a sea chest under the pontoons or externally along the column. Platforms are today moored at locations with increasingly harsher environmental conditions and at more extreme water depths. In order to minimize platform motions, especially the heave motion, they are designed with a very deep draught, Det Norske Veritas (2011a). This puts high requirements on strength and water integrity of the platform shell and penetration of the underwater hull, which is necessary in the case of internal piping, might be a risk. External piping for oil and gas productions as well as for ballast is becoming more common, thus avoiding penetration of the underwater hull and the possible problems related to internal piping.

Platforms may have a lot of external piping and other appendages on or along the column, as can be seen in Figure 1.1. These external appendages are exposed to wave and current loads. The extensions and magnitudes of these loads are dependent on wave elevation, wave direction and the interaction between waves and platform. Normally, one wants to avoid installing appendages in the so-called splash zone, as the area around the still water line normally experiences the greatest loads. Obviously, this is not possible for pipes extending from the deck box to the pontoon. According to Dalton and Nash (1976), external appendages have to be specially designed to accommodate the splash-zone environment where heavy water impact loads, i.e. slamming, is present in addition to drag and inertia loads.



*Figure 1.1 Modern production platforms may have a lot of external piping and other appendages attached to the columns. On the right-hand side, riser pipes and a riser guard which protects the pipes in case of collision can be seen. On the left-hand side, caissons and supports for sea water and ballast are installed.*

The design of several external appendages on a particular floating production unit designed for operation in the Gulf of Mexico has been presented in a report by GVA Consultants, GVA Consultants (2011a). The conclusion of this report was that a significant challenge lies in predicting the fatigue strength of the external appendages and their connections to the column shell. Uncertainties as to how applicable the method used resulted in a very conservative fatigue assessment. During the design, dimensions of the supports had to be increased and the fatigue limit state was considered a limiting factor.

The method used in the report, GVA Consultants (2011a), is in several classification societies Recommended Practice (RP) referred to as the simplified fatigue method. The simplified fatigue method is a stress-based fatigue assessment method. It uses the probability distribution of stress ranges to estimate the expected fatigue damage. One advantage with this method is that all stress ranges can be described by the distribution parameters, which makes it easy to compare or evaluate the fatigue loading of different structures. The expected fatigue damage can be evaluated with a Palmgren-Miner approach, where the only other inputs are an appropriate S-N curve and the design life in number of stress cycles.

The implementation of the method is left open in many respects by classification society rules, especially with regard to how distribution parameters should be determined. It was therefore interesting to identify and evaluate how different ways of applying the simplified fatigue method affects the outcome in fatigue damage estimation.

## 1.2 Objectives of Investigation

The simplified fatigue method, as well as fatigue assessment in general contains numerous uncertainties, Det Norske Veritas (2011a). Uncertainties in loads, material properties, fatigue resistance, stress calculations and fatigue calculations have been assessed by classification societies and the effects are often handled in the rules.

The objective of this thesis has been to identify and evaluate the factors in the simplified fatigue method that have the greatest effect on the calculated fatigue damage. A sensitivity analysis was performed with regard to the input parameters of the fatigue assessment. This was done in order to outline how these can be treated and what effects could be obtained by including different inputs or methods to derive parameters.

The effects were investigated in a case study regarding external piping on a semi-submersible platform. Two sets of classification society rules, the American Bureau of Shipping (ABS) and Det Norske Veritas (DNV), were used in this thesis. Differences in the interpretation of the simplified fatigue method between the two societies are pointed out.

One aim was also to suggest recommendations of how the simplified fatigue method should be applied and where efforts should be made in order to ensure greater certainty in future fatigue analyses of similar structures.

### 1.2.1 Sub-targets

The following sub-targets were identified in relation to the main objective of this thesis:

- Identify how the stress-range distribution parameters can be obtained and how they can be handled in order to represent the stress ranges as accurately as possible.
- Investigate how a variation in load input data propagates through the structural and fatigue analyses and affects the calculated fatigue damage. Primarily with respect to uncertainties in the load magnitude.
- Evaluate how the choice of different S-N curves that represent the fatigue resistance affects the calculated fatigue damage.

### 1.3 Methodology

In order to assess the simplified fatigue method, the following methodology was used.

A literature study was conducted in order to outline how the simplified fatigue method works, which assumptions are made, what information is included and what is lost. This study included classification society rules as well as the background and development of the method.

An investigation regarding the application of the method on the specific case study was carried out to see how the conditions and circumstances are treated. Different alternatives in the derivation of input parameters were identified to assess the sub-targets of the thesis.

The devised alternatives were compared in terms of corresponding fatigue damage, calculated using the following numerical analyses.

- Load analysis
- Structural response analysis
- Stress-range distribution analysis
- Fatigue evaluation

Each part is described briefly with respect to the methods and softwares used. The flowchart in Figure 1.2 represents the methodology of the numerical analysis used in this thesis.

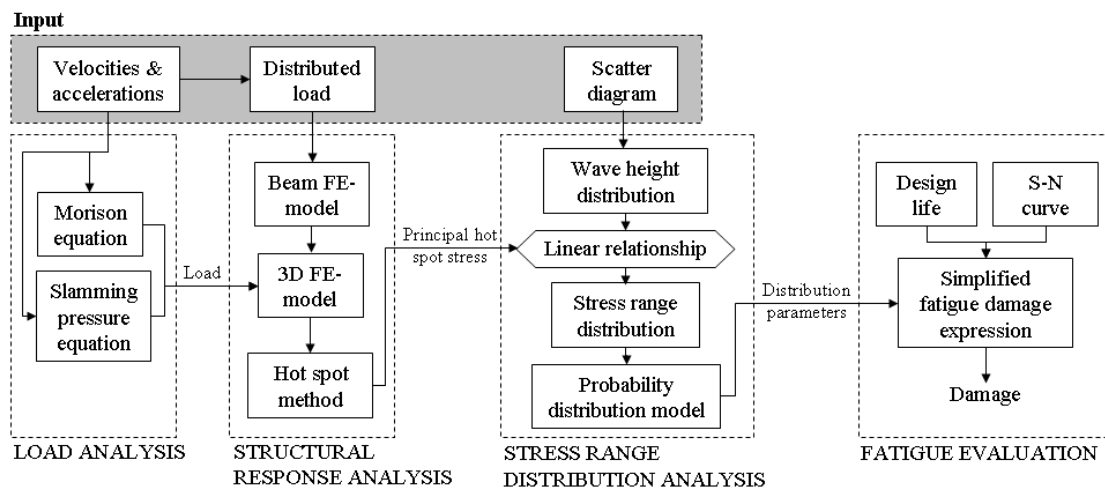


Figure 1.2 Numerical analysis flowchart.

Loads were derived using Morison equations as well as equations for space average slamming pressure presented in DNV RP, Det Norske Veritas (2010a). A simplified model of the support was used for estimating coefficients and for added mass and drag needed in the calculations, which were carried out in EXCEL 2003.

Two Finite Element (FE) models were used for the linear structural response analysis. One beam model of the caissons created in the DNV software NAUTICUS 3D BEAM (V.10.51.34.4522), Det Norske Veritas (2008), and one 3D model created in GENIE (V.5.1-11), Det Norske Veritas (2011b), containing the studied support and part of the column. Loads were applied on the beam model in order to obtain reaction forces and moments at the supports. Reaction forces and moments from the beam model were then applied together with remaining loads on the 3D FE-model. The GENIE model was solved in the DNV software SESTRRA (V.8.4-01), Det Norske Veritas (2010b), and stress results were gathered using the post-processing software XTRACT (V.3.0-00), Det Norske Veritas (2011c). Stresses in critical welds were calculated with the hot-spot method in the numerical software MATLAB (V.7.9.0), Mathworks (2013). GENIE, SESTRRA and XTRACT are all part of the DNV software package SESAM.

The stress-range distribution was obtained though assuming a linear relationship between wave height and stress range. The distribution of wave heights was based on scatter diagrams with measurements of significant wave height at the location of the platform. Each sea-state in the scatter diagram was assumed to be Rayleigh-distributed and a long-term wave height distribution could be obtained by a summation of the Rayleigh distributions together with their respective relative occurrence. The wave height distribution was scaled with a reference stress range using the assumed linear relationship resulting in a stress-range distribution. This distribution was then fitted to a probability distribution model in order to obtain the distribution parameters. All calculations were performed using MATLAB (V.7.9.0), Mathworks (2013).

The expected fatigue damage was calculated using the simplified fatigue damage expression. The expression requires parameters from an appropriate S-N curve, stress range distribution parameters and the design life defined in the number of cycles. The damage calculations were conducted in MATLAB (V.7.9.0), Mathworks (2013).

## 1.4 Limitations and Assumptions

The focus of this thesis has been on structural and fatigue analysis. Hence, no hydrodynamic analysis has been performed. Instead, results have been taken from a previous analysis performed by GVA Consultants on the semi-submersible platform, GVA Consultants (2010) and GVA Consultants (2011b). The loads have been taken as reference loads as the main objective was to evaluate the difference in calculated fatigue damage, not to predict the actual expected damage. The authors of this thesis take no credit or responsibility for the hydrodynamic analysis. However, methods used and results available are presented in Chapter 3.

A two-parameter Weibull model was chosen for describing the stress-range distribution, which is the case described in classification society rules and common practice in the industry, the American Bureau of Shipping (2013). The Weibull model is described by a shape parameter specifying the relative occurrence between stress ranges and a scale parameter specifying the magnitude of the stress ranges. The advantage is that the Weibull model can be fitted to the wave height distribution in order to obtain the shape parameter. The scale parameter can then be found with one stress-range cycle resulting from a reference wave with a specified occurrence. This

results in a linear relationship between the wave height and stress range. A linear relationship can be assumed to be valid for large floating column-stabilized offshore structures, American Bureau of Shipping (2010). Classification societies state that it is possible to use other distribution models, although this has not been studied.

In this thesis, only welds were considered in the fatigue assessment. It is known that welds are sensitive to cyclic loading. Tensile residual stresses due to welding decrease the fatigue resistance, IIW (2008). The influence of welds on the fatigue resistance has only been accounted for by the use of S-N curves together with the hot-spot method, hence welds were not modelled in the FE-analysis. The fatigue assessment has been limited to the caisson supports and the horizontal connection to the column shell. Because of the high requirements on water integrity of the column shell, this weld has been of interest. Possible failure might damage the column shell. It was also assumed that no macroscopic cracks existed in the structure after fabrication.

Only vertical slamming on the supports is considered in the load analysis, i.e. no horizontal slamming on either the caissons or the supports has been included. In the mentioned hydrodynamic analysis it was determined that the steepness of the most common waves was too low for any significant occurrence of horizontal slamming, GVA Consultants (2010) and GVA Consultants (2011b).

## **1.5 Outline of Thesis**

The first part of this thesis aims at assessing the simplified fatigue method both in general and in respect to the case study on which it is implemented Chapter 2 describes the fatigue assessment methods offered by classification societies, including the simplified fatigue method. The case study and input data is presented in Chapter 3. Factors in the simplified fatigue method with a great influence on calculated fatigue damage are identified in Chapter 4. Methods for assessing these factors individually are developed and presented. The numerical analyses required for evaluating the simplified fatigue method is presented through Chapters 5 to 8. A theory for the derivation of loads is presented in Chapter 5. The structural response analysis is presented in Chapter 6. Derivation of distribution parameters describing the stress ranges and the fatigue damage calculations is presented in Chapters 7 and 8. The results of calculated fatigue damage from the different methods identified in Chapter 4 are presented and discussed in Chapter 9. Conclusions based on these results can be found in Chapter 10. The methods used and the validity assumption used throughout the project are discussed in Chapter 11. Ultimately, future work for further evaluation of the simplified fatigue method is presented in Chapter 12.

## 2 Fatigue Assessment Alternatives

This chapter describes some fatigue assessment methods that are offered in classification society rules. Among these is the simplified fatigue method which is the main focus of this thesis. According to the two classification societies referenced in this thesis, ABS and DNV, fatigue analysis should be stress, strain or fracture mechanics based.

The stress-based approach is used when a linear relationship between stress and strain, Hooke's law, can be assumed throughout the sequence of the stress cycle, i.e. that the stress during the cycle is less than the yield limit of the material. The fatigue resistance is presented as the relationship between the number of cycles,  $N$ , of a constant stress range,  $S$ , that will result in fatigue failure, American Bureau of Shipping (2010). The relationship is often described in the form of an S-N curve, but can also be presented as a table or equation. The derivation of fatigue-inducing stress ranges needs to account for the local stress raisers such as notches or welds, American Bureau of Shipping (2010) and Det Norske Veritas (2011a). This can be done either by modifying the nominal stress in the considered detail through the use of stress concentration factors or through the use of reduced fatigue resistance. It is common to employ FE-modelling to account for geometric stress raisers, but tabulated values can also be obtained from handbooks, American Bureau of Shipping (2010). Welds are normally treated by modifying the fatigue resistance, i.e. using a reduced S-N curve. Depending on the type of weld and the geometry in the immediate vicinity, the weld is specified as a specific class governing the choice of S-N curve. In addition to weld class the fatigue resistance is also determined by environment - three different conditions are discussed by ABS and DNV, details in air, details in sea water with cathodic protection and details in sea water with free corrosion. With fatigue loading and resistance defined they are assessed using the Palmgren-Miner damage accumulation rule in order to obtain an estimate of the fatigue damage. In the case where damage is estimated using a stress-based approach, three alternatives are offered:

- Spectral based method
- Deterministic method
- Simplified fatigue method

The stress-based methods are mainly suited for high-cycle fatigue, whereas strain-based methods are suited for low-cycle fatigue. DNV defines low-cycle fatigue as  $N < 10^4$ , Det Norske Veritas (2011a). For evaluation of fatigue damage with a life lower than ten thousand cycles, the strain-based method generally gives improved estimates of fatigue damage, Dowling (2012). However, the number of cycles to failure is not the determining factor. The strain-based approach considers plastic behaviour that may occur in the localized regions where fatigue cracks are initiated. Material responses, such as elastic/plastic shakedown and ratchetting, can then be accounted for by material models describing the plastic behaviour. If the stresses during the sequence of a load cycle result in significant yielding the plastic strain range becomes more important than the stress range for defining the fatigue loading, Dowling (2012). The number of cycles at a constant strain range resulting in failure

determines the fatigue resistance. Since offshore structures are normally designed for other limit states, such as Ultimate Limit State (ULS), the detail is designed to avoid yielding. Even if stresses due to local notches are not accounted for in a ULS design, the ULS assessment implies that the actual strain ranges during a corresponding ULS loading is limited and that a further assessment of low-cycle fatigue is normally not required, Det Norske Veritas (2011a). ABS does not mention the use of a strain-based approach or low-cycle fatigue in its RP for fatigue assessment of offshore structures.

While fatigue assessments conducted using the stress-based approach are recommended for the design of offshore structures, the fracture mechanics method can be used as a complement to assess remaining life after a crack is discovered in the structure, American Bureau of Shipping (2013). Fracture mechanics may be used for fatigue analyses as a supplement for stress-based assessments, for example to assess acceptable defects, such as uncertainties in the quality of material or manufacturing discrepancies, Det Norske Veritas (2011a). In the fracture mechanics-based approach, fatigue damage is defined directly by the crack length. Fatigue resistance is defined as a relationship between the crack growth rate and the stress intensity factor range, using Paris law. An initial crack length and critical crack length are needed in order to determine when failure occurs. The critical crack length depends either on inspection period or failure such as: brittle fracture, yield, leakage, instability or creep of remaining section. The fracture mechanics approach for evaluating fatigue damage is suitable for inspection planning, American Bureau of Shipping (2013) and Det Norske Veritas (2011a). Since inspection is inconvenient for details located in the splash zone, the determination of an inspection time may be of less interest.

## 2.1 Spectral-based Method

The spectral-based method is a frequency domain assessment method which relies on the presumed linearity of wave-induced loads with respect to waves. Spectral-based fatigue analysis is a complex and numerically intensive technique, and there is more than one variant of the method that can be validly applied in a particular case, American Bureau of Shipping (2005). The spectral-based method contains five basic assumptions, American Bureau of Shipping (2013):

- Load analysis and associated structural analysis are linear or approximated as linear. Hence, scaling and the superposition of stress-range transfer functions from unit amplitude waves are considered valid.
- Non-linearities due to non-linear motions and wave loading are treated by the equivalent linearization.
- Structural dynamic response, such as springing and whipping is disregarded.
- Short-term stress processes are assumed to be stationary Gaussian and assumed to be narrowband so that the stress ranges have a Rayleigh distribution.
- The Palmgren-Miner damage accumulation rule applies.

As mentioned above, more than one variant of the spectral fatigue method may be applied. The method presented in ABS rules for column-stabilized and similar floating offshore installations is described briefly. For such floating structures, a linear relationship between wave height and stress range exists, American Bureau of Shipping (2010).

The sea environment is described by the occurrences of various sea-states defined by significant wave height,  $H_s$ , and zero up-crossing-period,  $T_z$ . These sea-states each define a short-term wave energy spectrum according to a spectrum relationship such as Pierson-Moskowitz. Wave direction probability should be considered when determining the wave energy spectra. A complex stress transfer function at the location of interest in the structure is determined through structural analyses performed for specified ranges of wave frequencies and headings. The stress energy spectrum can then be determined by scaling the wave energy spectrum with the stress transfer function. Spectral moments of the stress energy spectrum are determined which are used for defining the short-term Rayleigh distribution of stress response ranges and the average zero up-crossing period of stress cycles. The damage can then be calculated based on integration over stress ranges with the corresponding Rayleigh probability density function - the probability for each sea-state and fatigue resistance - based on the S-N curve, American Bureau of Shipping (2010).

The spectral-based method has the advantage of fewer calculations required compared to the deterministic stress-block method, but has the limitations of linearity and that it is hard to predict low-frequency fatigue stresses, American Bureau of Shipping (2010).

## 2.2 The Deterministic Method

The deterministic method, sometimes referred to as the direct calculation method, is a fatigue assessment presented in ABS RP, where the long-term distribution of stress is defined by block loading, American Bureau of Shipping (2010) and American Bureau of Shipping (2013). A stress spectrum is defined by blocks of constant amplitude stresses with the corresponding number of cycles. In the case of measured stress data, the number of blocks may be chosen somewhat arbitrarily as long as an appropriate resolution is achieved. If no measured stress history is available, recommendations exist in class rules for combinations of parameters to be evaluated in order to construct stress blocks, American Bureau of Shipping (2013). The requirements on which parameters to be considered vary depending on the type of the structure to be analysed. A rough approximation of the parameters to be considered for a permanently moored offshore platform is presented in Table 2.1. These are based on an example of an acceptable set of parameters for a self-evaluated drilling unit presented in ABS RP, American Bureau of Shipping (2013). The wave environment is evaluated in order to determine realistic ranges for the parameters together with the corresponding relative occurrence.

*Table 2.1 Approximation of parameters used for the creation of stress blocks in the deterministic method.*

Parameter	Number of cases / combinations
Number of wave/period combinations	At least 5
Number of cases of wave steepness	Between 12 and 15
Number of wave directions	Normally 8
Total number of combinations:	At least 480

The combinations are evaluated for the resulting wave loading and subsequent stress range through a structural analysis. Stress concentration factors and dynamic amplification should be considered - a single degree of freedom approach is adequate, American Bureau of Shipping (2013). Through this process, stress ranges of constant amplitudes are determined to be used together with their corresponding number of cycles. The number of cycles to failure for each stress block is determined using an appropriate S-N curve and the total fatigue damage is obtained through the Palmgren-Miner damage accumulation rule, American Bureau of Shipping (2013).

The deterministic method requires numerous stress calculations; one for every wave parameter combination and thus many combinations may be required.

### **2.3 The Simplified Fatigue Method**

The simplified fatigue method is a way of estimating fatigue damage based on long-term stress range distribution. Unlike the deterministic method, the simplified fatigue method uses the distribution of stress ranges instead of blocks of stress ranges. Any continuous distribution supported on the semi-infinite interval  $[0 \infty)$ , such as Rayleigh or Weibull, might be used for representing the stress ranges. The two-parameter Weibull distribution is common practice in the marine industry, American Bureau of Shipping (2013), and is thus presented here. The simplified fatigue method theoretically requires very few calculations compared to other methods in order to estimate the fatigue damage.

The method requires two major assumptions, American Bureau of Shipping (2010):

- The long-term distribution of the stress ranges can accurately be expressed by a probability distribution.
- The Palmgren-Miner damage accumulation rule applies, and that the fatigue resistance is defined by S-N curves.

The stress-range distribution is described by two distribution parameters, shape and scale. The shape parameter,  $\gamma$ , specifies the relative distribution between stress ranges - it affects the shape of the distribution rather than simply shifting or stretching it. The scale parameter,  $q$ , specifies the magnitude of the stress ranges; it stretches the distribution, see Figure 2.1.

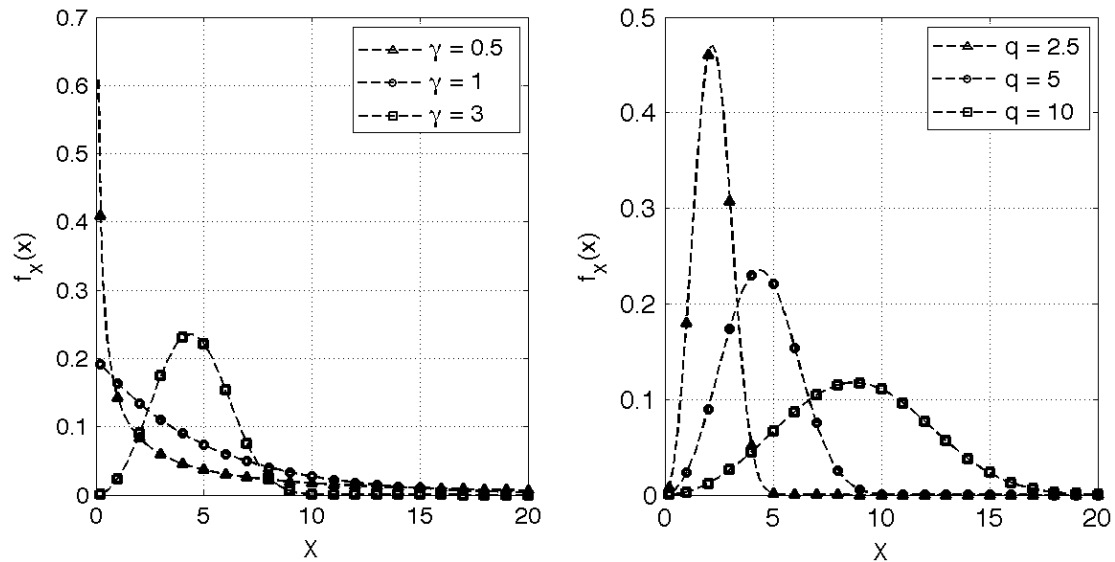


Figure 2.1 The influence of the two parameters describing the Weibull distribution. Left: Influence of varying the shape parameter,  $\gamma$ , with the constant scale parameter  $q=5$ . Right: Influence of varying the scale parameter,  $q$ , with the constant shape parameter  $\gamma=3$ .

The damage is obtained directly from Equation (2.1). The theory and derivation of the expression is presented in Appendix A.

$$D_d = \frac{N_d}{a} q^m \Gamma\left(\frac{m}{\gamma} + 1\right) \quad (2.1)$$

The scale parameter,  $q$ , which describes the magnitude of the stress ranges can be calculated from one specific stress range, given that the shape parameter is determined:

$$q = \frac{S_{ref}}{(\ln N_{ref})^{1/\gamma}} \quad (2.2)$$

where  $N_{ref}$  is a reference number of cycles for which  $S_{ref}$  is the maximum stress range that occurs during  $N_{ref}$  cycles.

The fatigue resistance is described by the S-N curve parameters,  $m$  and  $\bar{a}$ . The parameters are dependent on the principal stress direction and weld class.

The shape parameter,  $\gamma$ , that describes the relative relationship between stress ranges is harder to estimate. If measurements of stress ranges exist, the shape parameter can be determined directly by fitting a Weibull distribution to the measured stress ranges. If no measurements are available some different options are presented in rules. For ship structures, the shape parameter may be established from a long-term wave load analysis or be taken according to rules as a recommended value, American Bureau of Shipping (2012) and Det Norske Veritas (2005). The recommended value depends on location in the ship and the length of the ship. For offshore structures DNV does not offer any recommended values. However, two typical values exist, American Bureau of Shipping (2013):  $\gamma=0.7$  for fixed platforms in the Gulf of Mexico, and  $\gamma>1.0$  in the North Sea. For slender platforms that experience significant dynamics, the shape parameter can take on values as high as  $\gamma=1.4$ . In general, in the absence of data one might also choose a suitable value based on experience from fatigue analysis of similar structures, American Bureau of Shipping (2013).

If a linear relationship can be assumed between wave height and stress range, the shape parameter of the stress range distribution may be derived from the distribution of wave heights. In other words, the two distributions will have identical shape parameters but different scale parameters. One possibility is to employ spectral analysis in order to derive the wave-height distribution. This results in a method similar to the first steps of the spectral fatigue method. In this thesis, another assumption has been used for determining the long-range distribution of wave heights. Short-term distributions of wave heights,  $h$ , from each sea-state can be modelled by Rayleigh distributions that depend on the significant wave height,  $H_S$ . This is with a Rayleigh parameter equal to half the significant wave height, Det Norske Veritas (2010a) and Holthuijsen (2007).

### 3 Case Study

This chapter introduces the case studied in this thesis. The structure, its purpose, material and location is presented as well as available loads and a brief explanation of the methodology of the previously conducted hydrodynamic analysis.

#### 3.1 General

The case studied in this thesis regards the structural evaluation of external piping on a deep-draft semi-submersible production platform designed for operation in the Gulf of Mexico. External piping is used for oil and gas production as well as for ballast, sea water and fire water. To protect the piping and its associated equipment, such as pumps, they are often enclosed in caissons. Several pipes can be placed in each caisson, which will then serve as protection against environmental loads.

More particularly, this case deals with the fatigue assessment of a set of sea water caissons and its supporting structure. The studied caissons are located on one of the four columns as can be seen in Figures 3.1 and 3.2. The fifth support from the pontoon is situated closest above the still water line and was therefore selected for the study.

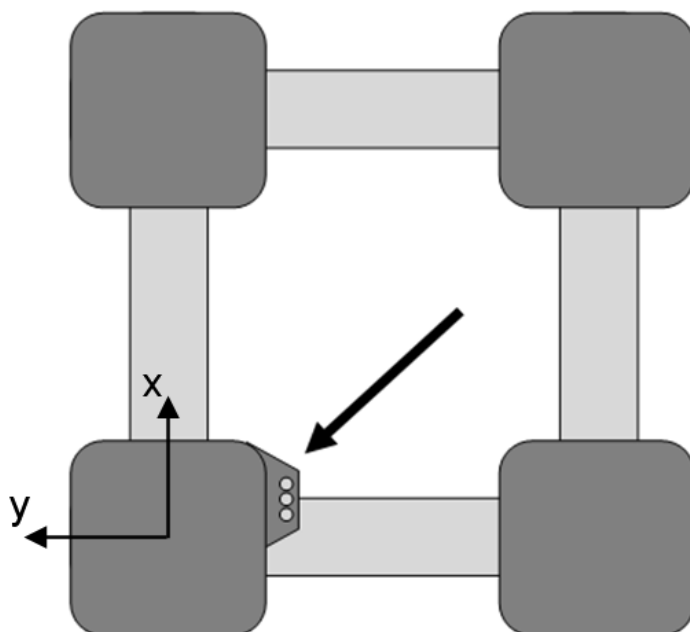


*Figure 3.1 Overview of the platform's four columns seen from above with position of sea water caissons and support indicated with an arrow. (Not to scale.)*



*Figure 3.2 Platform column viewed from pontoon deck. Studied support indicated with an arrow.*

## 3.2 Input Data

This section presents the input data needed for the numerical analyses presented in Section 1.3.

### 3.2.1 Structure

The caissons extend from the pontoon deck to the deck box with a total length of approximately 49 metres. The diameter of each caisson is 940 mm and they are supported by six identical supports along the column, as can be seen in Figure 3.2.

Drawings of the studied platform were used for designing the geometry model of the studied support and column. The material of column and support structure is a structural steel with a yield limit of 355 MPa - caissons are constructed in stainless steel with a yield limit of 500 MPa. Both materials have a Young's modulus of 206 GPa and a Poisson's ratio of 0.3. More information about dimensions and material parameters can be found in Appendix C.

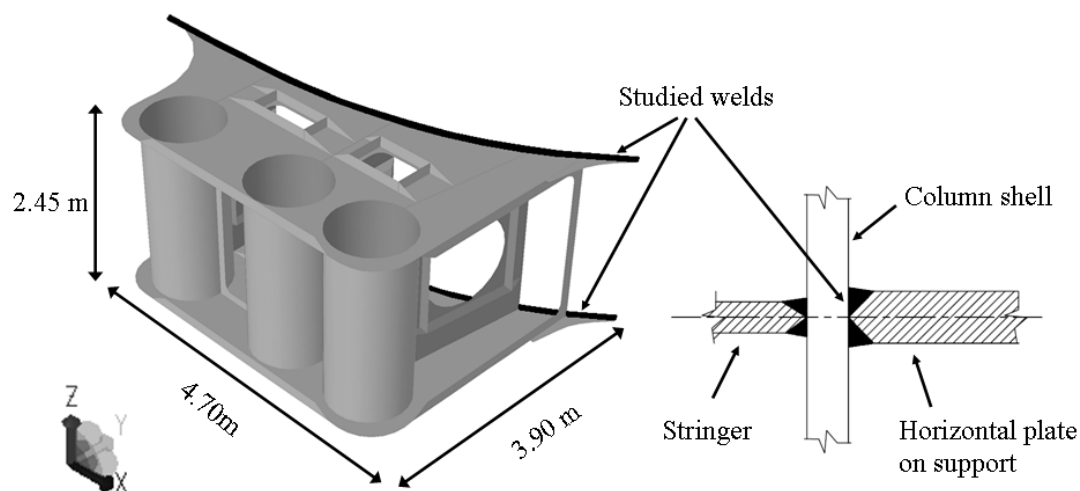


*Figure 3.3 Left: Sea water caissons support the model based on drawings. Roughly estimated dimensions and the studied weld are indicated. Right: Drawing of the connection between platform column and support.*

The support consists of a horizontal and vertical plate structure as well as three guiding-pipes for the caissons. The caissons and the supports have a sliding connection in the vertical direction. Cut-outs have been made in both the horizontal and vertical structure in order to decrease the loads acting on the structure when water flows around the support. The studied weld is a full-penetration fillet weld located in the connection between the horizontal plates of the support and the column shell. Roughly estimated dimensions of the support and the studied weld can be seen in Figure 3.3.

### 3.2.2 Environment

Wave statistics for the location of the platform have been available in form of scatter diagrams. Scatter data for eight different wave headings as well as a condensed scatter diagram describing all headings combined were available. The condensed scatter diagram has also been available for two different weather conditions; tropical and non-tropical. It is expected that the platform will be subjected to tropical weather, i.e. hurricane conditions during 3.4 % of the time. The wave headings relation to the studied support can be seen in Figure 3.4.

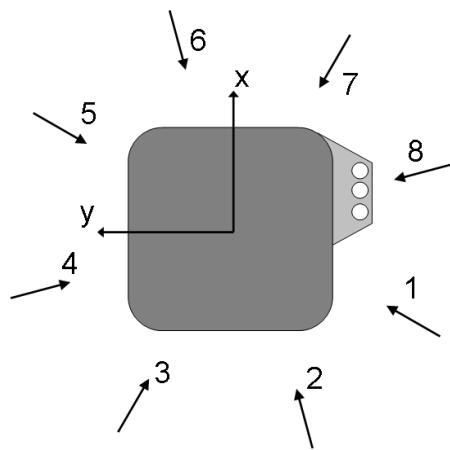


Figure 3.4 Loads and environmental data available are divided over eight wave headings. Heading 1 is in its positive direction rotated 13 degrees clockwise from the y-axis, with the subsequent seven headings spread 45° apart.

### 3.2.3 Loads

The support is exposed to both reaction forces from the caissons as well as Morison and slamming loads acting directly on the plate structure. Because of shielding effects from the platform columns, the velocities, accelerations and subsequent loads are heading-dependent.

A 10-year winter storm condition has been used as load input data. This is one of the conditions used for the global analysis and considered as the maximum operating condition. The winter storm data consists of distributed loads along the caissons, as well as the minimum and maximum relative velocities and accelerations at the location of the support for the eight wave headings.

All loads, velocities and accelerations are taken from a previously conducted hydrodynamic analysis of the platform carried out at GVA Consultants, GVA Consultants (2010) and GVA Consultants (2011b). The analysis is described briefly with respect to the methods and software used:

The hydrodynamic analysis was performed using environmental data from the Gulf of Mexico. A motion analysis was conducted using a panel model representing the platform on a global scale with no details included, such as appendages. The analysis was conducted using quasi-static coupling with damping and mass associated to the mooring system and risers were derived from linearization. Calculations were conducted both in the time and frequency domains, in accordance with DNV RP, Det Norske Veritas (2010a). Several different environmental conditions were considered, among them the 10-year winter storm which was specified by: wind speed, significant wave height, average peak crossing period and average current speed for five different depths. By applying the 10-year winter storm condition in different wave headings, the maximum relative velocities and accelerations at locations along the platform column could be estimated. These relative velocities and accelerations were then used as input for load calculations using the Morrison equations. The outputs of the load analysis were the maximum distributed Morrison loads along the position of the external piping spanning vertically along the platform columns during the 10-year winter storm.

Several software's included in the DNV software package SESAM were used in the load analysis. PREFEM (V.D7.1-05), Det Norske Veritas (2003) was used for creating the panel model, WADAM (V.8.1-05), Det Norske Veritas (2010c), which is a hydrodynamic panel program for the analysis of wave loads and motion responses, were used for conducting the motion analysis. In addition to WADAM, SIMO (V.3.6.6), Marintek (2007), and DEEPC (V.4.0), Det Norske Veritas (2010d), which calculates low-frequency responses in the time and frequency domains, respectively, were used. The distributed loads along the location of the external piping were conducted using the GVA Consultants software MORISLOAD.



## 4 Important Factors in the Simplified Fatigue Method

This chapter highlights and discusses factors that influence the simplified fatigue method. Identified challenges in applying the simplified fatigue method on the specific case study are presented.

In order to evaluate these factors and challenges individually, different methods for applying the simplified fatigue method on the case study have been developed. The four different methods are presented in Section 4.2.

### 4.1 Main Factors

The simplified fatigue method is described by three main factors:

- Shape parameter
- Reference stress range
- Fatigue resistance, governed by weld class

These factors are described in relationship to how they have been discussed in the current study.

#### 4.1.1 Shape Parameter

The shape parameter,  $\gamma$ , can have a significant influence on the result, Det Norske Veritas (2011a). In this thesis, the shape parameter was derived from the distribution of wave heights. The most straightforward way of determining the shape parameter is then to fit a Weibull distribution to the total wave height distribution. However, during the course of the project it was revealed that a satisfactory Weibull fit was hard to obtain for this condensed wave height distribution. The platform is designed for operation in the Gulf of Mexico, which is an area with an atypical wave climate compared to other areas such as the North Sea. In the North Sea severe storms occur frequently, which means that they can be described as a part of the general wave climate and thus will be quite constant over a larger time period. This is not the case for the Gulf of Mexico, where the only severe storms are hurricanes that occur infrequently for any given location, Nolte and Hansford (1977). As mentioned in Chapter 3, the area where the platform is moored is assumed to be affected by tropical weather during 3.4 % of the time. The two weather conditions vary from each other in such a way that they contribute to the problem of finding a satisfactory statistical fit. Similarly to how the two different weather conditions affect the wave height distribution, the location where the platform is moored is subjected to different wave climates dependent on wave heading. By partitioning the wave statistics for specific weather conditions or wave headings separately, more Weibull-like distributions of wave heights were obtained. The problems related to the fit still persisted to some

degree resulting in that a satisfactory fit could only be obtained for wave heights of either a high or low magnitude. The different ways of determining the shape parameter presented above could be used for determining the influence of this factor in two aspects. On the one hand, the influence of varying values of the shape parameter regardless of how the distributions were partitioned. On the other hand, how the partitioning of the distribution itself influences the calculated fatigue damage.

#### **4.1.2 Reference Stress Range**

The reference stress range depends on hydrodynamic loads and the flow in the proximity of the studied support. The relative velocities and accelerations of the fluid particles together with hydrodynamic coefficients determine the applied loads through Morison and slamming equations. The hydrodynamic panel model used for deriving the particle motions does not account for local wave-column interactions, GVA Consultants (2010) and GVA Consultants (2011b). Wave run-up and boundary layer effects were not considered. This may have caused the velocities and accelerations to be underestimated, especially in the vertical direction. However, it is hard to evaluate this further without the use of Computational Fluid Dynamics (CFD) software in which the flow close to the column could be analysed in detail. Another factor that could influence the reference stress range is dynamic response. Dynamic amplification could increase the magnitude of the reference stress range. Also, dynamic effects such as springing and whipping would increase the number of cycles contributing to the fatigue damage. The methods used in this thesis do not account for any dynamic effects. However, the possible consequences of a higher load magnitude was still of interest.

Effects from increasing the reference stress ranges were investigated by assuming a factor to multiply to the applied vertical load. The corresponding influence on the calculated damage could then be evaluated.

##### **4.1.2.1 Partitioning of the Stress Ranges Distribution**

The column will introduce shielding effects that reduce the load from waves in certain directions compared to others. Thus the wave load, and, in extension, the stresses are dependent on wave heading. The reference stress range will govern the distribution in the sense that all other stress ranges will effectively be similar to the reference, except for magnitude. If the simplified fatigue method is based on the condensed wave height distribution of all headings, all waves are accounted for with one reference stress range. This is as if they are propagating in the worst wave heading, i.e. the wave heading resulting in the highest stress range. This result in a conservative estimate, i.e. the fatigue damage is overestimated. This is alleviated to some extent by the partitioning of the wave height distribution. Since the maximum loads during the 10-year winter storm are available for eight wave headings, a more accurate description of the reference stress range could be obtained for the partitioned distributions.

#### 4.1.2.2 Passage of the Load Cycle

Loads acting on the structure can be divided into two contributions; impact loads, i.e. slamming, and Morison loads including drag, added mass and inertia loads. In the simplified fatigue method, the greatest obtained stress during a chosen number of cycles has to be determined. The maximum Morison force is assumed to occur when the wave crest passes the caissons, and at that point of time there should be no slamming loads. A possible impact load, i.e. slamming, is assumed to occur prior to the maximum Morison load even though some Morison loads will act simultaneously. If the slamming and Morison loads are assumed to not coincide, two stress ranges for every wave cycle can be added into the simplified fatigue expression. For the case where slamming occurs at the same time as a part of Morison force, it is more complicated. In order to investigate the total stress range during the slam event, the magnitude of the Morison load together with its extension along the caissons at the time of the slamming event had to be determined. Since limited load data was available, the cycles were dealt with separately and assumed to not coincide in time.

Waves with a wave height over 3 metres were assumed to reach the support and thus induce slamming. This then results in two stress ranges for every wave cycle instead of one. This could be handled in two ways: By using one distribution with the corresponding extra number of cycles added, the correct number of cycles could be represented. However, all cycles are governed by one reference stress range, i.e. the greater of either the impact or Morison stress range. The other option was to use two separate distributions with different reference stress ranges to represent the Morrison and impact stress ranges separately. The distribution, which was used for presenting the impact stress ranges could be accounted for in the simplified fatigue expression only for the part corresponding to waves of a wave height over 3 metres.

#### 4.1.3 Fatigue Resistance

The fatigue resistance is determined from S-N data, which, in turn, is dependent on weld class. S-N data presented in DNV RP corresponds to fatigue damage in the form of a fatigue crack along the weld, Det Norske Veritas (2011a). Fatigue crack growth is considered to be governed by maximum principal stress. If the principal stress direction is sufficiently different from the normal of the weld, the fatigue crack might no longer initiate along the weld. The notch at the weld toe will then no longer significantly influences the fatigue capacity and this S-N data will overestimate the fatigue damage, Det Norske Veritas (2011a). This is dealt with by using a different S-N curve.

Since stresses were derived using the hot-spot method the fatigue resistance is determined by an S-N curve of weld class D, or alternatively C2 depending on the principal stress direction in relation to the studied weld, Det Norske Veritas (2011a), see Figure 4.1.

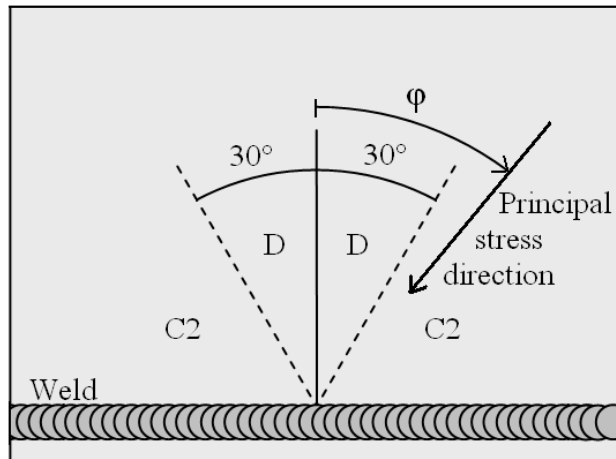


Figure 4.1 Weld class to be used in combination with the hot-spot method depending on principle stress direction in relation to the studied weld, according to DNV RP, Det Norske Veritas (2011a).

Since the reference stress range determines the whole stress-range distribution all stress ranges are dealt with as if they result in a principal stress direction identical to that of the reference. In order to determine the importance of this factor, two different weld classes were used, denoted D and C2 in DNV RP, Det Norske Veritas (2011a). The S-N data presented in ABS RP is very similar, American Bureau of Shipping (2010).

## 4.2 Alternatives in Methodology

This section describes how the challenges presented in the previous section were handled. Alternatives in methodology for applying the simplified fatigue method were devised in order to investigate the influence of the presented factors and challenges.

### 1. Nominal method (Nominal)

The simplified fatigue method applied for one stress range distribution. The condensed wave statistics were used for determining the shape parameter. The maximum stress range was used as the reference stress range and thus had to represent both impact and Morison loads for waves of all wave heights.

Applied as a reference method with the least complexity possible, according to rule requirements.

### 2. Morison and impact separated method (Separated)

The simplified fatigue method applied for two stress range distributions. The condensed wave statistics were used for determining the shape parameter. Two reference stress ranges were used. The maximum Morison stress range and the maximum slamming stress range. By dividing the stress-range distribution,

one distribution could be used to account for Morison loads and the other to account for impact loads.

Applied in order to investigate the influence of treating Morison and impact loads individually compared to the reference method.

### 3. Directional Morison method (Directional)

Partitioned simplified fatigue method applied for Morison stress ranges with partial damage from each heading. Eight different stress-range distributions were used, determined from the individual wave statistics of each heading. Resulting in eight shape parameters.

Different wave headings result in the maximum stress occurring at different locations along the studied weld. The damage were therefore determined at eight different hotspots along the weld and summed for each location.

Applied in order to investigate whether the more accurate estimations of the stress-range distributions resulted in a significant difference of calculated fatigue damage.

### 4. Weather conditional method (Weather)

Simplified fatigue method applied for tropical and non-tropical weather conditions and corresponding distributions. Resulting in two shape parameters.

Similar to the division of individual wave headings. Applied in order to investigate the difference in results from partitioned contributions from tropical and non-tropical weather.

The above methods all have advantages and drawbacks compared to each other, which is presented in Table 4.1.

Table 4.1 Pros and cons between the four methods.

Method:	Pros	Cons
(1) Nominal	<ul style="list-style-type: none"> <li>• Simple.</li> <li>• Only one location in the weld is considered (1 hotspot to evaluate).</li> <li>• Only one Weibull-fit is conducted. (One shape parameter and one scale parameter).</li> </ul>	<ul style="list-style-type: none"> <li>• Hard to obtain a satisfactory fit between the Weibull distribution and the wave distribution.</li> <li>• All loads are applied in the same way as the reference load cycle except for magnitude.</li> <li>• The location of maximum fatigue damage along the weld is uncertain.</li> </ul>
(2) Separated	<ul style="list-style-type: none"> <li>• Relatively simple.</li> <li>• Two locations in the weld are considered.</li> <li>• Only one Weibull-fit is conducted. (One shape parameter and two scale parameters).</li> <li>• Allows for Morison loads and impact loads to be applied differently from each other.</li> </ul>	<ul style="list-style-type: none"> <li>• Even if there is a distinction between impact and Morison loads, all Morison loads are identical except for magnitude. The same holds for impact loads, but since it is one-dimensional it has less significance.</li> <li>• Hard to obtain a satisfactory fit between the Weibull distribution and the wave distribution.</li> <li>• The location of maximum fatigue damage along the weld is uncertain.</li> </ul>
<i>Continued on next page.</i>		

<p>(3) Directional*</p>	<ul style="list-style-type: none"> <li>• A better fit is obtained, as the wave distributions of the individual wave headings are more Weibull-like than the condensed wave distribution.</li> <li>• Greater certainty with respect to where the highest damage in the weld is obtained.</li> <li>• Allows for greater difference in how loads are applied.</li> </ul>	<ul style="list-style-type: none"> <li>• 8 individual fits need to be done.</li> <li>• 8 locations along the weld need to be evaluated.</li> <li>• All loads within one heading are still applied identically except for magnitude.</li> <li>• The method is more time-consuming, which is not a problem when only one weld is considered but for an analysis including the whole structure it might be of significance.</li> </ul>
<p>(4) Weather*</p>	<ul style="list-style-type: none"> <li>• Relatively simple.</li> <li>• Better fit compared to the nominal method.</li> <li>• Relatively few fits need to be conducted. (Two shape parameters and two scale parameters)</li> <li>• Only one location in the weld is considered.</li> </ul>	<ul style="list-style-type: none"> <li>• The location of maximum fatigue damage along the weld is uncertain.</li> <li>• All loads within one type of weather are applied identically except for magnitude.</li> </ul>

\* Both methods are conducted only for Morison loads. Impact loads can be added similar to the *Separated* method but with information added about wave heading and/or weather. Theoretically, both methods can be combined to account for both wave heading and weather, given that input data is available.



## 5 Load Analysis

This chapter presents how loads acting on the structure have been calculated based on the relative water particle velocities and accelerations. Distributed loads along on the caissons were considered as input data for this thesis, as they have previously been calculated using the GVA Consultants software MORISLOAD, GVA Consultants (2011b). Equations used with this software are, however, presented in Section 5.1. Slamming and Morison loads acting on the support were calculated directly from the relative velocities and accelerations. Equations used for load calculations as well as the estimation of coefficients for added mass, drag and slamming are presented in Section 5.2.

### 5.1 Loads on Caissons

Loads along the caissons were needed in the analysis as the load is carried to the supports via reaction forces. The distributed loads vary along the caisson length. They were calculated for eight different headings as defined in Figure 3.4 and available as x- and y-components for both positive and negative lift coefficients. An example can be seen in Figure 5.1, and the remaining loads can be found in Appendix B.

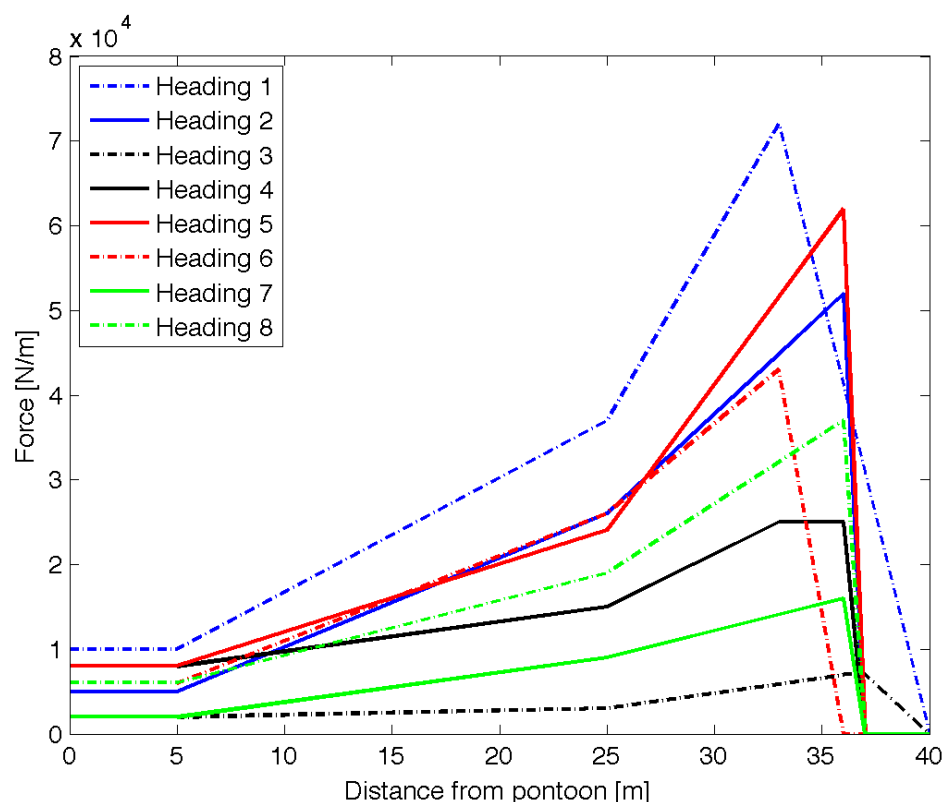


Figure 5.1 Example of distributed load along caissons for different headings. Loads in the x-direction for a positive lift coefficient are shown.

The loads were calculated using Morison's load formula for slender structural members given in DNV RP, Det Norske Veritas (2010a). The formula is applicable when the following conditions are satisfied:

$$\lambda > 5D \quad (5.1)$$

where  $\lambda$  is the wave length and  $D$  the diameter of the member. The length of the member also needs to be much larger than the transverse dimensions:

$$L \gg D \quad (5.2)$$

The resulting force per unit length acting on a cylinder in a fluid flow around a cylinder can be decomposed to; normal force,  $f_N$ , tangential force,  $f_T$ , and a lift force,  $f_L$ , Det Norske Veritas (2010a), see Figure 5.2.

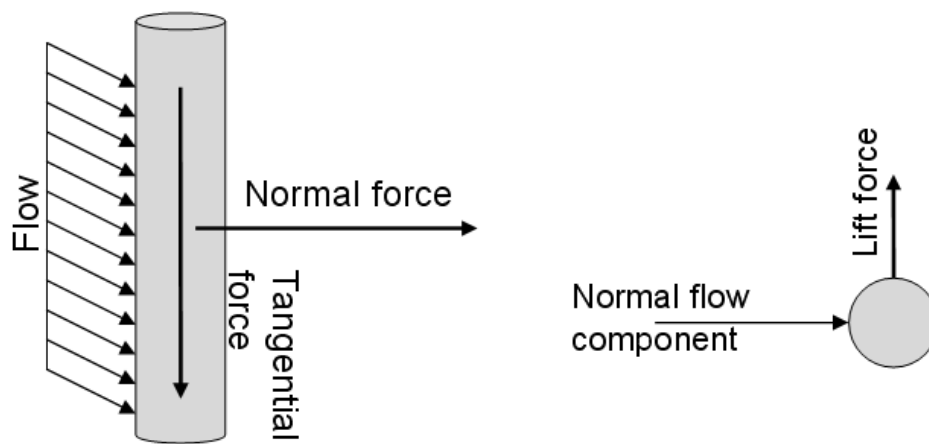


Figure 5.2 Morrison force components.

Since no vertical force is transferred from the caissons to the supports, due to the sliding connection, the tangential force was omitted. Only velocity components in the x- and y-directions were needed.

The forces were calculated for sections along the length of the cylinder in order to obtain the distributed load.

$$f_N = \rho(1 + C_A)A\dot{v} + \frac{1}{2}\rho C_D D_c v^2 \text{ N/m} \quad (5.3)$$

$$f_L = \frac{1}{2}C_L \rho D_c v^2 \text{ N/m} \quad (5.4)$$

Because of the cross section of the caissons, the lift force oscillates with time due to vortex shedding, Bishop and Hassan (1964). The direction of the lift force is thus unknown for any given time. When determining the reference stress range to be used in the simplified fatigue expression, the maximum magnitudes for both directions were evaluated.

## 5.2 Loads on Support

The sea water caisson supports are exposed to hydrodynamic loads as well as reaction forces from the caissons. Wave loads acting directly on the support can be divided into two contributions; slamming loads and Morison forces. Equations used for deriving these forces from relative water particle velocities and accelerations are presented in this section.

### 5.2.1 Morison Forces

To estimate the forces a Morison formulation for fluid flow around small-volume 3D objects was used. The formulation is described in DNV RP and applicable when the characteristic dimensions of the subjected member is small in relation to the wave length, Det Norske Veritas (2010a).

$$f_D = \rho V(1 + C_A)\dot{v} + \frac{1}{2} \rho C_D A_P v^2 \text{ N} \quad (5.5)$$

Because of the geometry of the support, its proximity to the wall and interactions between the different parts of the support, the loads were hard to estimate and would need to be modelled using a CFD simulation to get a more correct result. Since this thesis aimed at investigating the application of the simplified fatigue method, an exact prediction of the loads was not as important. The support was, instead, modelled as five rectangular plates, see Figure 5.3.

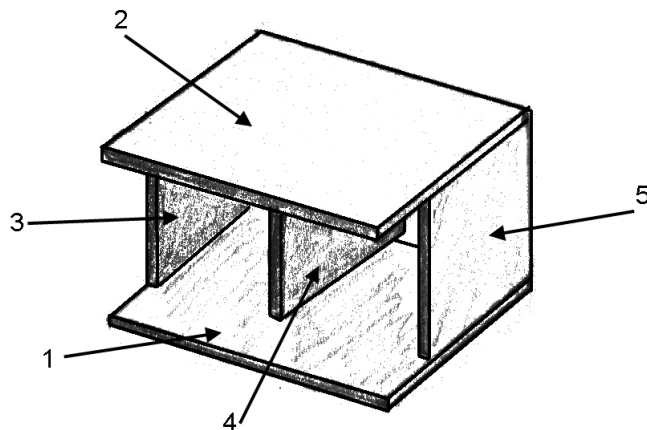


Figure 5.3 Simplified model of the support used to estimate coefficient for drag and added mass.

The reference volume of the thin plates, drag and added mass coefficients were taken from DNV RP, Det Norske Veritas (2010a), while the projected area was based on the geometry of the support, see Table 5.1.

Table 5.1 Properties of simplified support model.

Plate	Projected area, $A_p$ [m <sup>2</sup> ]	Added mass coefficient, $C_A$	Drag coefficient, $C_D$	Reference volume $V$ [m <sup>3</sup> ]
1	9.4	0.757	1.8	19.52
2	9.4	0.757	0.1	19.52
3	2	0.642	1.8	2
4	2	0.642	0.1	2
5	2	0.642	0	2

The vertical force was calculated using Plates 1 and 2 with vertical velocity and acceleration components. Horizontal force was calculated using Plates 3, 4 and 5 with horizontal velocity and acceleration components. Proximity to the column wall was not considered. The only interaction between the plates that were considered was a shielding effect included in the drag coefficient, corresponding to *Two thin plates in tandem* taken from DNV RP, Det Norske Veritas (2010a). The direction of the horizontal force applied according to the velocity components - for a negative velocity Plates 4 and 5 were considered loaded and for a positive velocity, Plates 3 and 4 were considered.

## 5.2.2 Slamming

Water impact loads on offshore structures have been of concern to designers for many years, Baarholm and Faltinsen (2004). A complete prediction of slamming phenomena is a complex task, which, in its entirety, is beyond the scope of any existing theory, Journée and Adegeest (2003). Wave slamming is caused when a structural part is being submerged, and wave slamming of a detail in the splash zone results in local effects, which does not usually result in a global response of the platform, Det Norske Veritas (2010a). The impact pressure is affected by the local geometry of the member, the relative velocity and angle (deadrise angle) between the water particles and the structure.

As mentioned above, the support under study consists of horizontal and vertical plate structures. It is located approximately two metres above the still water line, i.e. in the splash zone, which indicates that slamming loads will be a significant contributor to fatigue damage, Dalton and Nash (1976). Slamming loads are complicated loads with a very short time duration, which is often characterized by the peak pressure. The highest pressure during water entry of a wedge with a small deadrise angle is usually not relevant for steel structures, Det Norske Veritas (2010a). Instead, a closed-form solution, Wagner (1932), for water entry of a wedge was used for calculating the space average slamming pressure:

$$p_s = \frac{1}{2} \rho C_{pa} v^2 \text{ Pa} \quad (5.6)$$

The space average slamming pressure coefficient,  $C_{pa}$ , should be determined using recognized theoretical and/or experimental methods, Det Norske Veritas (2010a). For a flat bottom, when the deadrise angle is equal to zero the coefficient can be taken as  $2\pi$ , Det Norske Veritas (2010a).



## 6 Structural Response Analysis

In this chapter, method and models used for calculating the stress response resulting from the environmental loads is presented. Two FE-models were used for calculating the stresses in the studied welds. A beam model was used for evaluating the reaction forces on the caisson supports due to hydrodynamic loads acting along the caissons. The reaction forces from the beam model were then used together with the remaining loads acting on the support in a detailed FE-model of the caissons support connected to the column. The principal stresses in the studied weld were then determined using the hot-spot method.

### 6.1 Beam FE-model

The beam model was used for identifying the most critical supports along the caissons and for calculating the reaction forces and moments at each support. The DNV software NAUTICUS 3D BEAM (V.10.51.34.4522), Det Norske Veritas (2008), which is a tool for linear static analysis of 2D and 3D frame structures, was used for this analysis. The caissons were modelled as continuous beams extending from the pontoon deck to the deck box, which can be seen in Figure 6.2.

#### 6.1.1 Boundary Conditions

The caissons were considered rigidly fixed in all directions at both ends, i.e. at the pontoon deck and deck box. Global displacements of the hull will cause deflection of the members where the caissons are attached. A sliding connection in the z-direction between the caisson and its supports will allow the deck box to move without transferring any loads to the supports through the caissons. The extension of the supports in the vertical direction along the caisson has not been modelled. Instead, the boundary conditions have been set in the middle of each support, see Figure 6.1.

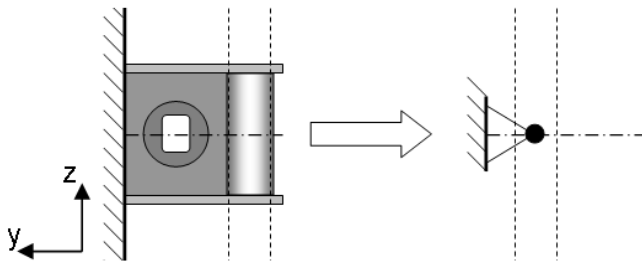


Figure 6.1 Approximation of support in the beam model.

This was considered a conservative simplification since the elastic length of the beam is increased, which will result in greater reaction moments. Two different boundary conditions, rigidly fixed and simply supported, were used for the supports in order to obtain the reaction forces and moments. The supports were considered rigidly fixed to

obtain the reaction moments, and the reaction forces were obtained by choosing the most conservative forces to apply to the 3D FE-model out of the results from both boundary conditions. More information about the beam model and the boundary conditions can be found in Appendix C.

### 6.1.2 Load Application

Forces were applied as distributed loads along the z-axis, both in the x- and y-directions, as can be seen in Figure 6.2. All applied loads can be found in Appendix B.

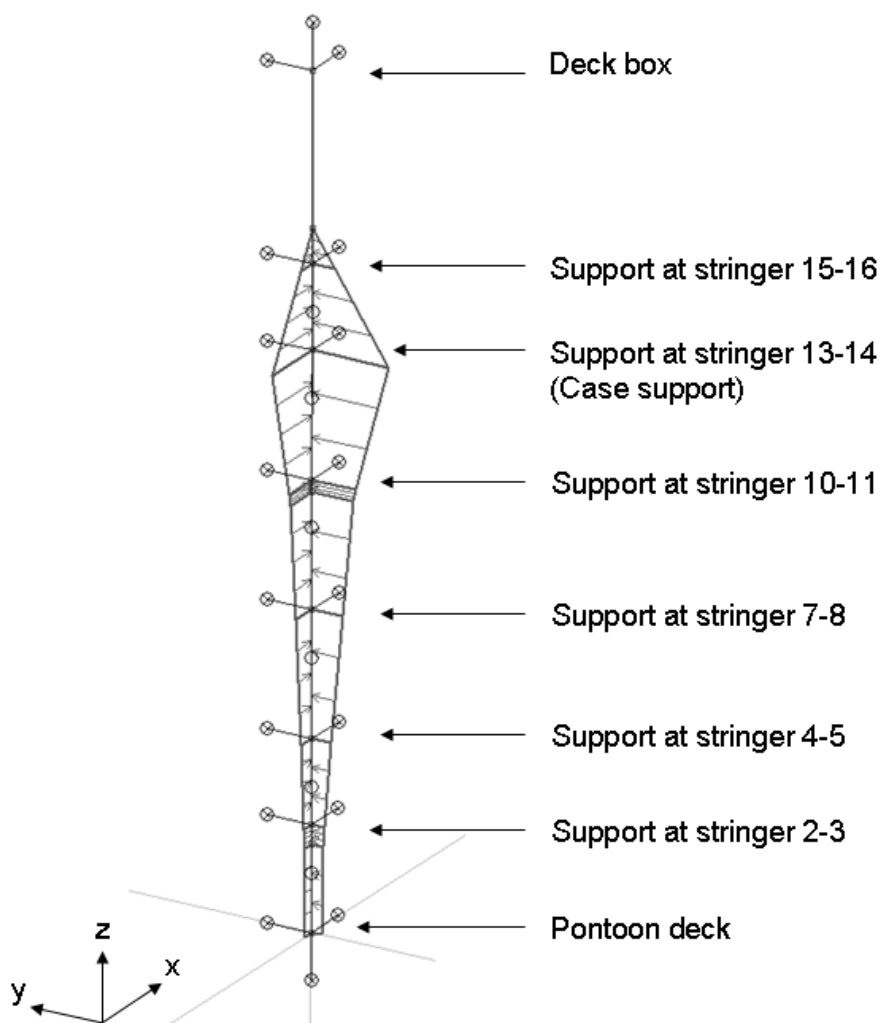


Figure 6.2 *Beam model from NAUTICUS 3D BEAM with applied distributed loads in both the x- and y-directions and boundary conditions at each support, denoted by their corresponding stringer planes.*

## 6.2 3D FE-model

The 3D FE-model was used for evaluating stresses in the area of the weld. Reaction forces from the beam model were applied together with the remaining loads acting directly on the support. The model was created in GENIE (V.5.1-11), Det Norske Veritas (2011b), which is a part of the DNV software package SESAM. The model spans over four stringer planes (12-15), see Figure 6.2, and includes approximately one third of the column cross section and the studied seawater caisson support, see Figure 6.3. The geometry and the dimensions of the model were based on drawings of the studied platform. Further information regarding the model can be found in Appendix C.

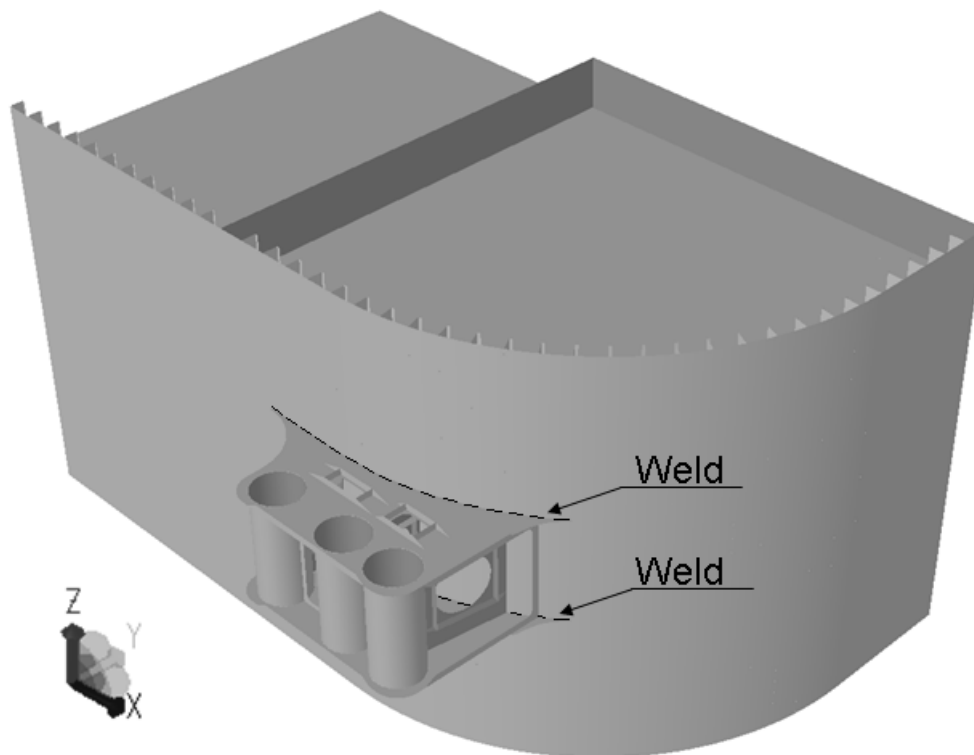


Figure 6.3 Geometry of a 3D FE-model, studied support and part of platform column.

### 6.2.1 Mesh

The FE-model was created using second-order elements. Plate fields were modelled with 8-node quadratic shell elements and the stiffeners were modelled using 3-node beam elements. Particulars of the element types used can be seen in Table 6.1. The hot-spot method requires a dense mesh in the weld region. An element size of  $t \times t$ , where  $t$  is the plate thickness at the weld, has been used in the weld area, which is recommended, Det Norske Veritas (2011a). The mesh size was then gradually increased to  $4t \times 4t$  on the support and approximately  $12t \times 12t$  on the column in order to shorten the computational time needed for running the model. The mesh density settings can be seen in Figure 6.4 and Appendix C. Resulting mesh in the weld

area can be seen in Figure 6.5. The length of the largest elements on the column is equal to half the stiffener spacing distance. The meshing tool was set to prefer quadratic elements, but where this was not possible triangular elements were used. Elements with odd geometry, skewed, taper-shaped or slender elements, were split in to triangular elements.

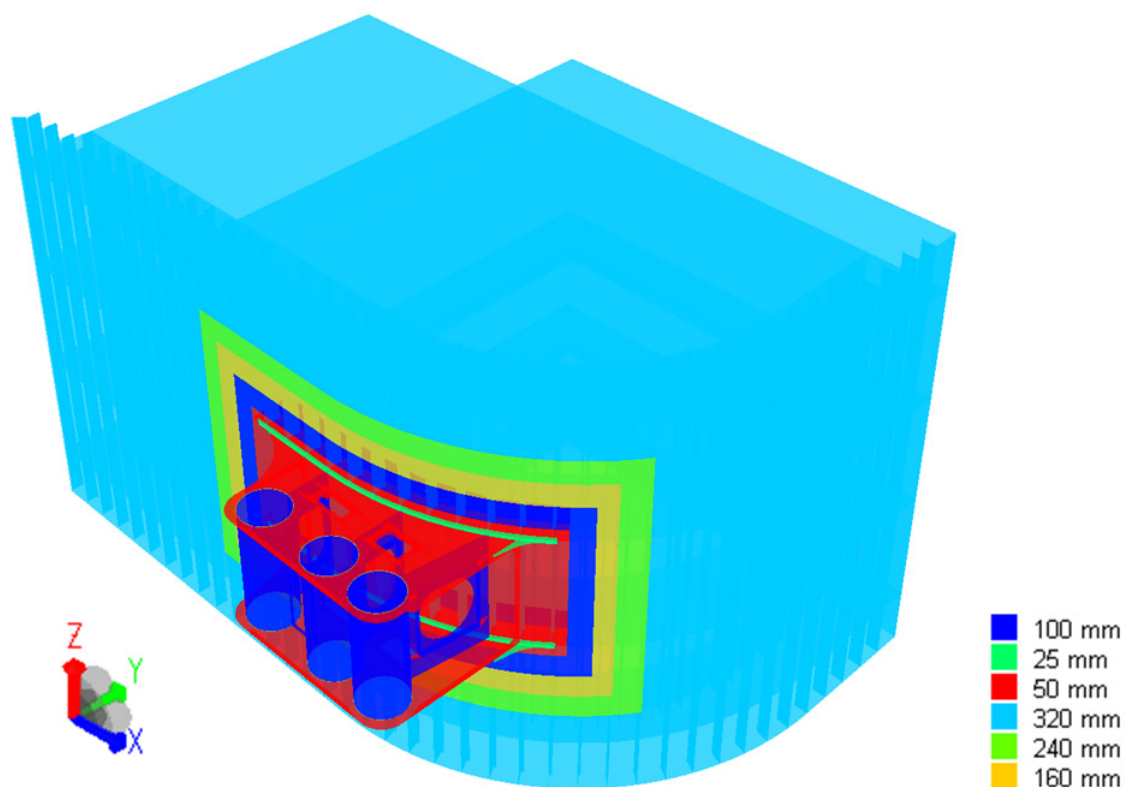


Figure 6.4 Mesh density settings used on the 3D FE-model. The mesh density is gradually decreased as the distance from the studied welds increases. The legend shows mesh density setting in terms of maximum element side length.

Table 6.1 Particulars of used element types.

Element name	Description	No. of nodes	No. of DOF/node	No. of Integration points	No. of elements
SCQS	Sub-parametric curved quadrilateral shell	8	6	8	50636
SCTS	Sub-parametric curved triangular shell	6	6	6	11549
BTSS	Curved beam	3	6	2	3716

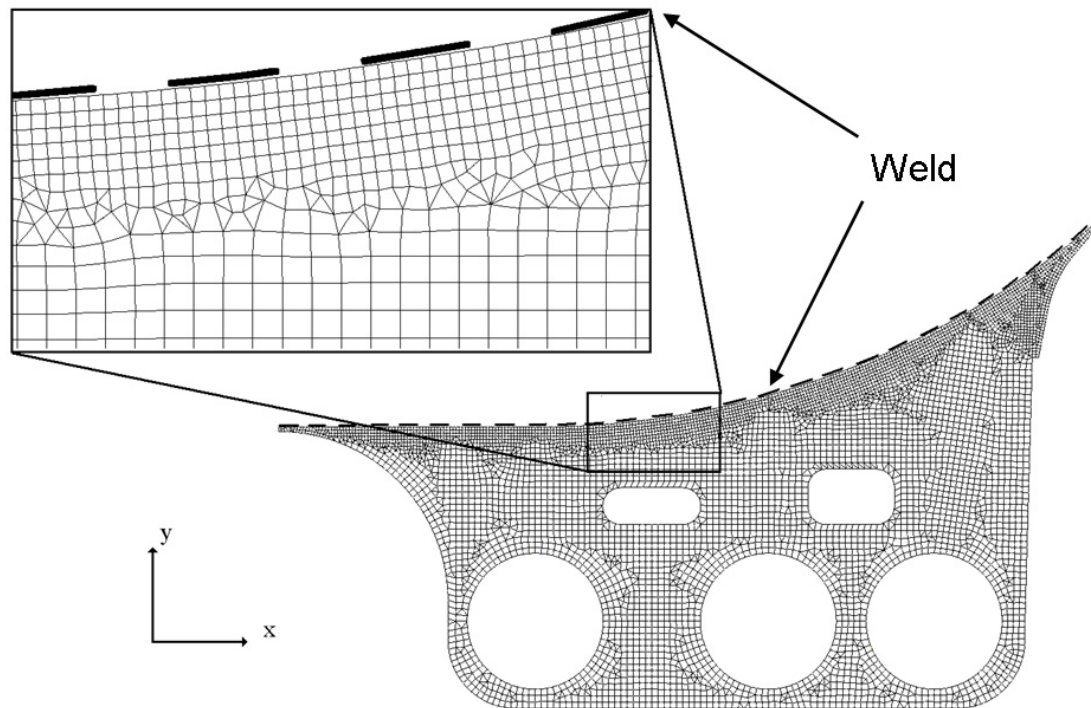


Figure 6.5 Resulting mesh in the weld area of the lower horizontal plate.

## 6.2.2 Boundary Conditions

Boundary conditions on the 3D FE-model was set on all free edges included in the model. Applied boundary conditions can be seen in Appendix C. Adjacent structures not included in the model were considered when applying the boundary conditions, for example intersections between bulkheads were considered to be rigidly fixed.

The extent of the local model has to be chosen in such a way that effects due to the boundaries on the structural detail considered are sufficiently small and reasonable boundary conditions can be formulated, Det Norske Veritas (2011a). This was verified by changing the boundary conditions on the edges of the outer and inner shell from rigidly fixed to allow rotation in all directions. The assumption was that stresses in the critical area would decrease with this change. The result from the reference calculations showed that stresses decreased with less than 1 %. It was then concluded that the effects of the boundary conditions on the results was sufficiently small.

## 6.2.3 Load Application

The reaction forces and moments were applied as distributed line loads at the upper and lower edges of the guiding pipes of the support. The x- and y-components were distributed over a quarter of the circumference as can be seen in Figure 6.6. By applying the reaction forces differently at the upper and lower plates, reaction moments could be represented.

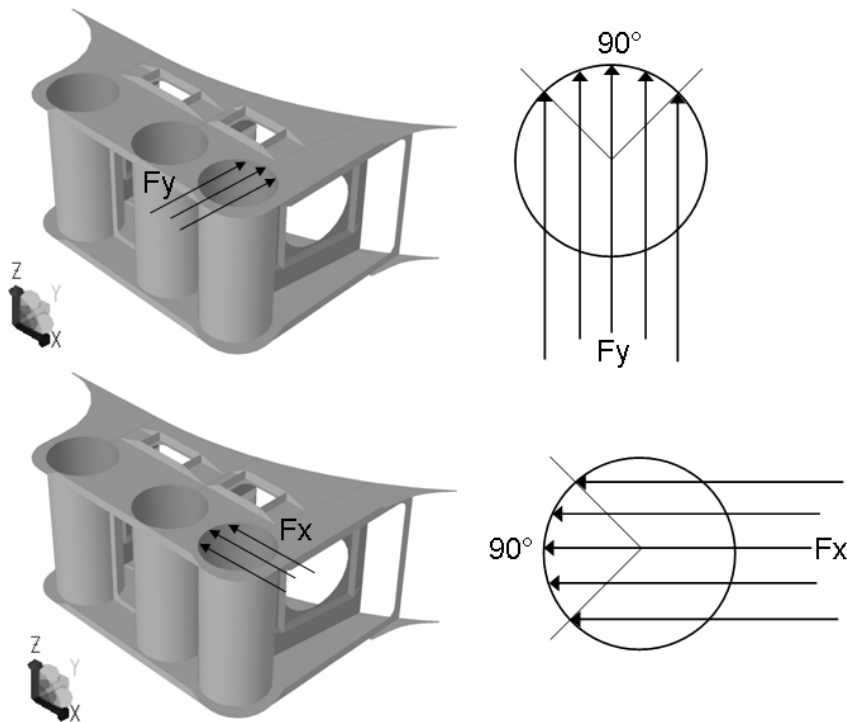


Figure 6.6 Load application of reaction force in the  $x$ - and  $y$ -directions. Note that the figure only shows the load applied at one of the 3 guiding pipes.

The loads acting directly on the support were applied as distributed surface loads. The drag forces have been determined for plates in tandem. It is assumed that shielding effects result in the pressure ratio between two plates being 1:18, Det Norske Veritas (2011a). So, for the horizontal plates only 1/18 of the pressure on the lower plate was applied on the upper plate, which can be seen in Figure 6.7. In the case of the vertical plates where there are three plates in tandem, it was assumed that the pressure on the third plate is negligible. The direction of pressure loads on the vertical plates is dependent on the wave direction. The slamming force was applied similarly to the vertical drag forces, but only on the lower plate - no other forces are applied simultaneously. All loads applied on the 3D FE-model can be seen in Appendix B.

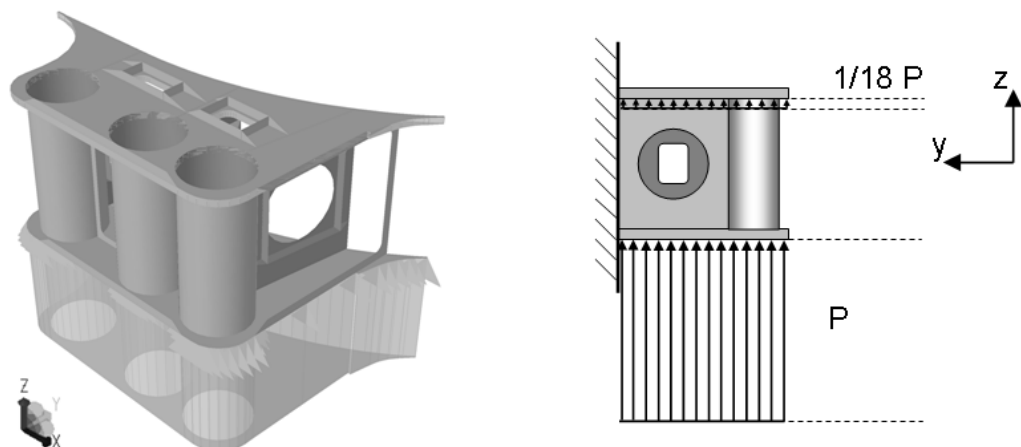


Figure 6.7 Application of vertical drag loads.

## 6.3 Local Stress Analysis

Due to local weld geometry and different types of imperfections welds are difficult to model in an FE-analysis, Det Norske Veritas (2011a). The influence of the weld, i.e. the weld geometry, residual stresses and the heat-affected zone is often more efficiently handled through use of an appropriate S-N curve, Det Norske Veritas (2011a).

### 6.3.1 The Hot-spot Method

The hot-spot method is a recognized method for calculation of the structural stress at the weld toe. The method only accounts for the geometry of the member, and the presence of the weld is then accounted for by a reduced S-N curve. The structural hot-spot stress approach is recommended for welded joints where there is no clearly defined nominal stress due to complicated geometric effects, and where the structural discontinuity is not comparable to a classified structural detail, IIW (2008). The hot-spot method is suitable for determining stresses at the weld toe. This was appropriate for the studied weld since it is a full penetration fillet weld at a cruciform joint. For such welds fatigue cracks normally start at the weld toe, Det Norske Veritas (2011a).

Hot-spot stresses were calculated assuming linear material behaviour and using an idealized structural model with no fabrication-related imperfections. The stress was calculated in the two read-out point;  $0.5t$  and  $1.5t$ , where  $t$  is the plate thickness at the hot-spot, see Figure 6.8. The principal stress at the hot-spot was derived from the linear extrapolated component values given as, Det Norske Veritas (2011a):

$$s_{HS} = \frac{1}{2}(s_{0.5t} - s_{1.5t}) + s_{0.5t} \quad (6.1)$$

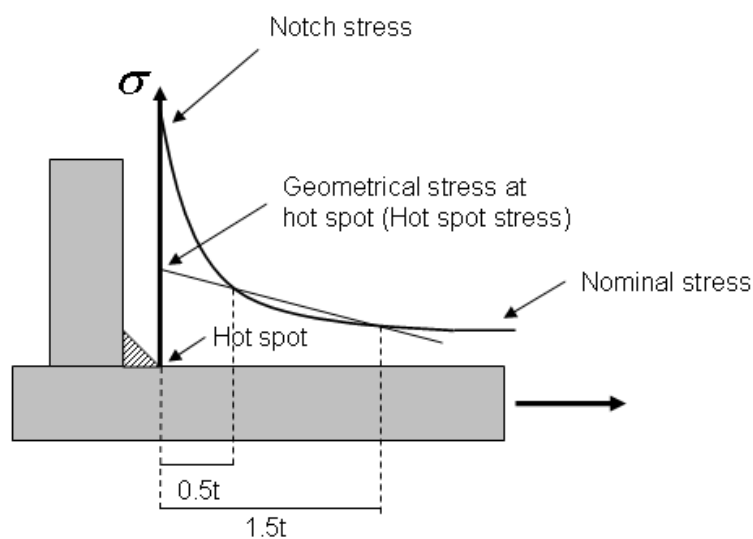


Figure 6.8 Visualisation of hot-spot stress compared to notch stress.

### 6.3.2 Stress Derivation

Stresses were derived for three different loading conditions in each wave heading. In one case for slamming loads and two for Morison loads, both positive and negative lift coefficients were considered. In the weld, the area with the maximum stress change depending on the load case and wave heading. Therefore, eight hot-spots were evaluated along the weld, which can be seen in Figure 6.9. The eight hot-spots correspond to locations where stiffeners are present on the opposite side of the column shell. Stresses were read out from the horizontal plate and the total damage was calculated for each hot-spot.

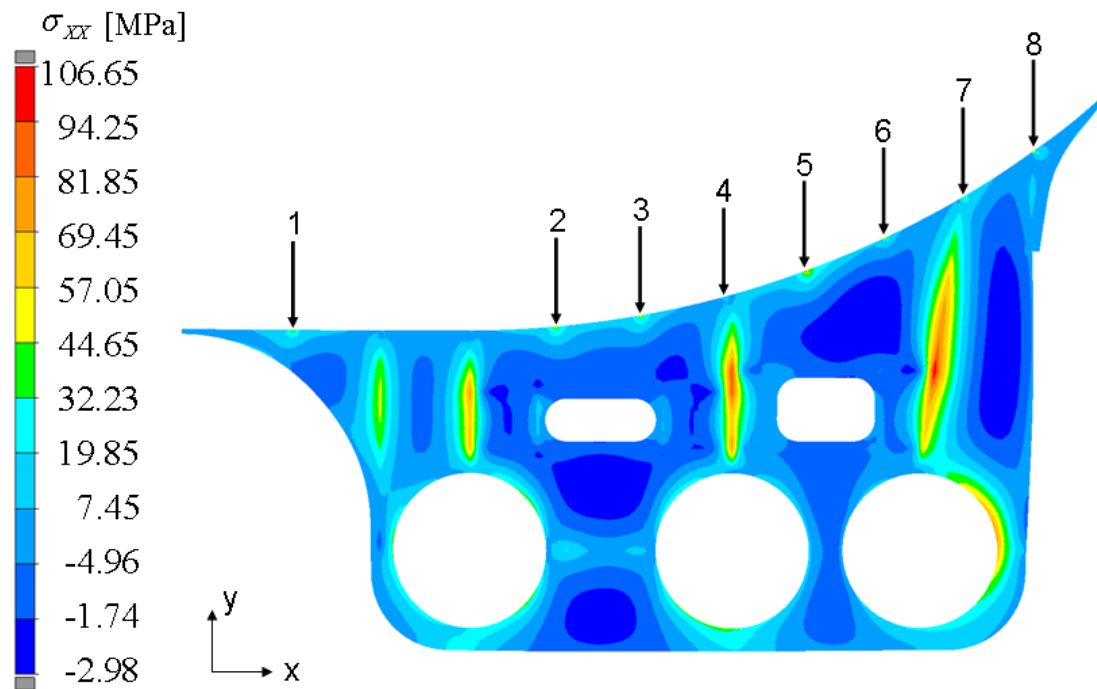


Figure 6.9 Evaluated hot-spots on the lower plate for one load case in one wave heading showing one stress component.

Obtained hot-spot stresses can be found in Appendix D.

## 7 Estimation of the Shape Parameter

This chapter presents the method used for deriving the shape parameter of the stress-range distribution. The shape parameter was derived based on the assumption of a linear relationship between wave height and stress range. According to ABS, this relationship exists for large floating column-stabilized offshore structures, American Bureau of Shipping (2010). As mentioned in Chapter 2, the result of this assumption was that the stress-range distribution and the wave height distribution have an equal shape parameter. Hence, the method used for estimating the long-term wave height distribution based on scatter diagrams with a measured significant wave height is presented. This distribution was then fitted to a Weibull model in order to obtain the shape parameter. Two estimates of the shape parameter were derived for each distribution. The particular procedure for each method mentioned in Chapter 4 is not presented - only the overall approach. All considered shape parameters and plots illustrating the fits for each of the methods presented in Chapter 4 can be seen in Appendix E.

### 7.1 Determining the Distributions of Waves

The estimation of the long-term distribution of wave heights,  $h$ , was based on scatter diagrams with measurements of the significant wave height,  $H_s$ . Each box of the scatter diagram represents the occurrence of a three-hour sea-state which is represented by a significant wave height and a peak crossing period. In order to estimate the distribution of wave height it was assumed that the short-term distribution of the wave height, i.e. within a sea-state, is Rayleigh-distributed, Holthuijsen (2007) and Det Norske Veritas (2010a). Sea-states with different periods but an equal significant wave height were condensed. The cumulative distribution function of the Rayleigh distribution is given as:

$$F(h) = P(H < h) = 1 - e^{\left(-\frac{h^2}{2\sigma^2}\right)} \quad (7.1)$$

with a significant wave height equal to 2 times the Rayleigh parameter, Holthuijsen (2007) and Det Norske Veritas (2010a):

$$F(h) = 1 - e^{\left(-2\left(\frac{h}{H_s}\right)^2\right)} \quad (7.2)$$

The probability density can be found by derivation:

$$f(h) = \frac{d}{dh} F(h) \quad (7.3)$$

An example of the short-term, Rayleigh, probability density can be seen in Figure 7.1.

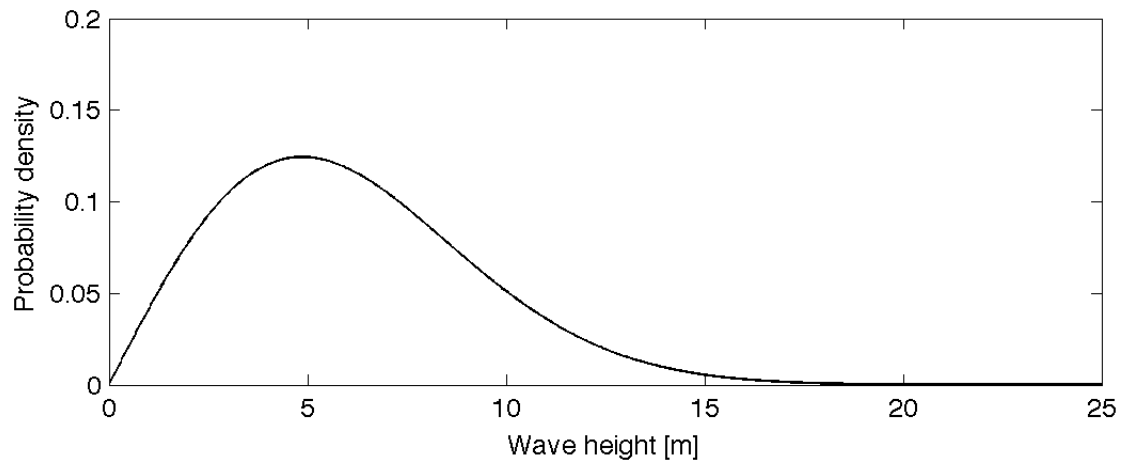


Figure 7.1 Example of a short-term probability density for the wave height in a sea-state with  $H_s=9.75$  m.

By using the probability of exceedance, Equation (7.2) was simplified to:

$$Q_{short-term}(h) = P(h > H) = e^{\left(-2 \cdot \left(\frac{h}{H_s}\right)^2\right)} \quad (7.4)$$

By summation of the short term individual sea-states, an estimation of the long-term distribution was obtained:

$$Q_{long-term}(h) = \sum_i f_{Sea-state_i} \cdot e^{\left(-2 \cdot \left(\frac{h}{H_{s,i}}\right)^2\right)} \quad (7.5)$$

where  $f_{Sea-state_i}$  is the relative frequency of the occurrence of the short-term sea-states with the significant wave height  $H_{s,i}$  compared to the occurrence of all sea-states.

An obtained probability density for the long-term distribution can be seen in Figure 7.2.

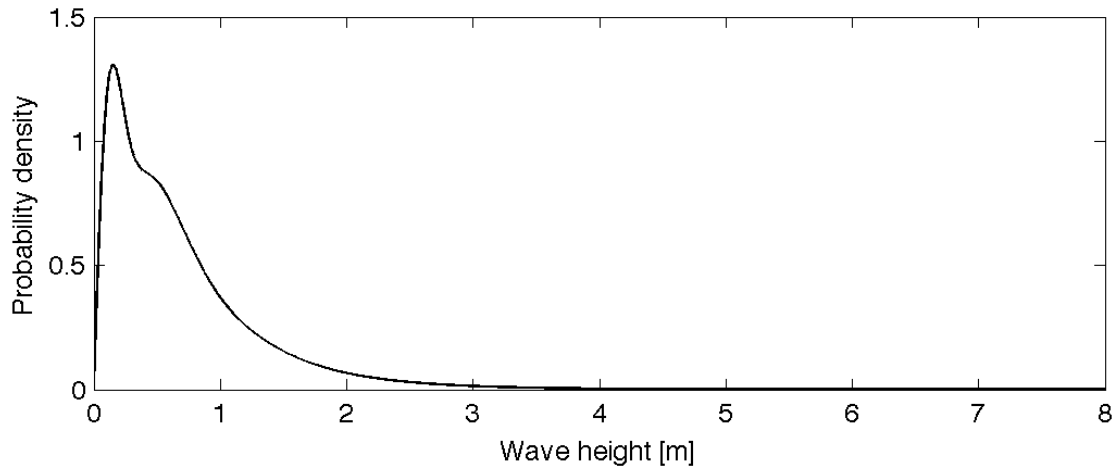


Figure 7.2 Example of long-term wave height distribution for all sea-states, obtained by summation of sea-states described as Rayleigh distributions.

## 7.2 Derivation of the Shape Parameter

The long-term wave height distribution obtained in the previous section was fitted to a Weibull model to obtain the shape parameter. Since it was not possible to obtain a satisfactory fit for both low and high wave heights simultaneously the fit was conducted twice.

In order to fit a Weibull distribution the exceedance probability was used.

$$Q_{Weibull}(h) = e^{-\left(\frac{h}{q}\right)^\gamma} \quad (7.6)$$

By minimizing the error between the calculated exceedance probability array and the Weibull exceedance probability the fit was obtained:

$$(q, \gamma) = \min\left(\left\| \left( \bar{Q}_{Weibull} - \bar{Q}_{long-term} \right) \cdot [1^p \ 2^p \ 3^p \ \dots \ n^p] \right\| \right) \quad (7.7)$$

An un-weighted fit where  $p = 0$ , resulted in a fit that represented low values of wave height rather well. However, this caused a difference in probability for higher wave heights, see Figure 7.3.

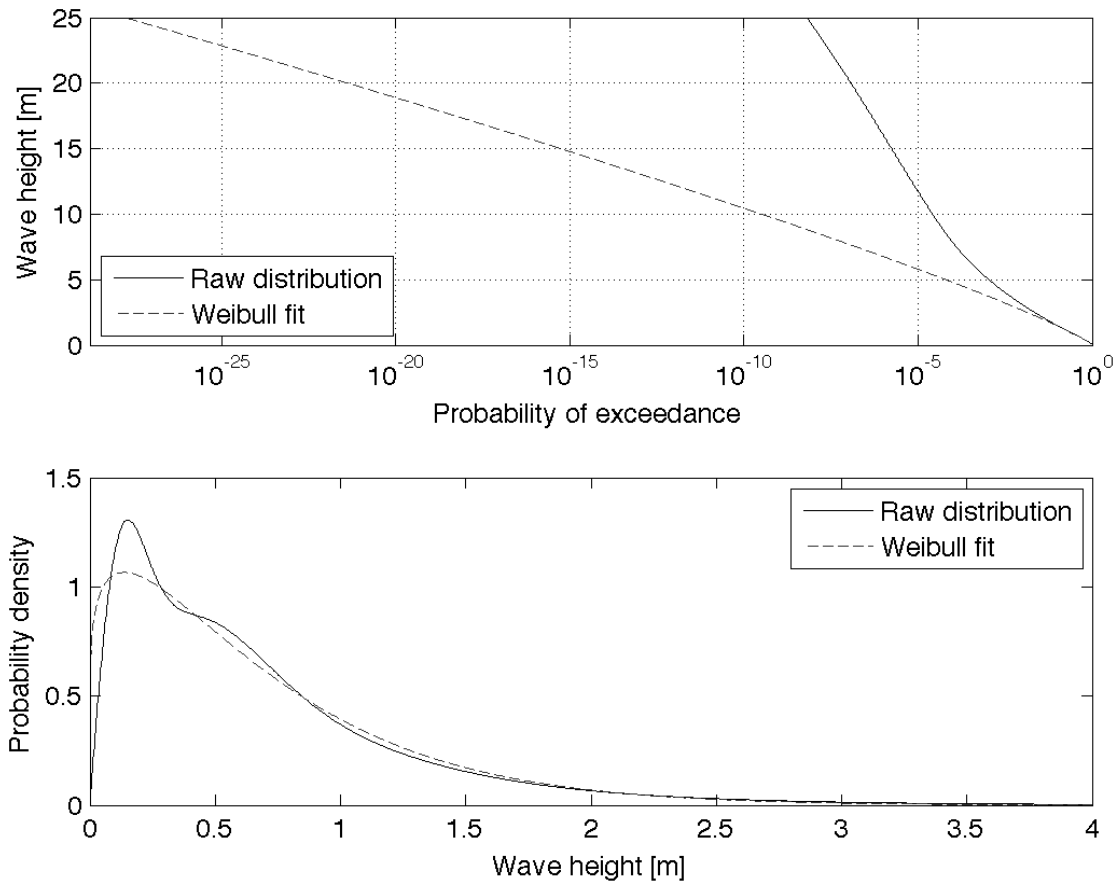


*Figure 7.3 Example of an un-weighted fit. Top: Probability of exceedance for all considered wave heights, a significant difference is seen for wave heights over 4 m. Bottom: Probability density for wave heights up to 4 m, the fit seems to follow the distribution fairly well except for the peak at  $h \sim 0.25$  m.*

As can be seen, there exists a substantial difference in probability for wave heights over  $\sim 4$  m. In order to obtain a fit that was representative of higher wave heights a weighting was used. The weighting exponent,  $p$ , was set to values in the range of  $5.5 < p < 7.5$ . This amplified the error between probabilities for high wave heights. The alternative fit can be seen in Figure 7.4.

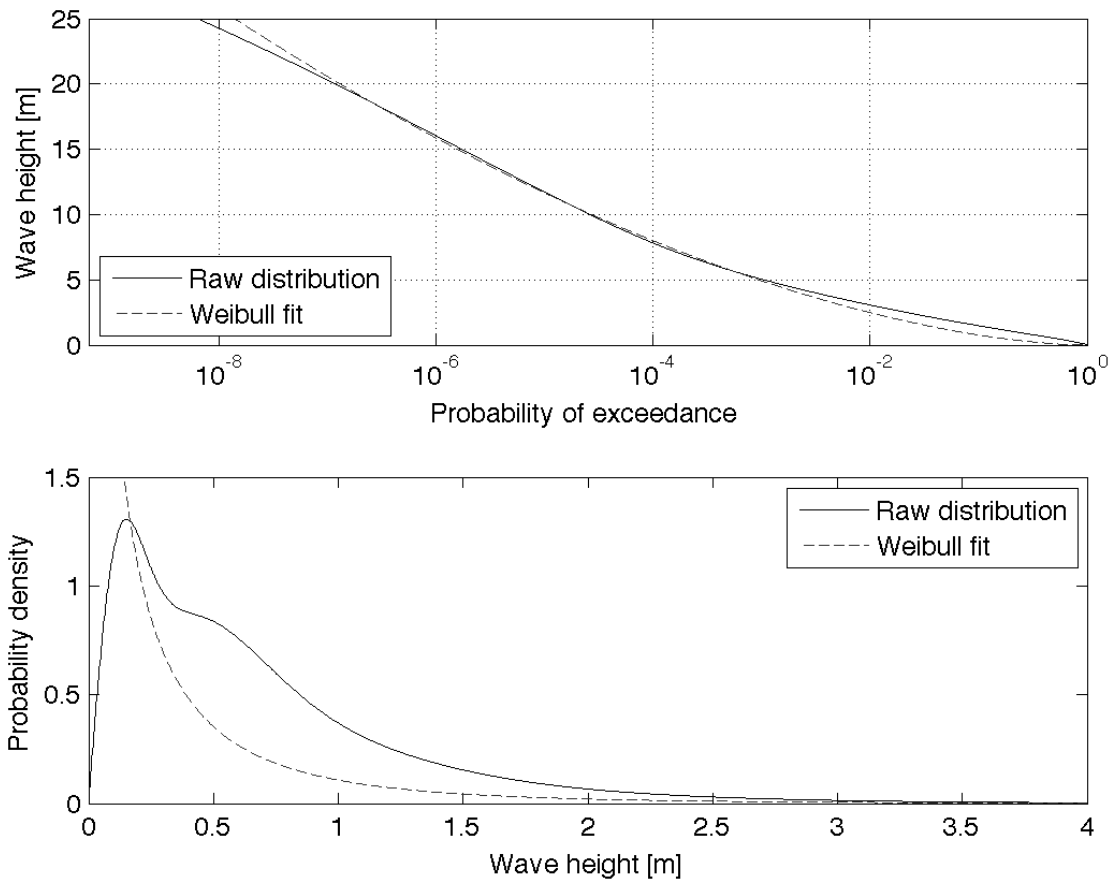


Figure 7.4 Example of a weighted fit. Top: Probability of exceedance for all considered wave heights, A much better fit compared with the un-weighted fit for wave heights over 5 m. Bottom: Probability density for wave heights up to 4 m. The weighted fit significantly overestimates the occurrence of wave heights below 0.25 m and underestimates wave heights between 0.25 and 4 m.

As can be seen, this results in a poorer fit for low wave heights and a much better result for high waves. This holds for all considered wave height distributions, although the difference in weighted and un-weighted fit was greatest for the condensed wave-height distribution.



## 8 Fatigue Damage

In this chapter, the final step of the numerical calculations is presented. A calculation is shown of the scale parameter and modifications to the simplified fatigue expression corresponding to each method presented in Chapter 4.

### 8.1 Calculation of Scale Parameter

The scale parameter describes the magnitudes of the stress ranges and is determined from one chosen stress range and its relative occurrence.

$$q = \frac{S_{ref}}{(\ln N_{ref})^{1/\gamma}} \quad (8.1)$$

The reference stress range,  $S_{ref}$ , was in all methods derived from the 10-year winter (= 10-year winter storm) storm. Since load data was available for the eight wave headings the reference stress range could be based on this. In Methods 1 and 2, see Chapter 4, the maximum stress range was determined from the load corresponding to wave heading 1, since this heading resulted in the highest stress. In Method 3 the simplified fatigue expression was divided to represent each heading with its own distribution. All eight stress ranges were thus used. The loads for the eight headings were applied differently on the structural model, the location along the weld that experiences the highest stress change for every heading. The damage and thus also the scale parameter was determined at 8 locations, or rather hot-spots, along the studied weld. In the 4:th method the reference stress range was taken as in Methods 1 and 2 as the highest stress range during the 10-year winter storm. The reference number of cycles was changed to correspond to the occurrence of this stress range in the tropical and non-tropical distribution.

The reference number of cycles,  $N_{ref}$ , was determined from the respective fits used. A nominal number of cycles for the 10-year winter storm in the condensed raw distribution was selected to correspond to  $0.5 \cdot 10^8$  waves during ten years, from an example in DNV RP, Det Norske Veritas (2011a). The corresponding reference number of cycles for the other fits were then determined from the difference to the condensed raw distribution.

The various alternatives in methodology presented in Chapter 4 employ either one, two or eight distributions. In combination with the two different alternatives for fitting the distribution presented in Chapter 7 and the fact that more than one location along the weld needed to be considered, several scale parameters are determined for each of the methods. Table 8.1 describes the information needed for determining the scale parameters for the 4 methods.

Table 8.1 Amount of variables needed for calculating the scale parameter.

Method:	Raw distributions	Shape parameters	Reference number of cycles	Reference stress ranges	Scale parameters
(1) Nominal	1 Based on the condensed wave statistics.	1 x 2 fits = 2	1 x 2 fits = 2	1 x 1 hot spot = 1	1 x 2 fits x 1 hot spot = 2
(2) Separated	1 Based on the condensed wave statistics.	1 x 2 fits = 2	1 x 2 fits = 2	2 x 1 hot spot = 2	2 x 2 fits x 1 hot spot = 4
(3) Directional	8 Based on the individual wave statistics of the eight headings.	8 x 2 fits = 16	8 x 2 fits = 16	8 x 8 hot spots = 64	8 x 2 fits x 8 hot spots = 128
(4) Weather	2 Based on the individual wave statistics of the two weather conditions.	2 x 2 fits = 4	2 x 2 fits = 4	1 x 1 hot spot = 1	2 x 2 fits x 1 hot spot = 4

Since the fit has been conducted in two different ways, see Chapter 7, two scale parameters needed to be considered for each method. Detailed information of how the scale parameters were determined is presented in Appendix F.

## 8.2 Calculation of Fatigue Damage

This section presents the different alternatives for calculating fatigue damage, based on the alternatives mentioned in Chapter 4. For a one-slope S-N curve the fatigue damage is given by Equation (8.2).

$$D_d = \frac{N_d}{a} q^m \Gamma\left(\frac{m}{\gamma} + 1\right) \quad (8.2)$$

Since a two slope S-N curve has been used the damage expression needs to account for stress ranges corresponding to the respective slopes in the S-N curve separately. Two cut-off gamma functions were used to accomplish this, see Equation 8.3 and 8.4.

$$\Gamma_1\left(\frac{m}{\gamma} + 1, z\right) = \int_z^{\infty} t^{\left(\frac{m}{\gamma} + 1\right) - 1} e^{-t} dt \quad (8.3)$$

$$\Gamma_0\left(\frac{n}{\gamma} + 1, z\right) = \int_0^z t^{\left(\frac{n}{\gamma} + 1\right) - 1} e^{-t} dt \quad (8.4)$$

The cut-off parameter,  $z$ , is determined by the stress range at the intersection of the two slopes,  $s_{s.i.}$ , see Equation (8.5).

$$z = \left(\frac{s_{s.i.}}{q}\right)^\gamma \quad (8.5)$$

In the case were the damage is given by the two slope S-N curve of type D:

$$s_{s.i.} = 83.4 \text{ MPa} \quad (8.6)$$

and if the damage is given by a S-N curve of type C2:

$$s_{s.i.} = 92.7 \text{ MPa} \quad (8.7)$$

Details of the two S-N curves can be seen in Appendix G.

The total number of cycles during 30 years,  $N_d$ , was set to  $N_d = 1.5 \cdot 10^8$  i.e. 3 times the number of waves during ten years in the above-mentioned example in DNV RP, Det Norske Veritas (2011a).

## 8.2.1 The Nominal Method

In the nominal simplified fatigue method the damage was given by the un-modified two-slope simplified fatigue expression given in DNV and ABS RP, Det Norske Veritas (2011a) and American Bureau of Shipping (2013).

$$D_d = N_d \left[ \frac{q^m}{a} \Gamma_1 \left( \frac{m}{\gamma} + 1, z \right) + \frac{q^n}{c} \Gamma_0 \left( \frac{n}{\gamma} + 1, z \right) \right] \quad (8.8)$$

## 8.2.2 Morison and Impact-separated Method

The damage was based on a division of Morison and impact loads with partial contributions to fatigue damage.

With the assumption that every wave with a wave height over  $H_{\text{lim}} = 3$  metres caused an impact stress range, the damage could be described by Equation (8.9):

$$D_d = \frac{N_d}{a} \left[ q_{\text{Morison}}^m \Gamma \left( \frac{m}{\gamma} + 1 \right) + q_{\text{impact}}^m \Gamma \left( \frac{m}{\gamma} + 1 \right) - q_{\text{impact}}^m \Gamma_0 \left( \frac{m}{\gamma} + 1, z_{\text{impact}} \right) \right] \quad (8.9)$$

with  $\Gamma$  as in equation (A.11) in Appendix A and:

$$z_{\text{impact}} = \left( \frac{H_{\text{lim}}}{q_{\text{wave}}} \right)^\gamma \quad (8.10)$$

where  $q_{\text{wave}}$  is the scale parameter of the condensed wave-height distribution.

Applied together with a two slope S-N curve:

for  $z_{\text{impact}} > z_{S-N, \text{impact}}$ :

$$D_d = \frac{N_d}{a} \left[ q_{\text{impact}}^m \Gamma \left( \frac{m}{\gamma} + 1 \right) - q_{\text{impact}}^m \Gamma_0 \left( \frac{m}{\gamma} + 1, z_{\text{impact}} \right) + q_{\text{Morison}}^m \Gamma_1 \left( \frac{m}{\gamma} + 1, z_{S-N, \text{Morison}} \right) \right] \\ + \frac{N_d}{c} q_{\text{Morison}}^n \Gamma_0 \left( \frac{n}{\gamma} + 1, z_{S-N, \text{Morison}} \right) \quad (8.11)$$

for  $z_{impact} < z_{S-N, impact}$  :

$$D_d = \frac{N_d}{a} \left[ q_{impact}^m \Gamma_1 \left( \frac{m}{\gamma} + 1, z_{S-N, impact} \right) + q_{Morison}^m \Gamma_1 \left( \frac{m}{\gamma} + 1, z_{S-N, Morison} \right) \right] + \frac{N_d}{c} \left[ q_{Morison}^n \Gamma_0 \left( \frac{n}{\gamma} + 1, z_{S-N, Morison} \right) + q_{impact}^n \Gamma_0 \left( \frac{n}{\gamma} + 1, z_{S-N, impact} \right) - q_{impact}^n \Gamma_0 \left( \frac{n}{\gamma} + 1, z_{impact} \right) \right] \quad (8.12)$$

where:

$$z_{S-N, Morison} = \left( \frac{s_{s.i.}}{q_{Morison}} \right)^\gamma \quad (8.13)$$

and:

$$z_{S-N, impact} = \left( \frac{s_{s.i.}}{q_{impact}} \right)^\gamma \quad (8.14)$$

### 8.2.3 The Directional Morison Method

Only stresses resulting from Morison forces were accounted for. The distribution of stress ranges were divided for the eight considered headings. As mentioned, eight hot-spots along the weld were evaluated, corresponding to index  $j$  below. Because of this, the fatigue damage was calculated for all eight hotspots, and subsequently compared in order to find the critical location along the weld. The relative occurrence of the eight wave headings can be seen in Table 8.2.

Table 8.2 Occurrence fractions for the eight wave headings.

Heading	1	2	3	4
$f_{Heading}$	0.09334	0.02837	0.02972	0.06716
Heading	5	6	7	8
$f_{Heading}$	0.09788	0.16327	0.24810	0.27217

$$D_{d,j} = \sum_i^8 f_{Heading,i} \cdot N_d \left[ \frac{q_{i,j}^m}{a} \Gamma_1 \left( \frac{m}{\gamma_i} + 1, z_{i,j} \right) + \frac{q_{i,j}^n}{c} \Gamma_0 \left( \frac{n}{\gamma_i} + 1, z_{i,j} \right) \right] \quad (8.15)$$

where:

$$q_{i,j} = \frac{S_{ref,i,j}}{(\ln N_{ref,i})^{1/\gamma_i}} \quad (8.16)$$

and:

$$z_{i,j} = \left( \frac{S_{s.i.}}{q_{i,j}} \right)^{\gamma_i} \quad (8.17)$$

## 8.2.4 The Weather Conditional Method

Only the damage due to Morison forces was considered. Partial contributions from non-tropical and tropical weather make up the total fatigue damage. Both distributions were assumed to share their shape parameters with their corresponding wave distributions.

The damage was given by Equation (8.18):

$$D_d = f_{Weather} \cdot N_d \left[ \frac{q_{tropical}^m}{\bar{a}} \Gamma_1 \left( \frac{m}{\gamma_{tropical}} + 1, z_{tropical} \right) + \frac{q_{tropical}^n}{\bar{c}} \Gamma_0 \left( \frac{n}{\gamma_{tropical}} + 1, z_{tropical} \right) \right] \\ + (1 - f_{Weather}) \cdot N_d \left[ \frac{q_{non-trop}^m}{\bar{a}} \Gamma_1 \left( \frac{m}{\gamma_{non-trop}} + 1, z_{non-trop} \right) + \frac{q_{non-trop}^n}{\bar{c}} \Gamma_0 \left( \frac{n}{\gamma_{non-trop}} + 1, z_{non-trop} \right) \right] \quad (8.18)$$

where:

$$z_{tropical} = \left( \frac{S_{s.i.}}{q_{tropical}} \right)^{\gamma_{tropical}} \quad (8.19)$$

and:

$$z_{non-trop} = \left( \frac{S_{s.i.}}{q_{non-trop}} \right)^{\gamma_{non-trop}} \quad (8.20)$$

and:

$$f_{Weather} = 0.0338 \quad (8.21)$$

## 9 Fatigue Damage Results

This chapter presents the results of the numerical analyses. Calculated fatigue damage for each method mentioned in Chapter 4 is presented.

In these calculations, the largest stresses were obtained in the bottom weld of the lower connection between the support and column shell. Fatigue damage results are thus presented for this weld. As mentioned, eight hot-spots were evaluated along the weld. Hot-spot 5, see Figure 6.9, proved to be the most critical for all methods and is therefore presented in this chapter.

Since the aim has been to evaluate the difference in calculated fatigue damage, only relative values are presented. All results are scaled with the result of the *Nominal* method with a shape parameter determined for a weighted fit,  $D_{ref} = 0.0025$ .

Fatigue damage results from the four methods formulated in Chapter 4 are presented in Tables 9.1 and 9.2. These results for the weighted and un-weighted fits were obtained from calculations with the nominal 10-year winter storm loads and a type D S-N curve representing the fatigue resistance.

Depending on method used, the cause of the fatigue damage may be identified. For example, in Method 2, the damage expression had two parts accounting for Morrison and impact load separately, see Equations (8.11) and (8.12) in Chapter 8. Method 1 did not distinguish between different types of loading and is therefore presented as indeterminate.

Table 9.1 *Relative damage for the four methods based on a shape parameter from an un-weighted fit.*

Method:	Nominal (1)	Separate (2)	Directional (3)	Weather (4)
$D_{indeterminate} / D_{ref}$	0.2835	-	-	-
$D_{Morrison} / D_{ref}$	-	0.0065	0.0013	0.0086
$D_{impact} / D_{ref}$	-	0.1160	0*	0*
$D_{tot} / D_{ref}$	0.2835	0.1225	0.0013	0.0086

Table 9.2 Relative damage for the four methods based on a shape parameter from a weighted fit.

Method:	Nominal (1)	Separate (2)	Directional (3)	Weather (4)
$D_{indeterminate} / D_{ref}$	1.0000	-	-	-
$D_{Morison} / D_{ref}$	-	0.0234	0.0024	0.0276
$D_{impact} / D_{ref}$	-	0.9013	0*	0*
$D_{tot} / D_{ref}$	1.0000	0.9247	0.0024	0.0276

\* The calculation has been conducted only for the Morison loads. The damage due to impact loading (slamming) can in theory be obtained using the same method.

To visualize the difference in calculated fatigue damage between methods and type of fit the results are plotted as stacked bar charts in Figure 9.1.

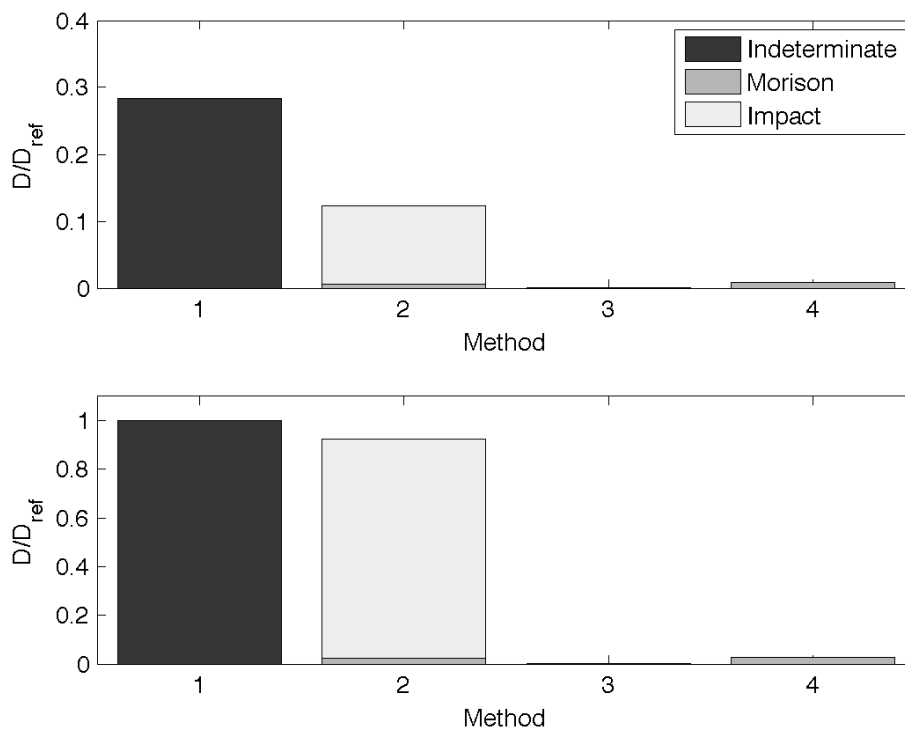


Figure 9.1 Relative fatigue damage. Top: Damage derived for a shape parameter based on an un-weighted fit. Bottom: Damage derived for a shape parameter based on a weighted fit.

The damage in Method 4 was based on a summation of the individual damage from the two weather conditions; tropical and non-tropical. Although tropical conditions were assumed to only occur during 3.4% of the time it still had a significant influence on the total damage. The relative contribution between both conditions, both for the weighted and un-weighted fit, can be seen in Table 9.3.

Table 9.3 Relative damage contribution in method 4 both for a weighted and un-weighted fit.

	Non-tropical conditions	Tropical conditions
Un-weighted fit	64 %	36 %
Weighted fit	43 %	57 %

Figure 9.2 shows the relative damage of the four methods with shape parameters varying linearly in five steps between the weighted and un-weighted value. Methods 1 and 2 had equal shape parameters for each row. This was not the case for Methods 3 and 4 which had different values for each row, since the difference between the weighted and un-weighted shape parameter was not the same for these methods.

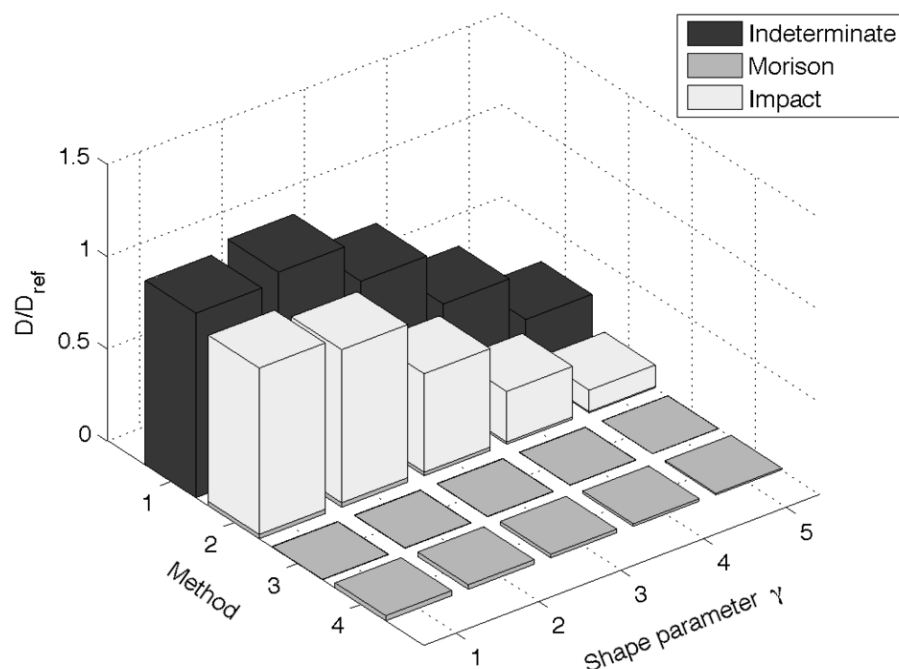


Figure 9.2 Relative fatigue damage for Methods 1 through 4. The shape parameter is varied linearly between the value obtained in the weighted fit (1) and the value obtained in the un-weighted fit (5).

The difference between the weighted and un-weighted fit varies depending on method. This was due to the different distributions from which the shape parameters were derived, see Table 9.4.

*Table 9.4 Difference in calculated fatigue damage based on the weighted and un-weighted fit for the respective methods.*

Method	Nominal (1)	Separate (2)	Directional (3)	Weather (4)
$\frac{D_{weighted}}{D_{un-weighted}}$	3.53	7.55 3.6 for Morrison part	1.85	3.21

As can be seen in Figure 9.2 the calculated damage varied heavily with the shape parameter. Methods 1 and 2 used the same shape parameter but different scale parameters. The fatigue damage was smaller for Method 2 than for Method 1, which was expected since the distribution in Method 1 was scaled with the slamming stress range, hence all stress ranges became similar to the slamming stress range. The relationship between the two methods also varies depending on shape parameter - the difference between the weighted and un-weighted fit was much greater for Method 2. However, the difference between the two methods was quite small for a weighted fit. This indicated that wave heights over 3 metres was the main contributor to fatigue damage for the weighted fit, but accounts for less than half of the damage for the un-weighted fit.

Methods 3 and 4 varied less with the shape parameter than the Morrison part of Method 2. The difference was greatest for Method 3, but can also be seen for Method 4. This was due to the fact that the shape parameter varied less between the fits, which, in turn, was due to the distribution of wave heights being divided depending on direction or that weather conditions were more Weibull-shaped compared to the condensed wave-height distribution. Some of the wave headings had wave-height distributions that were fairly Weibull-shaped, for example Heading 3 which can be seen in Figure E.2-5, Appendix E.

It was hard to evaluate the difference in calculated damage between the different methods since their relationship changed depending on the shape parameter. In order to determine how the fit should be weighted for getting the most accurate results, an investigation was made in order to verify which wave heights contributed most to the calculated fatigue damage.

This was done similarly to the first steps in the simplified fatigue method before the distribution is fitted to the Weibull model, which can be seen in Appendix A. see Equations A.1 through A.8. The distribution of stress ranges is the distribution of wave heights,  $h$ , multiplied with a constant,  $C$ , derived in the FE-analysis. The

damage can be said to follow a distribution corresponding to wave height multiplied by a constant raised to the power of the inverse slope of the S-N curve.

$$f_D(h) \sim P_H(h) \cdot (h \cdot C)^m \quad (9.1)$$

The damage distribution is shown together with the raw condensed wave-height distribution in Figure 9.5.

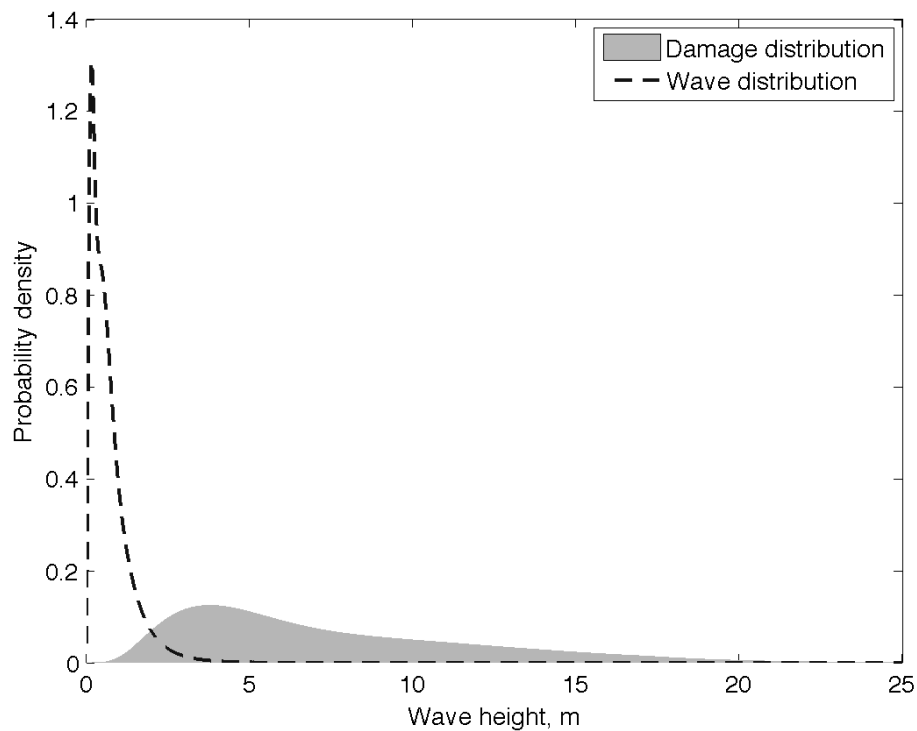


*Figure 9.5 Relative contributions of different wave heights to the calculated fatigue damage. The long-term wave height distribution shown is the condensed distribution.*

This indicated that the most common waves contributed very little to the calculated fatigue damage and that almost all damage was resulting from wave heights in the tail of the wave-height distribution.

By increasing vertical slamming and Morison loads, the effect of uncertainties in the hydrodynamic analysis and subsequent input loads could be investigated. This was done by increasing the vertical loads by 10%, while all other loads were left unchanged. The effects were calculated using the weighted fit for Methods 1, 2 and 4, which can be seen in Table 9.4 and Figure 9.3.

Table 9.4 Effect of a 10% increase in load magnitude for slamming and vertical Morison forces acting on the support. All other loads were left unchanged.

Method	Nominal (1)	Separate (2)	Weather (4)
Damage increase [%]	57.2	57.9	69.6

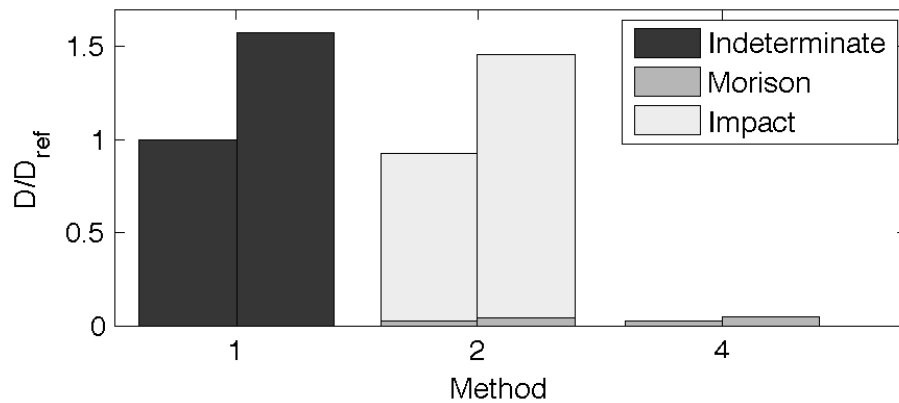
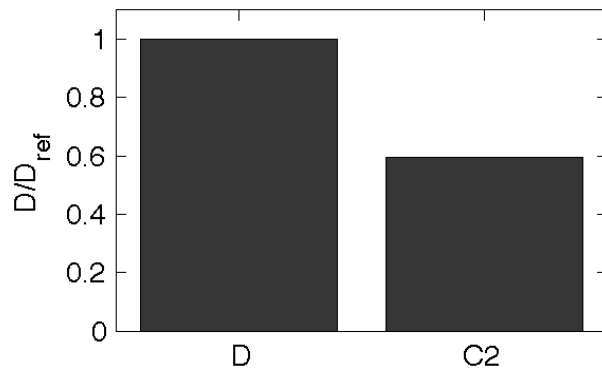


Figure 9.3 Effect of a 10% increase in load magnitude for slamming and vertical Morison forces acting on the support. The left bar represent the damage from nominal loads and the right bar gives the damage from the increased loads.

As can be seen in Figure 9.3, the simplified fatigue method was very sensitive to the reference stress cycle. When increasing the vertical load magnitude, the calculated fatigue damage increased by about 60% compared to the original loads.

Fatigue damage results presented so far have been calculated based on an S-N curve of type D. The result from changing to an S-N curve of type C2 can be seen in Figure 9.4.



*Figure 9.4 Relative fatigue damage of the Nominal SF method with a weighted fit for an S-N curve of types D and C2.*

Regarding the fatigue resistance it was also clear that the choice of S-N curve had a great impact on the calculated damage. The fatigue damage decreased by about 40% using the C2 curve instead of the D curve.



## 10 Discussion

In this chapter the methods, limitations and assumptions used during the course of the thesis project are discussed with regard to how these may have affected the results and conclusions arrived at in Chapters 9 and 10.

As stated in Chapter 1, one of the main assumptions has been a linear relationship between wave height and stress range, and while this is presented in classification rules, it may not hold for local details in the splash zone. This assumption has two major consequences: dynamic effects are not accounted for and a non-linear load application cannot be handled.

As for a non-linear load application, the extension of the distributed load applied along the caisson has been a problem that has not been possible to deal with the method used throughout the thesis project. Only the ten-year winter storm loads, which correspond to an extension of the distributed loads according to Figure C.1 through C.4 in Appendix C, have been discussed. The loads span over most of the caisson length - the linear relationship between wave height and stress range implies that this extension remains but that the magnitude changes. In reality, both the extension of the load and the magnitude change. This implies that stress ranges under the reference stress range are overestimated and that stress ranges above the reference stress range become underestimated in the current method. The loads distributed along the caissons are part of the Morison loads, which has been shown to contribute to a rather small part of the total fatigue damage. The impact loads due to slamming do not entail the same problem. As long as the wave height reaches the support a loading occurs, which only depends on the vertical particle velocity. For these loads, the assumption given by ABS of a linear relationship might still hold. However, the slamming loads depend on the square of the vertical particle velocity and further investigation might be needed - both in terms of how the particle velocity and the subsequent stress in the support relate to the wave height.

Dynamic effects could entail that the applied load are increased due to dynamic amplification for waves of certain frequencies and that impact loading, such as slamming, may result in additional stress cycles due to springing and whipping phenomena in the support structure. Another dynamic effect could occur because of the slender geometry of the caisson. Wind, current or fluid flow past a slender structural member may lead to oscillations normal to the longitudinal axis of the member due to vortex shedding, Det Norske Veritas (2010a). Vortex-induced oscillations may be a design issue in several limit states, including FLS. In particular, several cylinders in array formation may induce amplification of these oscillations, Det Norske Veritas (2010a).

The above-mentioned effects will definitely have an influence on the stress-range distribution. If dynamic amplification significantly increases the reference stress range it is clear that the method used in this thesis will heavily underestimate the fatigue damage, especially since the results show that the effects from a small change in load magnitude is amplified in the fatigue calculations. If each slamming event would result in a number of extra cycles, several stress ranges of a high magnitude would significantly raise the estimated fatigue damage. Dynamic effects concerning the

caisson may be of less importance. Even if extra cycles are caused by vortex-induced oscillations they will probably not reach a very high magnitude.

In total, the assumption that a linear relationship exists between wave height and stress range possibly underestimates the fatigue damage due to the fact that dynamic effects are not considered.

Another assumption that was made concerns how the distribution of wave heights was derived. The distribution of wave heights has been based on a relationship between the significant wave height of a sea-state and the distribution of regular wave heights during that sea-state, Holthuijsen (2007) and Det Norske Veritas (2010a). The relationship is based on a Rayleigh distribution of crest heights and that wave height can be taken as twice the height of the crest, Holthuijsen (2007). This should hold for narrowbanded waves in deep water. Wave crests with a negative height are not accounted for. Another problem regarding this is that the surface elevation can be disturbed due to wave breaking and non-linear wave-wave interactions, Holthuijsen (2007).

This is a relatively simple way of deriving the wave-height distribution, but it removes any information about wave period. A sea-state with a relatively low mean wave period will contain a greater number of waves during the three-hour measurement period compared to a sea-state with a relatively high mean wave period. If waves with a large wave height are assumed to correspond to long wave periods they will obtain a higher occurrence than they should in the long-term distribution. This ultimately leads to an overestimation of the fatigue damage.

The Weibull distribution has been used for describing stress ranges in this thesis. As mentioned above, other distributions may be used in the simplified fatigue method. In theory, this should not change the outcome in any other way than that a satisfactory fit becomes either harder or easier to achieve. Using the Weibull distribution model it was hard to achieve a satisfactory fit for both high and low wave heights simultaneously. However, since almost all damage is due to waves with a high wave height a weighted fit could be used for representing these quite well. This method is assumed to work equally well if other distribution models would be used.

As was seen in Chapter 9, the calculated fatigue damage is low. The main reason for this low value is probably that the reference number of cycles used was taken from an example in DNV RP. This value of numbers of cycles corresponds to a very high wave height in the distribution obtained in Chapter 7. The ten-year winter storm loads probably do not correspond to this very high wave height, and in reality these loads should be more common for the distribution used. If the wave height corresponding to these loads was instead found in the distribution and that the occurrence was determined to correlate to a ten-year return value, the fatigue damage would be much higher. It is also possible that more common waves will give a higher contribution to the fatigue damage. This is obviously related to the method used for deriving the wave-height distribution as discussed above.

# 11 Conclusions

Based on the results presented in the previous chapters, the following observations and conclusions could be made in order to address the three sub-targets presented in Section 1.2:

- Identify how the stress-range distribution parameters can be obtained and how they can be handled in order to represent the stress ranges as accurately as possible.
- Investigate how a variation in load input data propagates through the structural and fatigue analyses and affects the calculated fatigue damage - primarily with respect to uncertainties in the load magnitude.
- Evaluate how the choice of different S-N curves representing the fatigue resistance affects the calculated fatigue damage.

The first sub-target was addressed by an investigation in several parts. First, how the fit to the Weibull model should be conducted in order to get a good representation of the most important stress ranges. Secondly, it was investigated whether a partition into several wave height/stress-range distributions could result in more Weibull-like distributions and hence a better representation of stress ranges. This approach influences both the shape and scale parameter as the shape parameter is then less dependent on the type of fit and the scale parameter can be obtained with a more appropriate reference stress range. The partition was conducted for different headings, weather conditions and load contributions.

The results showed that contributions from stress ranges with a high magnitude dominated, even though the occurrences of such stress ranges were very low. It is then important that the fit describes the tail of the distribution well. The conclusion is that a weighted fit must be used both for obtaining an appropriate shape parameter and for being able to scale the distribution correctly. This applies if the reference stress range is associated with an occurrence located in the tail of the distribution as was the case in this thesis.

Because of this, the results to be compared are the ones from the weighted fits for the respective methods. As previously mentioned, the difference between Methods 1 and 2 was quite small. For the specific case it could be concluded that there was not much to gain by dividing the stress ranges into contributions from Morison and slamming, other than to highlight what causes most fatigue damage. Partly, this was due to the fact that Morison forces accounted for a very small part of the damage. However, it is worth mentioning that the influence might be larger for other cases with different circumstances. A subdivision like this can be done only for stress ranges that are considered separated in time.

When comparing the Morison contribution investigated in Methods 2, 3 and 4 it was found that a subdivision of stress ranges from different headings had a great impact on the calculated damage. This is most likely due to the fact that all distributions were scaled with an individual reference stress range instead of the one from the worst heading. A better Weibull fit for each heading compared to the fit of the condensed

distribution might also have been a reason. This approach was only investigated for the Morison stress ranges, but the same effect can be assumed to occur when applying it to the stress ranges from slamming. This method resulted in the greatest effect on the calculated fatigue damage, since the calculated result was about 10% of the damage calculated in Method 2. The conclusion is that this subdivision has a great influence on the damage estimate if the extensions and magnitude of loads acting on the structure are very heading-dependent.

It was also found that Method 4 resulted in a larger damage than the Morison part of Method 2, the difference being roughly 18 %. In this case, tropical conditions only occurred during 3.4 % of the time, but contributed to roughly half of the estimated fatigue damage. As with the subdivision of wave headings, only Morison loads were investigated. If the same difference can be assumed for damage due to slamming stress ranges, using this approach can have a significant influence. It is interesting to note that, in this case, the *Nominal* method was not conservative, i.e. it underestimated the fatigue damage.

Another conclusion from the results of Methods 3 and 4 is that the subdivision of stress ranges result in more Weibull-like distributions. The shape parameter is then less dependent on the type of fit and a more accurate reference stress range can be used for scaling the distribution, which increases the accuracy in the estimate.

The second sub-target resulted in an investigation of how the calculated fatigue damage changes due to an increase in vertical load, both for slamming and Morison loads. The investigation was based on finding the influence of uncertainties in the hydrodynamic analysis mentioned in Chapter 4.

It was noted that small changes in load data significantly increased the estimated fatigue damage. The 10 % increase in reference load corresponds to approximately a 5 % increase in the relative velocities and accelerations used for calculating the loads. By increasing the reference stress range magnitude, all accounted stress ranges were increased. Since the S-N curve is not linear the effect of increasing the loads was amplified. It is also possible that the most common stress ranges, which previously accounted for almost none of the estimate fatigue damage, attained a high enough magnitude to significantly contribute to the total damage. This also means that it is very important to have an accurate estimate of the reference number of cycles which is used for calculating the scale parameter. Uncertainty in occurrence of the reference stress range will essentially cause the same problem as uncertainty in the load input data. The conclusion is that if more detailed methods are not used that can improve the accuracy of the loads, it is important to have an understanding of the uncertainties and scatter in this data.

The last sub-target was addressed by using different S-N curves to represent the fatigue resistance.

As specified in Chapter 4, the choice of S-N curve depends on the principal stress direction. The estimated fatigue damage was reduced by approximately 40 % through using the C2 curve rather than the D curve. It is thus important to know which S-N curve that is appropriate for the studied case. The S-N curve was selected based on the principal stress direction at the weld. A type D curve correspond to a principal stress direction perpendicular to the weld, while C2 is used for directions along the weld,

see Figure 4.1 in Chapter 4. In the studied case, vertical forces from slamming and Morison loads seemed to dominate the stress response in the lower plate. If this is the case, the bending moment from these loads around the neutral plane of the support should induce tensile stresses perpendicular to the weld in the lower plate. This corresponds to observations made during stress derivations in the FE-analysis. Hence, it is concluded that a type D S-N curve should be appropriate for this case. Also, if the principal stress direction of the reference stress range indicates the use of an S-N curve of type C2, it is important to know whether this is the case for all stress ranges in the stress-range distribution. Otherwise, a crack might be initiated along the weld corresponding to the D curve from one of the other cycles and lowering the fatigue resistance. If any uncertainties in this information exist, an S-N curve of type D should be used, which in the worst case will give conservative results.



## 12 Future Work

This chapter presents possible procedures for further evaluating the simplified fatigue method. Aspects that could not be represented in the method used in this thesis are presented in Chapter 11. Future alternative methods for investigating these aspects are presented below.

Dynamic effects might significantly affect the fatigue damage, both in terms of increased stress-range magnitude and an increased number of stress cycles. Mass properties should be added to the structural FE-models used for deriving the stress in order to be able to calculate eigenfrequencies of the structure. DNV presents recommendations of how dynamic effects due to slamming can be dealt with in its RP, Det Norske Veritas (2010a). This can be used as a first investigation of how dynamic effects might influence the method. Each slam can be associated with 20 approximate linear decaying stress ranges, Det Norske Veritas (2010a). This is a quick correction that could be conducted to evaluate the influence of dynamic effects of the impact loading. Since it has been shown that the main contribution to fatigue damage is due to slamming loads and waves with a wave height over 3 metres, this correction is assumed to increase the fatigue damage. In order to more fully investigate the effects of dynamic loading, a more accurate application of loads would also be needed with information about the frequency included and extension along the caisson during the time of a passing wave. This obviously depends on a better understanding of the loads.

A better understanding of the loads and the load cycles would be needed for solving a number of problems - CFD simulation or basin experiments may be needed to determine the detailed flow phenomena in the proximity of the support. If the full load cycle during the course of a passing wave is determined, the problem relating to separating the stress ranges into Morison and impact parts can also be solved. A CFD analysis verified by basin experiments would also lead to greater certainty in the particle velocity. As can be seen in Chapter 9, this has a significant impact on the fatigue damage.

Since the distribution of wave heights within each sea-state was assumed to be Rayleigh-distributed. The damage could have been determined from each sea-state and then summed with the occurrence from the scatter diagram, without the problems relating to finding a satisfactory fit. This is a method resembling the last step in the spectral fatigue method, where the stress-range distribution is assumed to be Rayleigh-distributed within each sea-state and subsequently summed. However, the methods leading up to the stress-range distribution parameter would be different from the spectral method.

A relatively simplistic model for deriving the wave-height distribution was used in this thesis. The MATLAB toolbox WAFO, WAFO group (2011), could be used for simulating waves using the significant wave height and peak period from the available scatter diagrams as spectral parameters. A rainflow count can then be conducted in order to derive wave heights. This would also allow for information about the wave period to be obtained. This means that rainflow cycles are considered, rather than the min-max cycles used throughout this thesis. Rainflow cycle counting is, for example, in Downing's book considered to be the preferred method, Dowling (2012). A more

realistic wave-height distribution could also alleviate some of the problems relating to the reference stress range.

In order to verify the results obtained through the simplified fatigue method in this thesis one of the other fatigue assessments offered in the class rules should be employed. An analysis using the spectral fatigue method as specified in Chapter 2, with an assumed linearity between wave height and stress range, i.e. no motion analysis included, would be the most similar to the method used in this thesis in terms of assumptions used. This would make a comparison between both the resulting damage and the difference in the stress-range distribution possible.

A stress-block method could be used for bypassing the problems associated with fitting the distribution altogether. If small increments of the wave-height distribution are used as stress blocks the damage can be calculated directly from the stress-range distribution without having to use the simplified fatigue expression. This would make a comparison between the damage from the weighted fit to be compared to the raw distribution. A verification of whether the damage caused by stress ranges with a low magnitude really is negligible would be possible.

Since it was shown that tropical weather causes a significant contribution to fatigue damage, a more stochastic approach can be used for handling the occurrences of tropical storms. This could be handled in a reliability point of view estimating an expected number of tropical storms experienced during the design life with a suitable safety margin.

The weld was not modelled during the structural response analysis. Instead, the effects of the weld were assumed to be handled through the use of an appropriate S-N curve. However, it was found that the choice of weld class to be used was not completely trivial. If the weld is instead modelled in the FE-model, this problem could be avoided. A denser mesh would be needed and material properties corresponding to the heat-affected zone has to be used.

## 13 References

- American Bureau of Shipping (2005): *Guidance notes on: Spectral-based fatigue analysis for floating offshore structures*, American Bureau of Shipping, Huston, United States of America, 2005.
- American Bureau of Shipping (2010): *Guide for the: Fatigue assessment of offshore structures*, American Bureau of Shipping, Huston, United States of America, 2010.
- American Bureau of Shipping (2012): *Rules for Building and Classing Steel Vessels: Part 5C Specific Vessel Types*, American Bureau of Shipping, Houston, United States of America, 2012.
- American Bureau of Shipping (2013): *Commentary on the guide for the: Fatigue Assessment of Offshore Structures*, American Bureau of Shipping, Houston, United States of America, 2013.
- Baarholm R., Faltinsen O.M. (2004): Wave impact underneath horizontal decks, *Journal of Marine Science and Technology*, Vol. 9, No. 1, May 2004, pp. 1-14.
- Bishop R.E.D., Hassan A.Y. (1964): The lift and drag forces on a circular cylinder in a flowing fluid. *Proceedings of the Royal Society of London. Series A, Mathematical and Physical Science*, Vol. 227, No. 1368, January 1964, pp.33-49
- Dalton C., Nash J.M. (1976): Wave Slam on Horizontal Members of an Offshore Platform, *8<sup>th</sup> Annual Offshore Technology Conference*, Proc. OTC 2500, May 1976, pp. 769-775
- Det Norske Veritas (2001): *Offshore Standards: DNV-OS-C106: Structural Design of Deep Draught Floating Units*, Det Norske Veritas, Høvik, Norway, 2001.
- Det Norske Veritas (2003): *SESAM User Manual Prefem*, Det Norske Veritas, Høvik, Norway, 2003.
- Det Norske Veritas (2005): *Classification notes No. 30.7: Fatigue assessment of ship structures*, Det Norske Veritas, Høvik, Norway, 2005.
- Det Norske Veritas (2008): *Nauticus Hull User Manual 3D Beam*, Det Norske Veritas, Høvik, Norway, 2008.
- Det Norske Veritas (2010a): *Recommended Practice: DNV-RP-C205: Environmental Conditions and Environmental Loads*, Det Norske Veritas, Høvik, Norway, 2010.
- Det Norske Veritas (2010b): *SESAM User Manual Sestra*, Det Norske Veritas, Høvik, Norway, 2010.
- Det Norske Veritas (2010c): *SESAM User Manual Wadam*, Det Norske Veritas, Høvik, Norway, 2010.
- Det Norske Veritas (2010d): *SESAM User Manual DeepC*, Det Norske Veritas, Høvik, Norway, 2010.

- Det Norske Veritas, (2011a): *Recommended Practice: DNV-RP-C203: Fatigue Design of Offshore Steel Structures*, Det Norske Veritas, Høvik, Norway, 2011.
- Det Norske Veritas (2011b): *SESAM User Manual GeniE*, Det Norske Veritas, Høvik, Norway, 2011.
- Det Norske Veritas (2011c): *SESAM User Manual Xtract*, Det Norske Veritas, Høvik, Norway, 2011.
- Dowling, N.E. (2012): *Mechanical Behaviour of Materials, Fourth edition*. Pearson Education Limited, Essex, United Kingdom, 2012.
- Fruedenburg W.R., Gramling R. (2011): *Blowout in The Gulf: The BP Oil Spill Disaster and the Future of Energy in America*. MIT Press, Cambridge, United States of America, 2011.
- GVA Consultants (2011a): *Caisson Foundation Analysis: Report No. I0250-ST-RP-117-1601*, GVA Consultants, Göteborg, Sweden, 2011.
- GVA Consultants (2011b): *Hydrodynamic Loads on Appurtenances Report: Report No. I0250-HY-RP-050-0013*, GVA Consultants, Göteborg, Sweden, 2011
- GVA Consultants (2010): *Design Brief Hydrodynamic Analysis: Report No. I0250-HY-DB-050-0001*, GVA Consultants, Göteborg, Sweden, 2010.
- Holthuijsen L.H. (2007): *Waves in Oceanic and Coastal Waters*. Cambridge University Press, New York, United States of America, 2007.
- International Institute of Welding (2008), *Recommendations for Fatigue Design of Welded Joints and Components*, Abington Publishing, Cambridge, United Kingdom, 2008.
- Journée J.M.J., Adegeest L.J.M. (2003): *Theoretical Manual of Strip Theory Program "SEAWAY for Windows"*, AMARCON, Report No. 1370, Dalfsen, Netherlands, 2003.
- Marintek (2007): *SIMO - User's Manual Version 3.6*, Norwegian Marine Technology Research Institute, Trondheim, Norway, 2007.
- Mathworks (2013): *MATLAB Documentation Center homepage*: <http://www.mathworks.co.uk/help/matlab/index.html>, [Accessed: 2013-05-21].
- Nolte K.G., Hansford J.E. (1977): Closed-Form Expressions for Determining the Fatigue Damage of Structures Due to Ocean Waves. *Society of Petroleum Engineers Journal*, Vol. 17, No. 6, December 1977, pp. 431-440.
- The World Commission on Environment and Development (1987): *Our Common Future*, Oxford University Press, Oxford, United Kingdom, 1987.
- WAFO group (2011): *WAFO – a Matlab Toolbox for Analysis of Random Waves and Loads*, Lund University, Lund, Sweden, 2011.

Wagner H. (1932): Über Stoss- und Gleitvorgänge an der Oberfläche von Flüssigkeiten (On the impact and sliding phenomena on the surface of liquids. In German), *Zeitschrift für Angewandte Mathematik und Mechanik*, Vol. 12, No. 4, August 1932, pp. 193-215.

World Resource Institute (2000): *World Energy Assessment: Energy and the challenge of sustainability*. United Nations Development Programme Bureau for Development Policy, New York, United States of America, 2000.



## Appendix A: The Theory of the Simplified Fatigue Method

This appendix presents the theory and general procedure for determining the fatigue damage according to the simplified fatigue method.

Fit the data of long-term stress ranges to a statistical model for the distribution. The Weibull distribution is standard practice in the marine industry, American Bureau of Shipping (2013). Define the stress range as a random variable,  $S$ . An example of the probability density can be seen in Figure A.1.

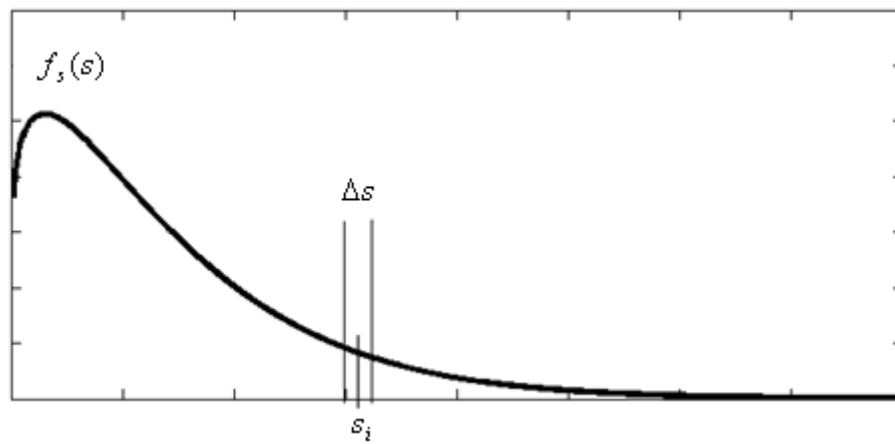


Figure A.1 Example probability density of the stress ranges.

For any stress range  $s_i$ , the number of cycles to failure obtained from an appropriate S-N curved based on weld geometry and environment is denoted:

$$N_i = N(s_i) \quad (\text{A.1})$$

And the number of cycles at the stress range  $s_i$ :

$$n_i = N_{life} [f_s(s_i) \Delta s] \quad (\text{A.2})$$

Where  $N_{life}$  is any reference life in terms of cycles and  $f_s(s_i) \Delta s$  is the ratio out of the entire distribution for a small increment around stress range  $s_i$ .

The partial damage according to PM is thus:

$$d_i = \frac{n_i}{N_i} = \frac{N_{life} f_s(s_i) \Delta s}{N(s_i)} \quad (\text{A.3})$$

And the total damage during the reference life  $N_{life}$  :

$$D_{life} = \sum_i \frac{N_{life} f_s(s_i) \Delta s}{N(s_i)} \quad (A.4)$$

As the increment  $\Delta s$  goes towards zero, Equation (A.4) is expressed as the integral:

$$D_{life} = N_{life} \int_0^{\infty} \frac{f_s(s_i) ds}{N(s_i)} \quad (A.5)$$

The number of cycles to failure at a specific stress range,  $N(s)$ , for a one slope S-N curve, can be expressed as:

$$N(s) = \bar{a} \cdot s^{-m} \quad (A.6)$$

Where  $\bar{a}$  is the interception of the N-axis and the curve, and  $m$  is the inverse slope of the S-N curve.

By using Equation (A.6) in (A.5):

$$D_{life} = \frac{N_{life}}{\bar{a}} \int_0^{\infty} s^m f_s(s_i) ds \quad (A.7)$$

The integral part of Equation (A.7) is by definition the expected value of  $s^m$ .

$$E(s^m) = \int_0^{\infty} s^m f_s(s_i) ds \quad (A.8)$$

Equation (A.8) in (A.7):

$$D_{life} = \frac{N_{life} E(s^m)}{\bar{a}} \quad (A.9)$$

For the Weibull distribution, the expected value can be expressed according to the gamma function:

$$E(s^m) = q^m \Gamma\left(\frac{m}{\gamma} + 1\right) \quad (A.10)$$

$$\Gamma\left(\frac{m}{\gamma} + 1\right) = \int_0^{\infty} t^{\left(\frac{m}{\gamma} + 1\right) - 1} e^{-t} dt \quad (A.11)$$

Where  $q$  is the scale parameter and  $\gamma$  is the shape parameter of the Weibull distribution.

By combining Equation (A.10) with (A.9):

$$D_{life} = \frac{N_{life}}{a} q^m \Gamma\left(\frac{m}{\gamma} + 1\right) \quad (\text{A.12})$$

Since the reference number of cycles used,  $N_{life}$ , can be set arbitrarily. The damage for the design life,  $D_d$ , is obtained when the reference number of cycles is set to the number of cycles for the design life,  $N_d$ .

$$D_d = \frac{N_d}{a} q^m \Gamma\left(\frac{m}{\gamma} + 1\right) \quad (\text{A.13})$$

With  $N_d$  expressed as:

$$N_d = v_0 T_d \quad (\text{A.14})$$

Where  $v_0$  is the average zero-crossing frequency for the stress ranges, and  $T_d$  is the design life in seconds.

By using Equation (A.14) in (A.13) the final expression for the fatigue damage, according to the simplified fatigue method, is obtained:

$$D_d = \frac{v_0 T_d}{a} q^m \Gamma\left(\frac{m}{\gamma} + 1\right) \quad (\text{A.15})$$

It is also possible to use a two-slope S-N curve by evaluating the gamma function in two steps:

$$D_d = \frac{v_0 T_d}{a} q^m \Gamma_1\left(\frac{m}{\gamma} + 1, z\right) + \frac{v_0 T_d}{c} q^n \Gamma_0\left(\frac{n}{\gamma} + 1, z\right) \quad (\text{A.16})$$

For fatigue strength is defined as:

$$N(s) = \bar{a} \cdot s^{-m} \text{ for } s > s_{s.i.} \quad (\text{A.17})$$

$$N(s) = \bar{c} \cdot s^{-n} \text{ for } s < s_{s.i.} \quad (\text{A.18})$$

Where  $s_{s,i}$  is the stress corresponding to the intersection of the two slopes.

$$\Gamma_1\left(\frac{m}{\gamma} + 1, z\right) = \int_z^{\infty} t^{\left(\frac{m}{\gamma} + 1\right) - 1} e^{-t} dt \quad (\text{A.19})$$

$$\Gamma_0\left(\frac{n}{\gamma} + 1, z\right) = \int_0^z t^{\left(\frac{n}{\gamma} + 1\right) - 1} e^{-t} dt \quad (\text{A.20})$$

$$z = \left(\frac{s_{s,i}}{q}\right)^\gamma \quad (\text{A.21})$$

## Appendix B: Loads

In this appendix, loads calculated and applied on the FE-models are presented. Distributed loads acting on the caissons are considered as input data in this thesis and they are applied on the beam FE-model. The loads are available in the x- and y-directions for both a positive and negative lift coefficient, as can be seen in Figure B.1-4. Reaction forces and moments at the studied support are obtained from the beam FE-model. They were then recalculated as reaction forces that could be applied on the 3D FE-model. Applied reaction forces can be seen in Tables B.1 and B.2. Loads acting directly on the support, slamming and Morison loads, can be seen in Table B.3-B.5.

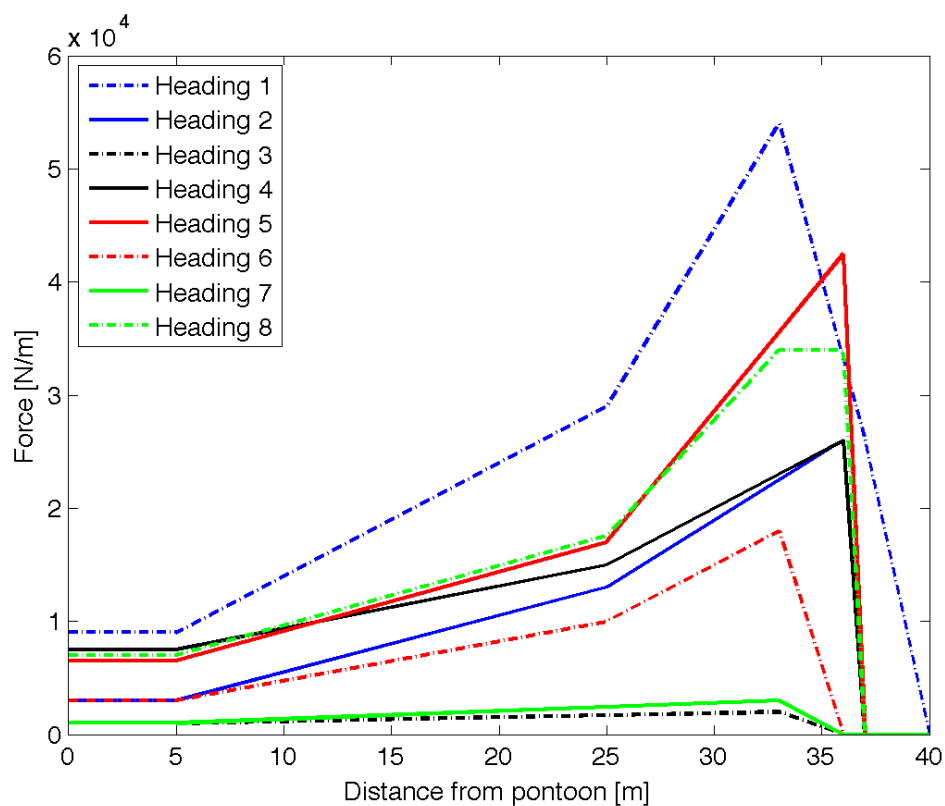


Figure B.1 Distributed load along the caisson in the x-direction with a negative lift coefficient.

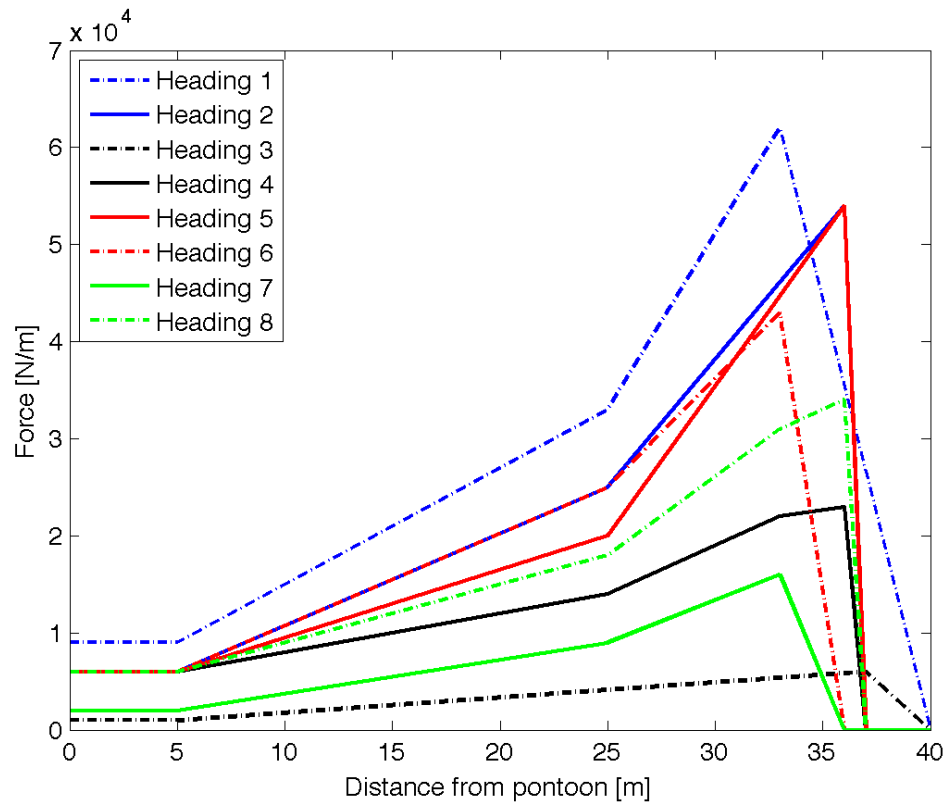


Figure B.2 Distributed load along the caisson in the y-direction with a negative lift coefficient.

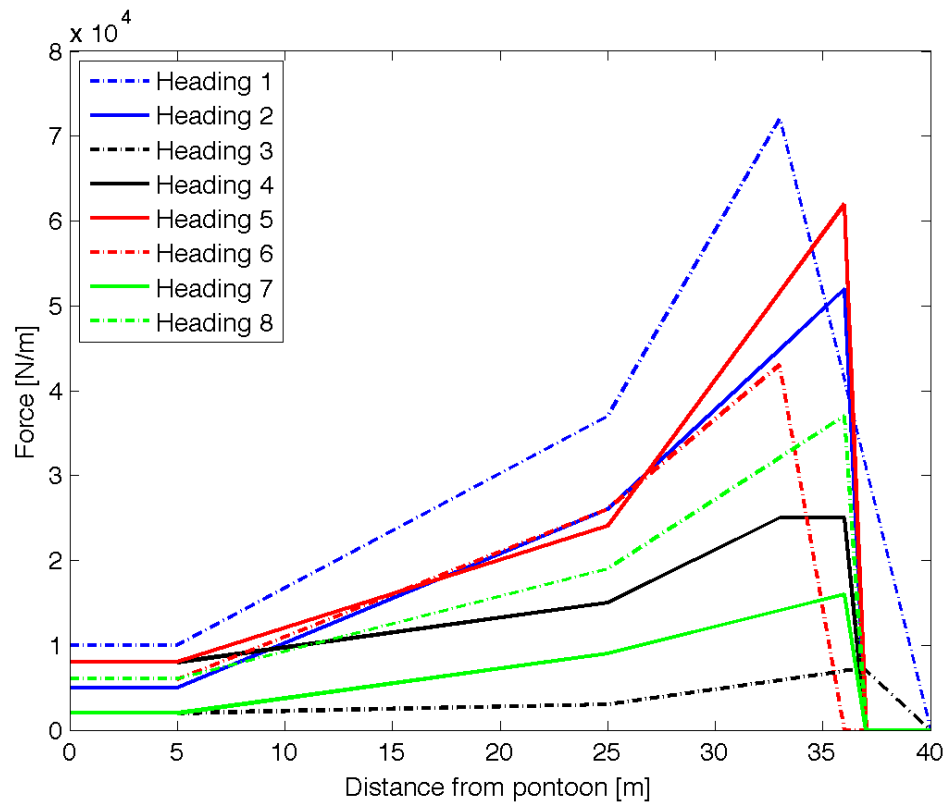


Figure B.3 Distributed load along the caisson in the x-direction with a positive lift coefficient.

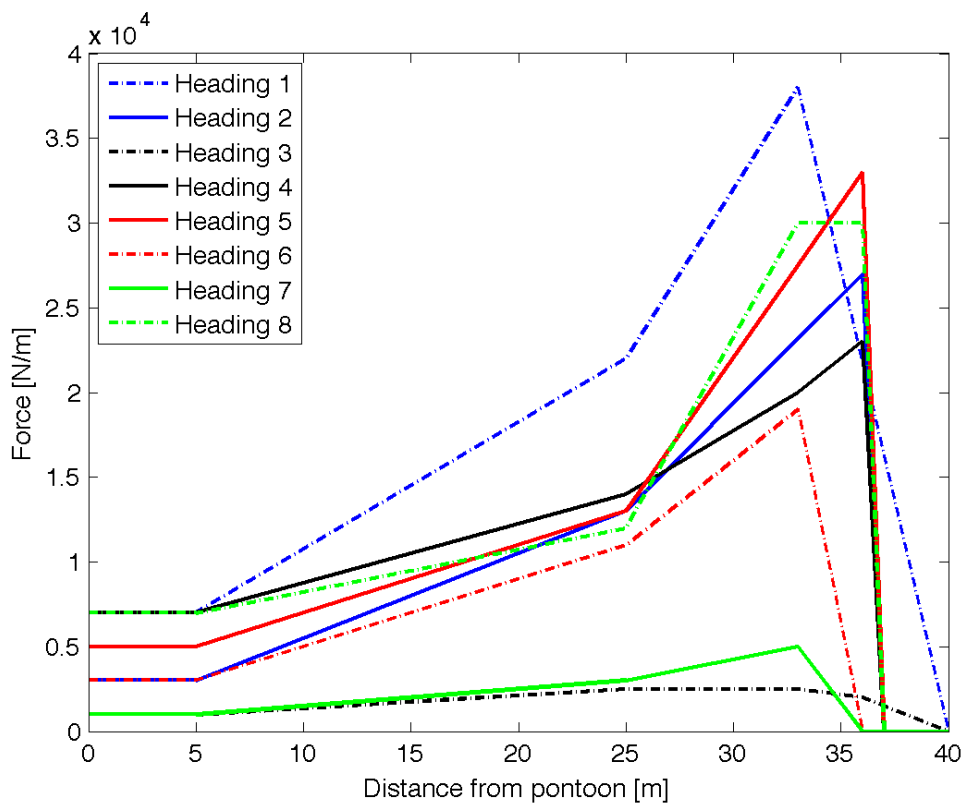


Figure B.4 Distributed load along the caisson in the y-direction with a positive lift coefficient.

Three loading cases are investigated for each wave heading. One case is with only the slamming pressure applied on the lower plate - pressures are given in Table B.3. The two other cases are for Morison loads with a positive and negative lift. Vertical and horizontal Morison forces acting directly on the support are the same for both cases - pressures are given in Tables B.4 and B.5. Applied reaction forces from the beam model can be seen in Tables B.1 and B.2.

*Table B.1 Applied reaction forces from the beam model, positive lift.*

Positive Lift	Upper plate		Lower plate	
Heading	$F_x$ [N/m]	$F_y$ [N/m]	$F_x$ [N/m]	$F_y$ [N/m]
1	154075.3	80631.8	309138.8	166404.1
2	122490.1	-63565.6	201748.3	-103701.8
3	17859.5	5747.1	25944.9	12412.6
4	-63210.1	-53653.6	-112271.4	-92914.7
5	-145080.0	-77097.2	-224627.2	-119925.9
6	-56553.3	25128.1	-185971.0	81547.9
7	-37832.3	-6580.1	-64372.6	-21592.3
8	86799.7	82224.1	148981.6	139000.5

Table B.2 Applied reaction forces from the beam model, negative lift.

Negative Lift	Upper plate		Lower plate	
Heading	$F_x$ [N/m]	$F_y$ [N/m]	$F_x$ [N/m]	$F_y$ [N/m]
1	-115203.5	132364.2	-233489.8	267703.0
2	61314.5	126961.4	101046.7	205049.0
3	2486.0	-15158.9	9289.495	-25344.6
4	61463.1	-56629.0	105358.7	-100015.7
5	99481.2	-126258.5	155134.5	-193628.1
6	-23914.1	56833.4	-76705.1	184685.1
7	-3771.0	21232.8	-13764.9	68332.1
8	-87220.6	77525.2	-144712.2	127002.6

Table B.3 Applied slamming pressure on the lower plate.

Heading	Applied slamming pressure [Pa]
1	120608.0
2	69328.1
3	77947.8
4	69627.3
5	43371.6
6	15727.4
7	25972.3
8	48727.3

Table B.4 *Applied Morison force in the vertical direction.*

	Applied vertical (z-dir) drag force pressure [Pa]	
Heading	Upper plate	Lower plate
1	3895.1	66216.8
2	2205.5	37493.4
3	2473.6	42050.6
4	2139.7	36374.7
5	1364.2	23190.6
6	489.6	8323.9
7	814.2	13840.8
8	1592.4	27070.9

Table B.5 *Applied Morison force in the horizontal direction.*

	Applied horizontal (x-dir) drag force pressure [Pa]	
Heading	First plate	Second plate
1	112409.5	6612.3
2	68808.0	4047.5
3	13231.6	778.3
4	-48756.2	-2868.0
5	-80366.0	-4727.4
6	-11914.9	-700.9
7	8531.9	501.9
8	-2619.1	-154.1

## Appendix C: Structural Models

This appendix aims at presenting complimentary information about the two FE-models needed in order to perform the structural response analysis. Information about the beam FE-model such as is used in boundary conditions, dimensions, material parameters and cross section properties is presented in Section C.1. Information regarding the 3D FE-model such as boundary conditions, material parameters and mesh density settings as well as the resulting mesh is presented in Section C.2.

### C.1 The Beam FE-model

Two boundary condition settings are used in order to obtain the most conservative reaction forces to apply on the 3D FE-model. These are simply supported and rigidly fixed, the set-up can be seen in Tables C.1 and C.2. Material parameters, cross section properties and dimensions of the modelled caissons can be seen in Tables C.3 and C.4.

Table C.1 *Boundary conditions for beam model (simply supported).*

Simply supported	Degrees of freedom						
	Support:	Trans. x	Trans. y	Trans. z	Rot. x	Rot. y	Rot. z
Pontoon deck	Fixed	Fixed	Fixed	Fixed	Fixed	Fixed	Fixed
Stringer 2-3	Fixed	Fixed	Free	Free	Free	Free	Free
Stringer 4-5	Fixed	Fixed	Free	Free	Free	Free	Free
Stringer 7-8	Fixed	Fixed	Free	Free	Free	Free	Free
Stringer 10-11	Fixed	Fixed	Free	Free	Free	Free	Free
Stringer 13-14	Fixed	Fixed	Free	Free	Free	Free	Free
Stringer 15-16	Fixed	Fixed	Free	Free	Free	Free	Free
Deck box	Fixed	Fixed	Fixed	Fixed	Fixed	Fixed	Fixed

Table C.2 Boundary conditions for beam model (rigidly fixed).

Rigidly fixed	Degrees of freedom						
	Support:	Trans. x	Trans. y	Trans. z	Rot. x	Rot. y	Rot. z
Pontoon deck	Fixed	Fixed	Fixed	Fixed	Fixed	Fixed	Fixed
Stringer 2-3	Fixed	Fixed	Free	Fixed	Fixed	Fixed	Fixed
Stringer 4-5	Fixed	Fixed	Free	Fixed	Fixed	Fixed	Fixed
Stringer 7-8	Fixed	Fixed	Free	Fixed	Fixed	Fixed	Fixed
Stringer 10-11	Fixed	Fixed	Free	Fixed	Fixed	Fixed	Fixed
Stringer 13-14	Fixed	Fixed	Free	Fixed	Fixed	Fixed	Fixed
Stringer 15-16	Fixed	Fixed	Free	Fixed	Fixed	Fixed	Fixed
Deck box	Fixed	Fixed	Fixed	Fixed	Fixed	Fixed	Fixed

Table C.3 Material properties of beam model.

Material	Stainless steel
Young's modulus, $E$	206 GPa
Density, $\rho$	7850 kg / m <sup>3</sup>
Poissons ratio, $\nu$	0.3
Yield stress	500 MPa
Ultimate strength	600 MPa

Table C.4 Caisson dimensions and cross section properties.

Sea Water Caisson	
Outer diameter	940 mm
Thickness	18 mm
Length	49 m
Cross section area, $A$	26076 mm
Second moment of inertia, $I_{x,y}$	$5.5423 \cdot 10^9 \text{ mm}^4$
Second moment of inertia, $I_z$	$1.1085 \cdot 10^{10} \text{ mm}^4$

## C.2 3D FE-model

Mesh density settings of the 3D FE-model can be seen in Figures C.1 and C.2. The generated mesh on the entire model can be seen in Figure C.3. Applied boundary conditions can be seen in Table C.5 - edges are explained in Figures C.4 and C.5. Material parameters of the 3D FE-model can be seen in Table C.6.

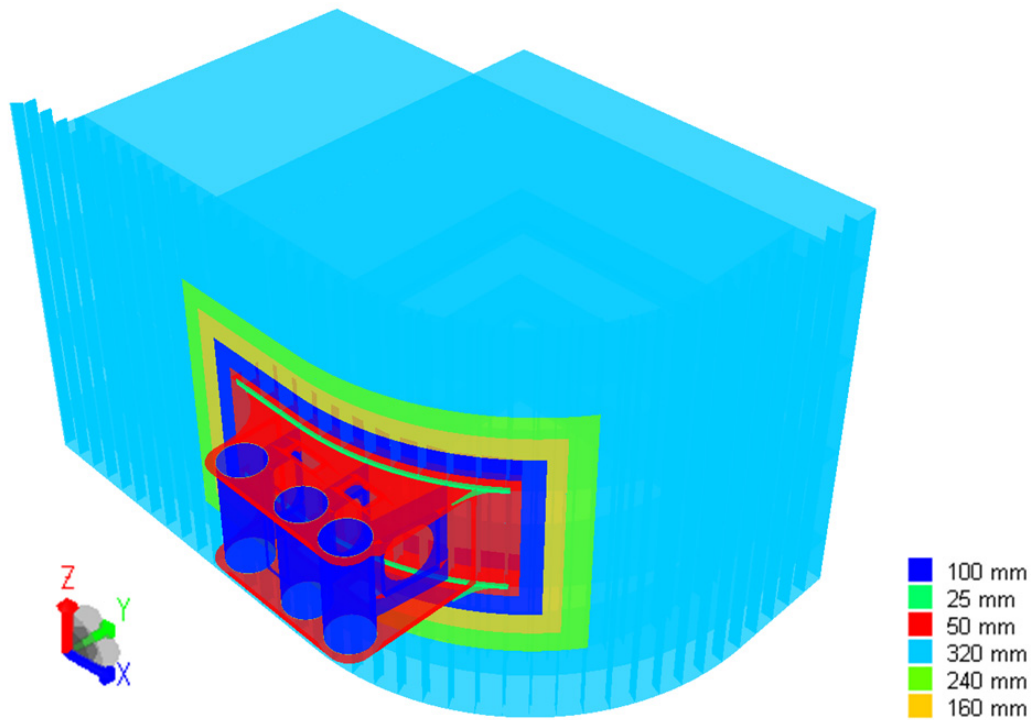


Figure C.1 Mesh density settings. The mesh density is gradually decreased as the distance from the studied weld increases.

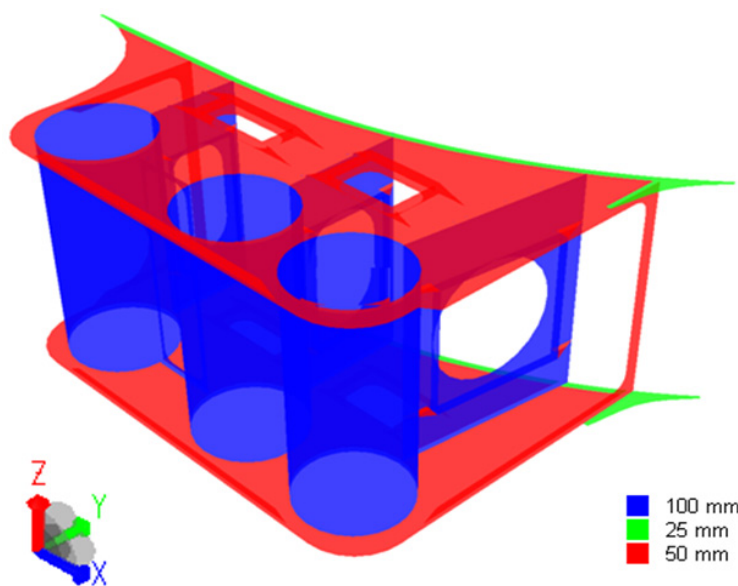
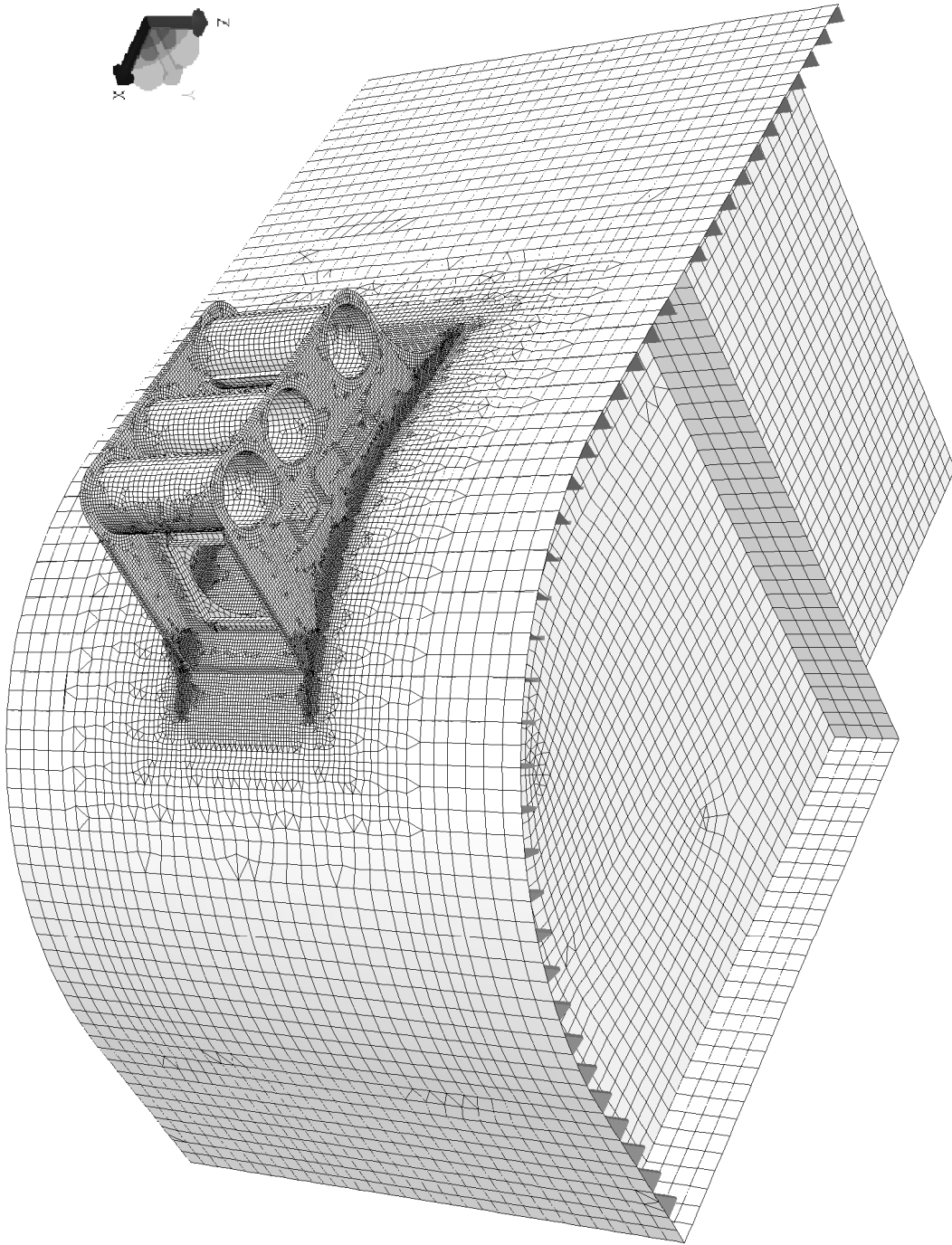


Figure C.2 Mesh density settings on support.



*Figure C.3 Resulting mesh on the entire 3D FE-model.*

Table C.5 *Boundary conditions applied on the 3D FE-model - edges are explained in Figures C.5 and C.6.*

Edge:	Degrees of freedom					
	Trans. x	Trans. y	Trans. z	Rot. x	Rot. y	Rot. z
1	Fixed	Fixed	Fixed	Fixed	Fixed	Fixed
2	Fixed	Fixed	Fixed	Fixed	Fixed	Fixed
3	Fixed	Free	Fixed	Fixed	Fixed	Fixed
4	Fixed	Fixed	Fixed	Fixed	Fixed	Fixed
5	Fixed	Fixed	Fixed	Fixed	Fixed	Fixed
6	Fixed	Fixed	Free	Fixed	Fixed	Fixed
7	Fixed	Fixed	Free	Fixed	Fixed	Fixed
8	Fixed	Free	Fixed	Fixed	Fixed	Fixed
9	Fixed	Fixed	Fixed	Fixed	Fixed	Fixed
10	Fixed	Fixed	Fixed	Fixed	Fixed	Fixed
11	Fixed	Fixed	Fixed	Fixed	Fixed	Fixed
12	Fixed	Fixed	Fixed	Fixed	Fixed	Fixed

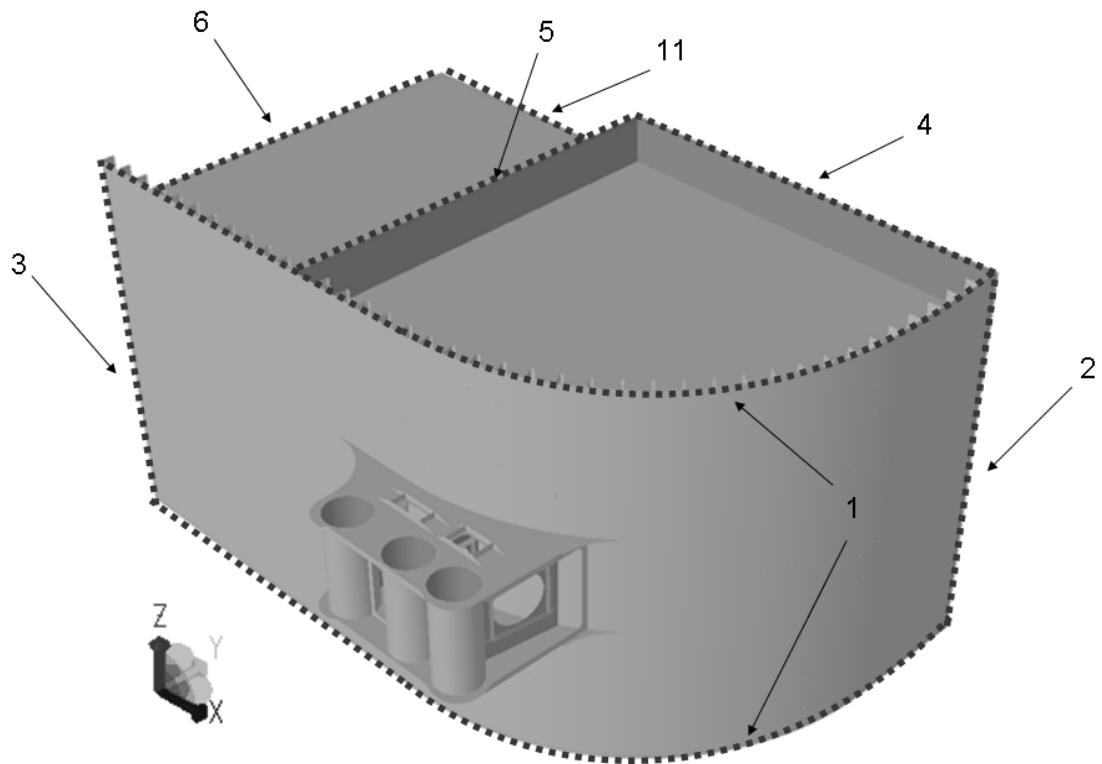


Figure C.5 Boundary edges on the 3D FE-model.

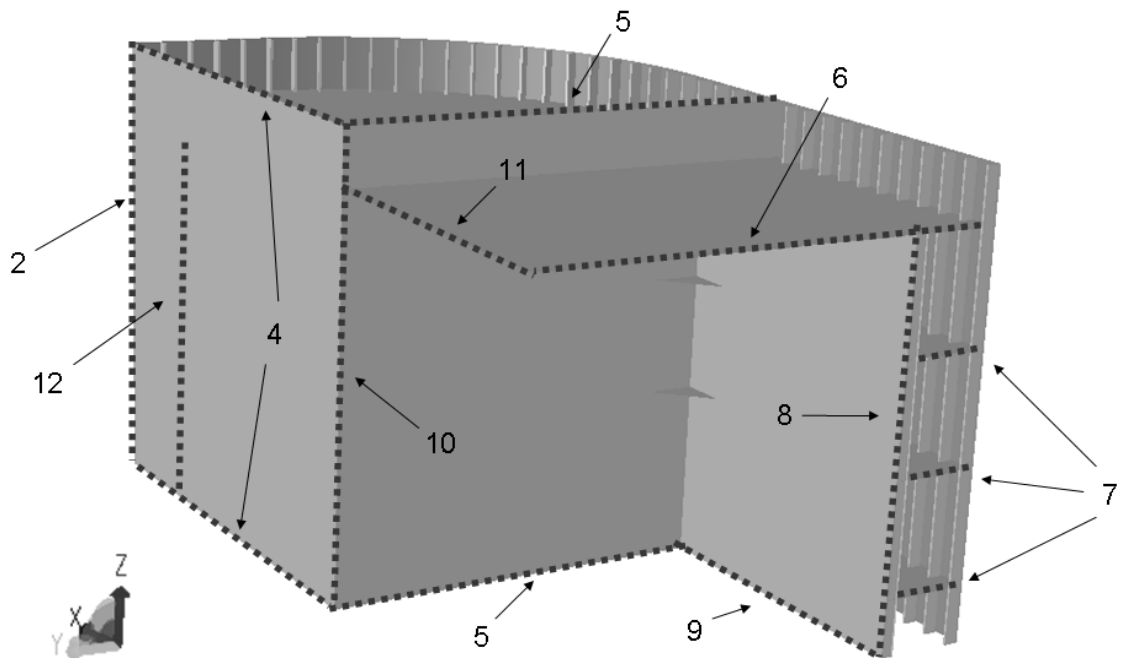


Figure C.6 Boundary edges on the 3D FE-model.

Table C.6 Material properties of FE-model

Material	Steel
Young's modulus, $E$	206 GPa
Density, $\rho$	7850 kg / m <sup>3</sup>
Poissons ratio, $\nu$	0.3
Yield stress	355 MPa

## Appendix D: Stress Results

The maximum principal stress range for each load case and hot-spot as defined in Chapter 6 is presented in Table D.1-8. Stress component values have been read out in the hot-spot read-out points and extrapolated to the hot-spot in order to calculate the principal stresses. The principal stress with the largest magnitude has been recorded for the damage calculations.

Table D.1 Hot-spot stresses, Heading 1.

Heading 1	Principal stress range [MPa]		
Hot spot	Morison -negative lift	Morison - positive lift	Impact
1	35.08	55.46	86.81
2	45.23	54.96	104.43
3	46.54	49.50	100.67
4	6.04	19.02	37.08
5	51.22	53.02	111.81
6	30.35	27.37	72.16
7	19.64	21.99	45.28
8	26.30	19.53	56.33

Table D.2 Hot-spot stresses, Heading 2.

Heading 2	Principal stress range [MPa]		
Hot spot	Morison - negative lift	Morison - positive lift	Impact
1	26.28	38.24	49.90
2	26.21	37.18	60.03
3	23.98	35.08	57.87
4	5.45	19.73	21.32
5	25.84	38.04	64.27
6	11.47	24.43	41.48
7	11.24	16.47	26.03
8	11.85	16.21	32.38

Table D.3 Hot-spot stresses, Heading 3.

Heading 3	Principal stress range [MPa]		
Hot spot	Morison - negative lift	Morison - positive lift	Impact
1	31.33	31.01	56.11
2	37.46	36.27	67.49
3	36.28	34.81	65.06
4	14.92	13.24	23.97
5	40.40	38.50	72.26
6	26.61	24.43	46.64
7	16.84	15.78	29.26
8	20.60	18.49	36.41

Table D.4 Hot-spot stresses, Heading 4.

Heading 4	Principal stress range [MPa]		
Hot spot	Morison - negative lift	Morison - positive lift	Impact
1	32.30	23.91	50.12
2	36.27	33.68	60.29
3	33.99	34.03	58.12
4	17.27	15.66	21.41
5	35.83	37.81	64.55
6	20.64	23.91	41.66
7	24.45	25.57	26.14
8	19.43	25.41	32.52

Table D.5 Hot-spot stresses, Heading 5.

Heading 5	Principal stress range [MPa]		
Hot spot	Morison - negative lift	Morison - positive lift	Impact
1	27.49	11.87	31.22
2	28.47	22.34	37.55
3	26.17	24.36	36.20
4	17.61	13.34	13.34
5	26.09	27.77	40.21
6	13.26	16.35	25.95
7	27.08	27.66	16.28
8	16.36	24.36	20.26

Table D.6 Hot-spot stresses, Heading 6.

Heading 6	Principal stress range [MPa]		
Hot spot	Morison - negative lift	Morison - positive lift	Impact
1	5.84	8.99	11.32
2	1.12	4.59	13.62
3	2.37	6.31	13.13
4	7.95	4.46	4.84
5	1.41	5.78	14.58
6	4.58	3.05	9.41
7	5.13	3.49	5.90
8	3.57	5.97	7.35

Table D.7 Hot-spot stresses, Heading 7.

Heading 7	Principal stress range [MPa]		
Hot spot	Morison - negative lift	Morison - positive lift	Impact
1	8.03	8.32	18.69
2	9.42	12.00	22.49
3	9.08	12.60	21.68
4	0.89	5.45	7.99
5	9.82	14.61	24.08
6	5.08	10.62	15.54
7	3.87	6.50	9.75
8	3.84	9.38	12.13

Table D.8 Hot-spot stresses, Heading 8.

Heading 8	Principal stress range [MPa]		
Hot spot	Morison - negative lift	Morison - positive lift	Impact
1	21.75	13.01	35.07
2	21.20	17.97	42.19
3	17.99	19.00	40.67
4	5.86	1.77	14.98
5	18.99	20.64	45.17
6	7.70	12.32	29.15
7	8.60	8.18	18.29
8	11.03	11.71	22.76

## Appendix E: Shape Parameters

In this Appendix, results obtained from applying the method described in Chapter 7 to the alternative assessment methods in Chapter 4 is presented. Two different fits of the Weibull model were conducted for each wave-height distribution used, one weighted and one un-weighted. The weighted fit results in a good representation of high wave heights while the un-weighted describes low wave heights well. Plots illustrating all the fits can be seen in Figures E.1-E.7. Shape parameters used for each method presented in Chapter 4 can be seen in Subchapter E.1.

Figure E.1 illustrates the Weibull fit to the long-term wave-height distribution obtained from the condensed scatter diagram. Both weather conditions, tropical and non-tropical, and all headings are condensed in this diagram. The shape parameters from this fit were used in Methods 1 and 2.

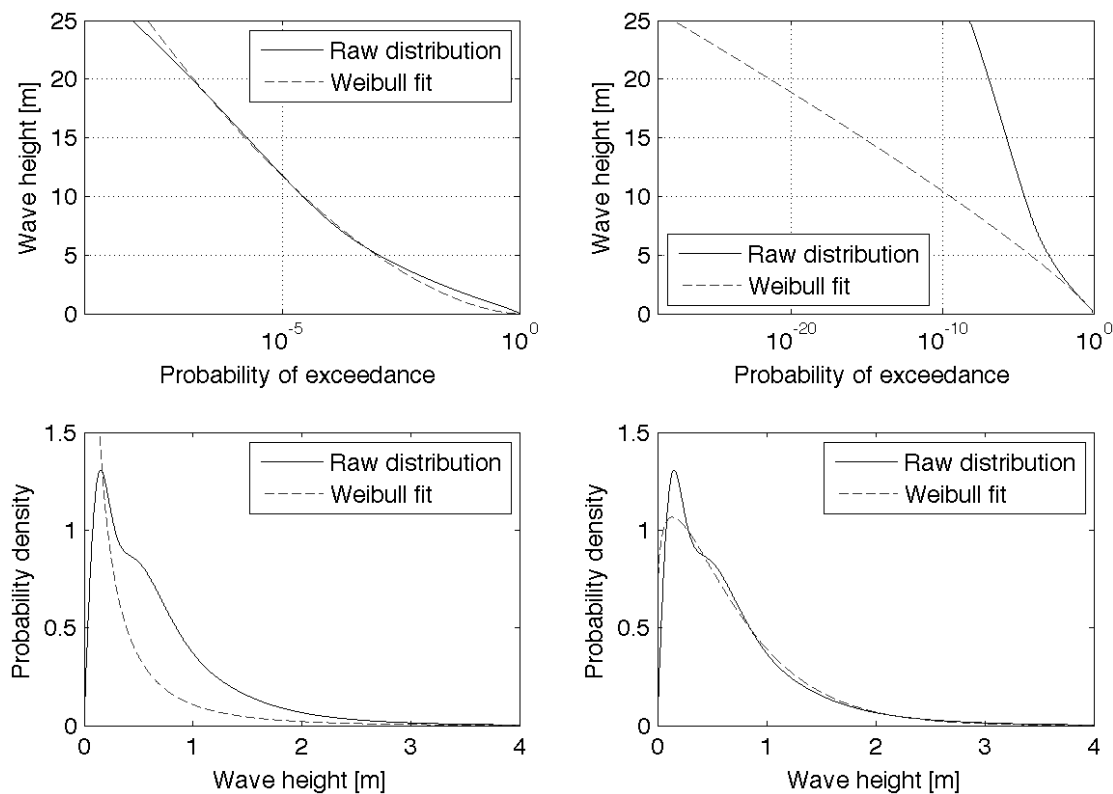


Figure E.1: Wave-height distribution and fit based on the condensed scatter diagram representing all sea-states and headings. Left: weighted fit. Right: un-weighted fit.

Figure E.2-E.5 illustrates the fits performed for Method 3. The long-term wave height distribution for each heading is based on the individual heading scatter data. Figure E.2 shows the un-weighted fit for each heading for a wave height up to 4 metres and Figure E.3 shows the fit for all wave heights. Figures E.4 and E.5 show the same thing as Figures E.2 and E.3 but for the weighted fit.

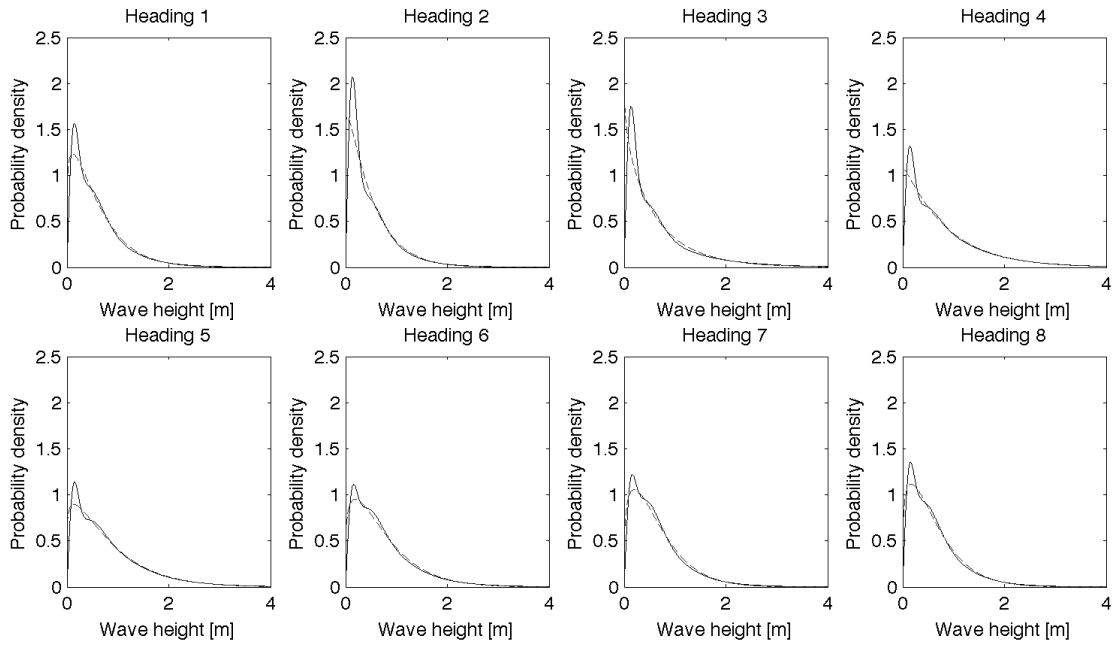


Figure E.2: Wave-height distribution and un-weighted fit based on the individual headings of the condensed scatter diagram. The figure shows the probability density function for wave heights up to 4 metres.

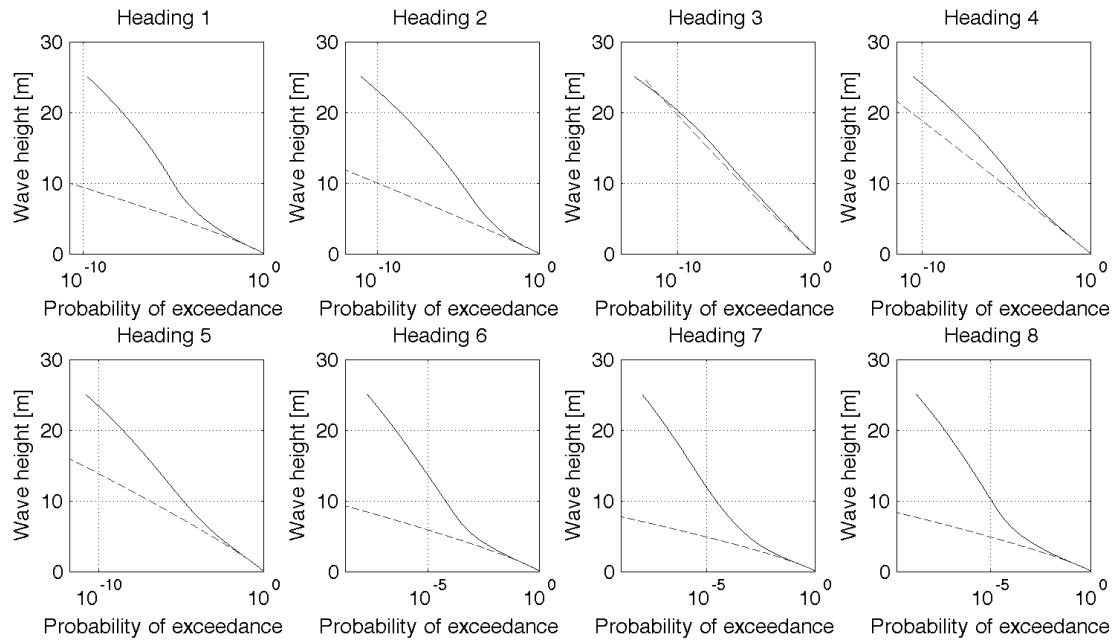


Figure E.3: Wave-height distribution and un-weighted fit based on the individual headings of the condensed scatter diagram. The figure shows the probability of exceedance for all considered wave heights.

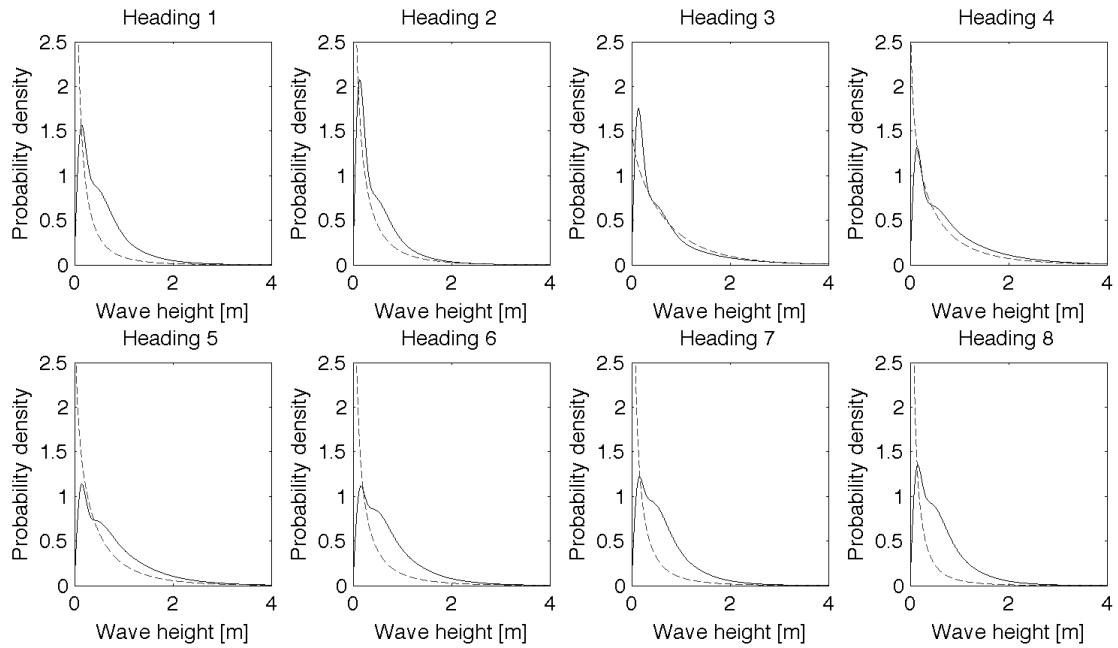


Figure E.4: Wave-height distribution and weighted fit based on the individual headings of the condensed scatter diagram. The figure shows the probability density function for wave heights up to 4 metres.

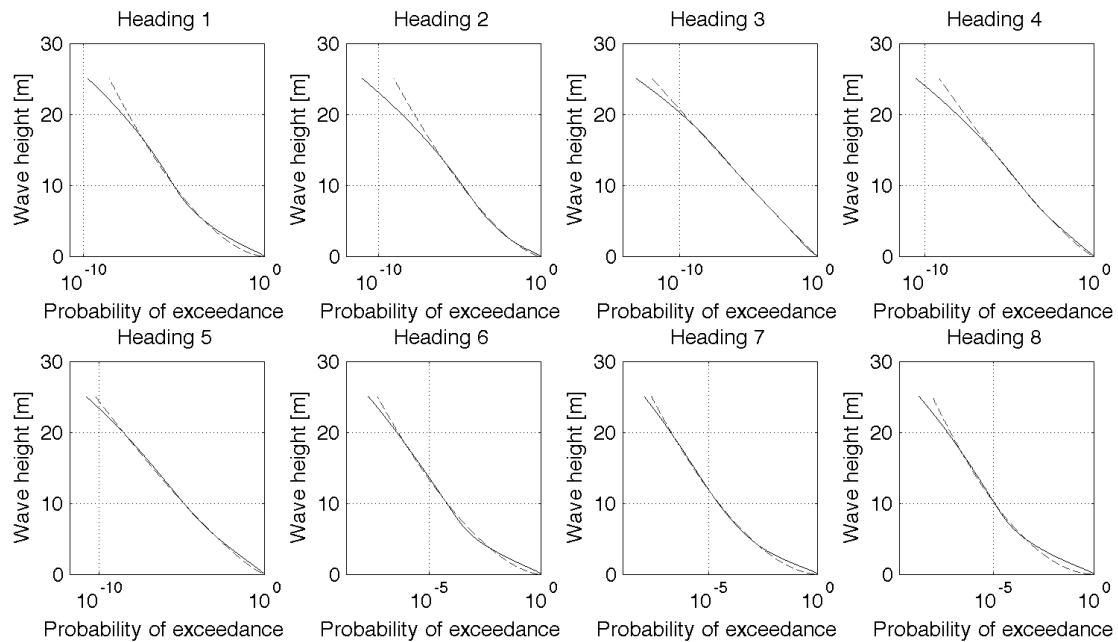


Figure E.5: Wave-height distribution and weighted fit based on the individual headings of the condensed scatter diagram. The figure shows the probability of exceedance for all considered wave heights.

Figures E.6 and E.7 shows the Weibull fit to the wave-height distribution obtained from the non-tropic and tropic scatter diagrams, respectively. All headings in these diagrams were condensed to obtain the wave-height distribution. Shape parameters from these fits were used in Method 4.

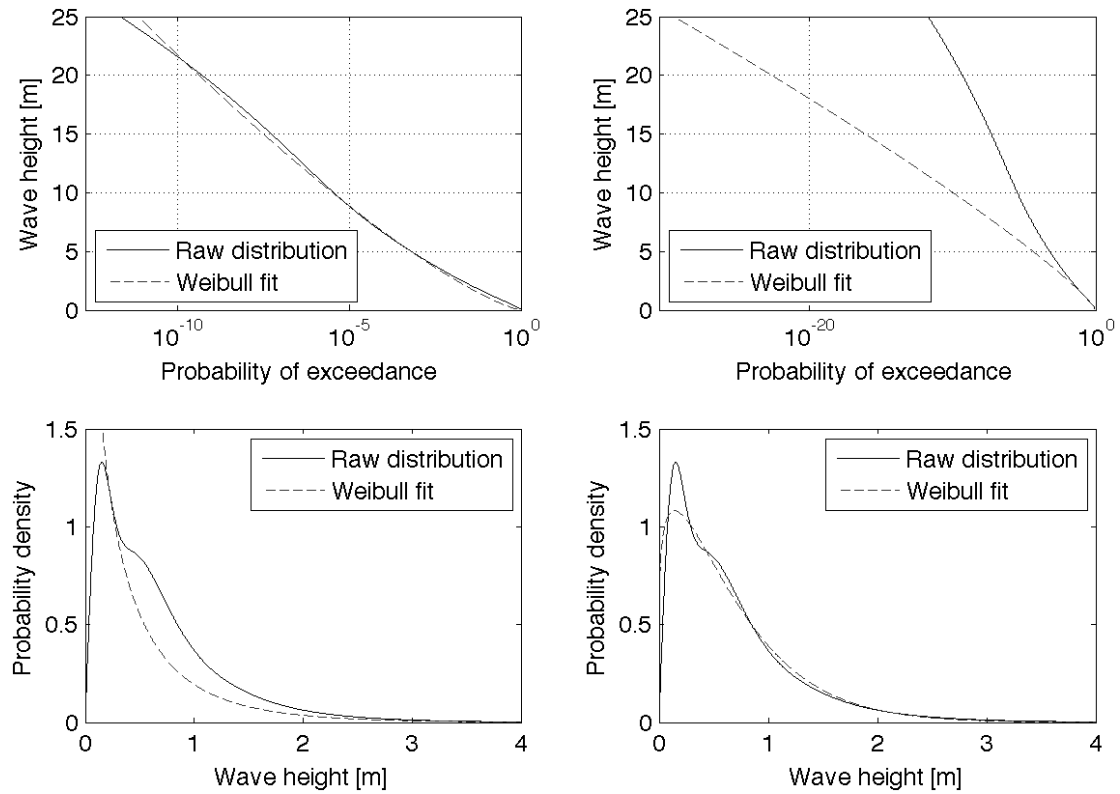


Figure E.6: Wave-height distribution and fit based on the non-tropical scatter diagram with all headings condensed. Left: weighted fit. Right: unweighted fit.

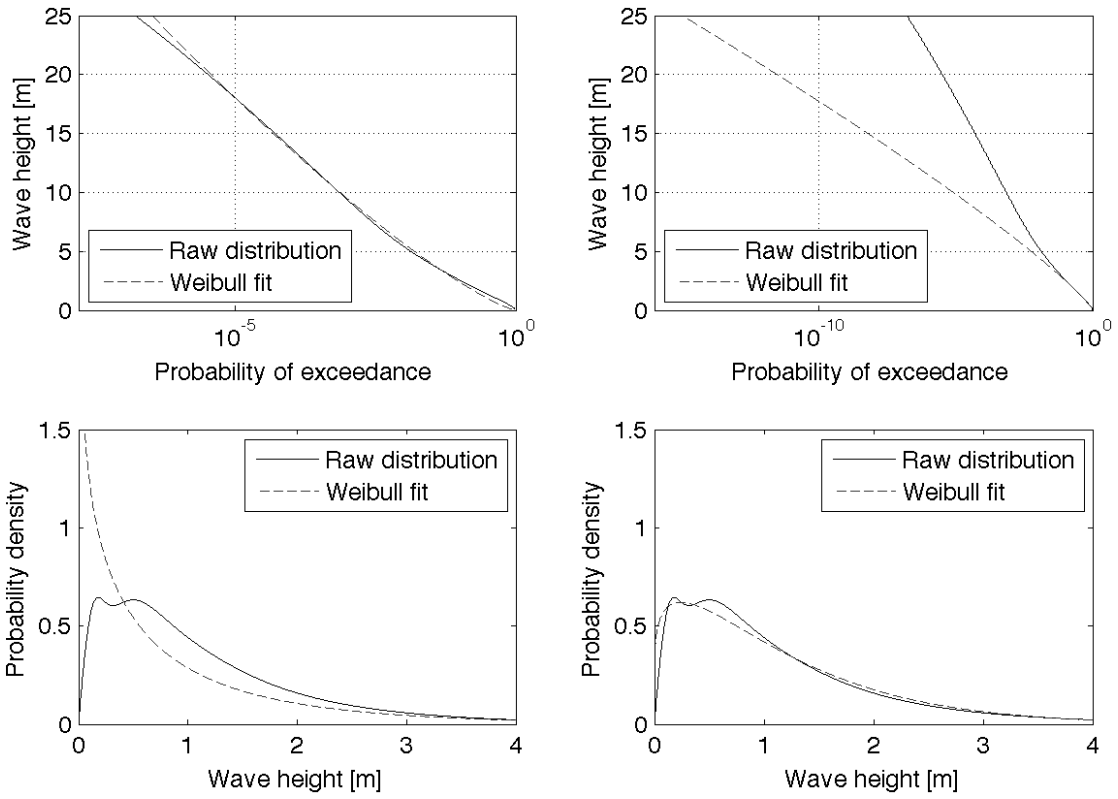


Figure E.7: Wave-height distribution and fit based on the tropical scatter diagram with all headings condensed. Left: weighted fit. Right: un-weighted fit.

## E.1 List of Shape Parameters

Below, all the derived shape parameters are presented with respect to the various methods.

### Nominal method (1), Morison and impact separated method (2)

Condensed wave distribution

$$\gamma_{un-weighted} = 1.171$$

$$\gamma_{weighted} = 0.592$$

### Directional Morison method (3)

Heading 1:

$$\gamma_{un-weighted} = 1.157$$

$$\gamma_{weighted} = 0.585$$

Heading 5:

$$\gamma_{un-weighted} = 1.136$$

$$\gamma_{weighted} = 0.803$$

Heading 2:

$$\gamma_{un-weighted} = 1.060$$

$$\gamma_{weighted} = 0.670$$

Heading 6:

$$\gamma_{un-weighted} = 1.216$$

$$\gamma_{weighted} = 0.606$$

Heading 3:

$$\gamma_{un-weighted} = 0.932$$

$$\gamma_{weighted} = 0.953$$

Heading 7:

$$\gamma_{un-weighted} = 1.261$$

$$\gamma_{weighted} = 0.567$$

Heading 4:

$$\gamma_{un-weighted} = 1.020$$

$$\gamma_{weighted} = 0.810$$

Heading 8:

$$\gamma_{un-weighted} = 1.229$$

$$\gamma_{weighted} = 0.529$$

#### **Weather conditional method (4)**

Non-tropical distribution

$$\gamma_{un-weighted} = 1.181$$

$$\gamma_{weighted} = 0.773$$

Tropical distribution

$$\gamma_{un-weighted} = 1.176$$

$$\gamma_{weighted} = 0.792$$



## Appendix F: Scale Parameters

In this Appendix, values used for determining the scale parameters described in Chapter 8 to the alternative assessment methods devised in Chapter 4 are presented. Details are presented for the four assessment alternatives, respectively.

### (1) The nominal method

The maximum stress range for the ten-year winter storm is used as the reference stress cycle. This corresponds to Heading 1.

$$S_{ref} = \max \begin{cases} S_{impact,max,10} \\ S_{Morison,max,10} \end{cases} = S_{impact,max,10} = 111.81 \text{ MPa} \quad (\text{F.1})$$

The shape parameters were derived from the condensed scatter diagram.

$$\gamma_{un-weighted} = 1.171 \quad (\text{F.2})$$

$$\gamma_{weighted} = 0.592 \quad (\text{F.3})$$

Two values of the reference number of cycles were used, corresponding to the two Weibull fits. Extra numbers of cycles were added corresponding to the fact that waves above 3 metres cause two stress ranges instead of one.

$$N_{ref,un-weighted} = 2.25 \cdot 10^{25} \text{ cycles} \quad (\text{F.4})$$

$$N_{ref,weighted} = 3.18 \cdot 10^7 \text{ cycles} \quad (\text{F.5})$$

### (2) The Morison and impact-separated method

The second method is very similar to the first and was conducted with the same values for the reference number of cycles and shape parameters as the first method.

Two stress ranges are used to determine scale parameters for Morison and impact respectively.

$$S_{ref,Morison} = S_{Morison,max,10} = 53.02 \text{ MPa} \quad (\text{F.6})$$

$$S_{ref,impact} = S_{impact,max,10} = 111.81 \text{ MPa} \quad (\text{F.7})$$

It is worth noting that 53.02 MPa was not the highest stress obtained along the weld due to Morison loads. Hot-spot 1, for example, experienced 55.46 MPa. However, when the stresses due to both Morison and impact loads were combined, hot-spot 5

obtained the greater fatigue damage. (Hot-spot 1 maximum impact loading stress = 86.81 MPa)

### (3) The Directional Morison method

Eight distributions were used in the method, one for each of the headings considered. Since the critical location along the weld changed depending on which load was applied, eight hot-spots were considered, see Figure 6.9. Only Morison stress ranges were investigated. Because of the eight headings and eight hotspots, 64 reference stress cycles were used. The reference stress ranges can be seen in Table F.1.

Table F.1 Reference stress ranges used in the third method. [MPa]

Hotspot\Heading	1	2	3	4	5	6	7	8
1	55.46	38.24	31.33	32.30	27.49	8.99	8.32	21.75
2	54.96	37.18	37.46	36.27	28.47	4.59	12.00	21.20
3	49.50	35.08	36.28	34.03	26.17	6.31	12.60	19.00
4	19.02	19.73	14.92	17.27	17.61	7.95	5.45	5.86
5	53.02	38.04	40.40	37.81	27.77	5.78	14.61	20.64
6	30.35	24.43	26.61	23.91	16.35	4.58	10.62	12.32
7	21.99	16.47	16.84	25.57	27.66	5.13	6.50	8.60
8	26.30	16.21	20.60	25.41	24.36	5.97	9.38	11.71

The shape parameters used vary for the eight different wave headings, see Appendix B Section E.1.

Due to the different distributions eight reference number of cycles - one for each heading and fit - were used, see Table F.2.

Table F.2 Reference number of cycles used for the third method.

Heading	$N_{ref,un-weighted}$ [cycles]	$N_{ref,weighted}$ [cycles]
1	$2.12 \cdot 10^{28}$	$1.42 \cdot 10^8$
2	$2.23 \cdot 10^{24}$	$3.81 \cdot 10^8$
3	$4.39 \cdot 10^{11}$	$1.25 \cdot 10^{11}$
4	$2.28 \cdot 10^{12}$	$3.71 \cdot 10^8$
5	$9.31 \cdot 10^{17}$	$5.66 \cdot 10^9$
6	$2.42 \cdot 10^{26}$	$9.38 \cdot 10^6$
7	$4.28 \cdot 10^{35}$	$2.08 \cdot 10^7$
8	$5.97 \cdot 10^{33}$	$4.92 \cdot 10^7$

Due to the eight headings, eight hot-spots and the two methods used for conducting the fit, 128 scale parameters were needed.

#### (4) The Weather conditional method

Two scale parameters were used to represent tropical and non-tropical-weather. The maximum ten-year winter storm was once again used as the reference stress range.

$$S_{ref,non-trop} = S_{ref,tropical} = S_{Morison,max,10} = 53.02 \text{ MPa} \quad (\text{F.8})$$

Different shape parameters are used depending on the individual distributions and are derived from the non-tropical and tropical scatter diagrams, respectively.

$$\gamma_{non-tropical,un-weighted} = 1.181 \quad (\text{F.9})$$

$$\gamma_{non-tropical,weighted} = 0.773 \quad (\text{F.10})$$

$$\gamma_{tropical,un-weighted} = 1.176 \quad (\text{F.11})$$

$$\gamma_{tropical,weighted} = 0.792 \quad (\text{F.12})$$

Four values of the reference number of cycles were used corresponding to the two weather conditions and two Weibull fits.

$$N_{ref,un-weighted,non-trop} = 6.68 \cdot 10^{26} \text{ cycles} \quad (\text{F.13})$$

$$N_{ref,weighted,non-trop} = 3.19 \cdot 10^{10} \text{ cycles} \quad (\text{F.14})$$

$$N_{ref,un-weighted,tropical} = 4.77 \cdot 10^{13} \text{ cycles} \quad (\text{F.15})$$

$$N_{ref,weighted,tropical} = 1.26 \cdot 10^6 \text{ cycles} \quad (\text{F.16})$$

## Appendix G: S-N Curves

This appendix specifies the two S-N curves used throughout the thesis.

A two-slope S-N curve, for type D in sea water with cathodic protection, Det Norske Veritas (2011a). See table G.1

Table G.1 DNV S-N curve D

$N < 10^6$	$N > 10^6$
$m = 3.0$	$n = 5.0$
$\log_{10}(\bar{a}) = 11.764$	$\log_{10}(\bar{c}) = 15.606$

$$s_{s.i.} = 10^{\frac{\log(\bar{a}) - \log(10^6)}{m}} = 10^{\frac{\log(\bar{c}) - \log(10^6)}{n}} = 83.4 \text{ MPa} \quad (\text{G.1})$$

A two-slope S-N curve, for type C2 in sea water with cathodic protection, Det Norske Veritas (2011a). See table G.2

Table G.2 DNV S-N curve C2

$N < 10^6$	$N > 10^6$
$m = 3.0$	$n = 5.0$
$\log_{10}(\bar{a}) = 11.901$	$\log_{10}(\bar{c}) = 15.835$

$$s_{s.i.} = 10^{\frac{\log(\bar{a}) - \log(10^6)}{m}} = 10^{\frac{\log(\bar{c}) - \log(10^6)}{n}} = 92.68 \text{ MPa} \quad (\text{G.2})$$

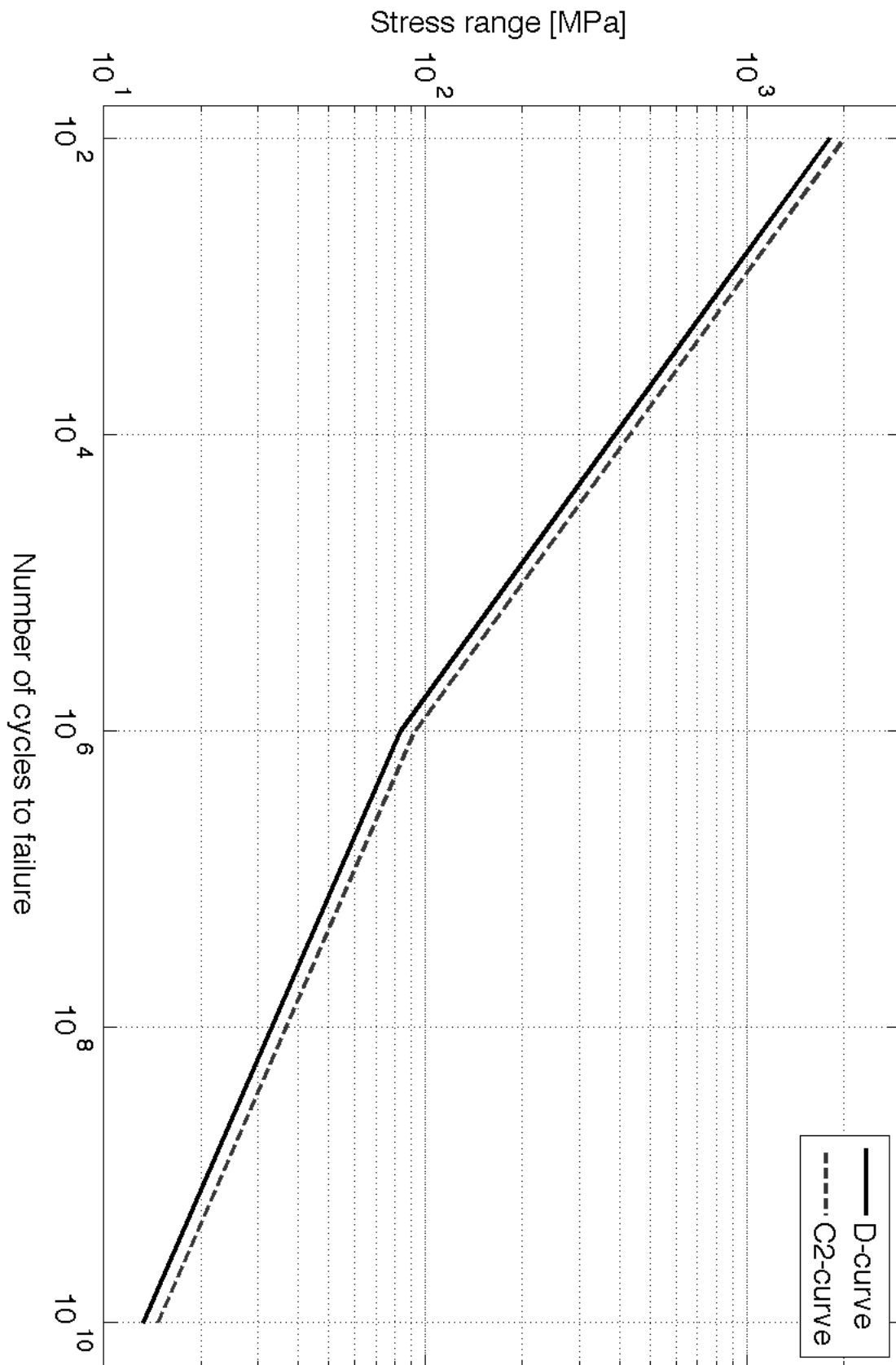


Figure G.1 The two S-N curves used in the thesis, DNV S-N curve D and C2